AD_____

Award Number: W81XWH-11-2-0071

TITLE:
The Importance of Neurogenic Inflammation in Blast-Induced Neurotrauma

PRINCIPAL INVESTIGATOR:
Dr. Brock Wester, Ph.D.

CONTRACTING ORGANIZATION:
Johns Hopkins University Applied Physics
Laurel, MD 20723

REPORT DATE:
May 2014

TYPE OF REPORT:
Final Report

PREPARED FOR:
U.S. Army Medical Research and Materiel Command
Fort Detrick, Maryland 21702-5012

DISTRIBUTION STATEMENT:
Approved for public release; distribution unlimited

REPORT DOCUMENTATION PAGE

Form Approved
OMB No. 0704-0188

1. REPORT DATE	2. REPORT TYPE	3. DATES COVERED
May 2014	Final	1 Jan 2011 - 31 Dec 2013

4. TITLE AND SUBTITLE
The Importance of Neurogenic Inflammation in Blast- Induced Neurotrauma

5a. CONTRACT NUMBER

5b. GRANT NUMBER
W81XWH-11-2-0071

5c. PROGRAM ELEMENT NUMBER

6. AUTHOR(S)
Michele Schaefer, Ph.D., Brock Wester, Ph.D., Nathan Boggs, and Chris Bradburne,

email:

Email: brock.wester@jhuapl.edu

5d. PROJECT NUMBER

5e. TASK NUMBER

5f. WORK UNIT NUMBER

7. PERFORMING ORGANIZATION NAME(S) AND ADDRESS(ES)
Johns Hopkins University Applied Physics
Laurel, MD 20723

8. PERFORMING ORGANIZATION REPORT NUMBER

9. SPONSORING / MONITORING AGENCY NAME(S) AND ADDRESS(ES)
U.S. Army Medical Research and Materiel Command
Fort Detrick, Maryland 21702-5012

10. SPONSOR/MONITOR'S ACRONYM(S)

11. SPONSOR/MONITOR'S REPORT NUMBER(S)

12. DISTRIBUTION / AVAILABILITY STATEMENT
Approved for Public Release; Distribution Unlimited

13. SUPPLEMENTARY NOTES

14. ABSTRACT
This study investigates the role of blood-borne immune cells as important mediators of damage and neuropathology resulting from blast-induced neurotrauma (BINT). We hypothesized that macrophages, along with their secreted cytokines and chemokines from the periphery, migrate via blood and infiltrate the CNS where they contribute to neuronal damage caused by activated microglia both in acute and chronic injury phases of BINT. We have used MRI and molecular techniques in mice with mild/moderate blast injury generated in a compressed helium-driven shock tube, as well as measurements of motor performance and behavioral assessment, observed temporally over 1 month. Groups of animals with mild/moderate BINT are imaged (MRI) and validated by immunocytochemistry, to visualize potential macrophage infiltration; blood-brain barrier (BBB) disturbance; reactive gliosis; or astrocyte activation. We show that a single exposure to mild/moderate blast induces both acute and chronic glial activation, levels of cytokines/chemokines, and motor impairment

15. SUBJECT TERMS- blast, traumatic brain injury, brain, inflammation, magnetic resonance imaging, mice

16. SECURITY CLASSIFICATION OF:			17. LIMITATION OF ABSTRACT	18. NUMBER OF PAGES	19a. NAME OF RESPONSIBLE PERSON
a. REPORT	b. ABSTRACT	c. THIS PAGE			USAMRMC
U	U	U	UU	72	19b. TELEPHONE NUMBER *(include area code)*

Table of Contents

Page

Introduction

Nearly 80% of U.S. wartime causalities since 2001 have been caused by improvised explosive devices (IEDs), contributing to a huge incidence of blast-induced neurotrauma (BINT) leading to both acute and long-term, chronic effects in survivors. From 2000 to 2011, nearly 220,000 service members have been reported to be affected by traumatic brain injury (TBI; Effgen et. al., 2012). While moderate and severe TBIs are easily identified and aggressively treated, milder TBIs or concussions, previously thought insignificant, frequently remain undiagnosed. Recent studies suggest blast exposure may cause inflammation in the brain, which could lead to long-term neurological deficits. We believe that blast injury mobilizes and activates immune cells from the systemic circulation, which then secrete cytokines and chemokines into the blood as well as migrate through blood and lymph and enter the brain through a disturbed blood-brain barrier (BBB). These chemicals and cells, once in the brain, activate glia and/or worsen the neuronal damage caused by activated microglia both in acute and chronic phases of BINT. Among the major challenges in defining the pathobiology of TBI-induced neurogenic inflammation is the morphological similarity between macrophages that originate from the periphery and then enter the brain, and the activated resident microglia. Clarifying these mechanisms would significantly help in developing novel diagnostic tests that would be capable of identifying patients with a higher risk of developing long-term neurological problems, in assessing disease progression, in generating therapeutics that will slow and/or decrease morbidity and long term effects and in monitoring the success of therapeutic interventions.

Understanding these unique pathological responses to blast exposure requires a holistic approach, taking into account the interaction between all vital injury mechanisms, not only those originated in the central nervous system. We hypothesized that in response to blast exposure that blood-borne immune cells that migrate via blood and lymph circulation infiltrate the CNS and contribute to neuronal damage caused by activated microglia both in acute and chronic injury phases of BINT. In evaluating this hypothesis, we used state-of-the-art imaging and molecular techniques in mice exposed to simulated blast environments throughout a one-month post-exposure observation period. In an additional test series through each Aim, we also evaluated the efficacy of a near-ideal instantiation of torso protection to successfully mitigate the effects of BINT. In Aim 1, imaging investigations were performed to assess macrophage infiltration (SPIO-enhanced T2-weighted magnetic resonance imaging (MRI)), BBB disturbance (Gf-enhanced T1-weighted MRI), reactive gliosis (manganese-enhanced MRI or MEMRI), and astrocytic activation (bioluminescence IVIS imaging of transgenic GFAP-reporter mice). In Aim 2, molecular mechanisms and presence of neurogenic inflammation cellular responses were examined. In Aim 3, high level functional outcomes such as motor, cognitive, and behavioral evaluations were performed. Lastly, in Aim 4, a final imaging modality was selected, and the imaging outcomes from additional experiments were compared with molecular analyses and functional data.

In this final report, we disclose the findings from these imaging and molecular assessments, which provide insights into the physiologic responses to blast exposure generated in a compressed helium-driven shock tube. Our neuropathology and molecular biology methods validate the imaging findings and can be compared with functional tests measuring motor performance, memory, and behavior. Furthermore, we can begin to deconstruct injury mechanisms by assessing the contribution of the direct shock wave to the head versus shock wave to the torso on the immune response.

Body

Aim 1 (18 months-October 1, 2010 to March 31, 2012) MRI Imaging of Macrophage Infiltration, BBB Disturbance, and Glial Response in Mice Exposed to Mild, Moderate, or Severe Blast Exposure

Overall, animals were imaged over multiple time points at the Georgetown University Medical Center Preclinical Imaging Research Laboratory (PIRL) generating hundreds of images. To investigate various imaging markers and contrasting agents, mice received Feraspin particles (Task 1.1. and Figure 1), gadolinium (Task 1.2. and Figure 2-4), or MnCl2 (Task 1.3. and Figure 5-7). Pre- and post-contrast images were acquired for all mice and representative images are included here (Figure 1-7). For this phase of the effort, only sham (Sham) and non-protected blast-exposed animals (NP) were evaluated. Torso protected (TP) blast-exposed and torso-protected sham (TP-Sham) animals were not evaluated. To ensure consistency of animal positioning and orientation within the machine, a custom-designed stereotaxic holder was constructed to fit the PIRL 4-channel phased-array radiofrequency mouse brain coil and corresponding transmit volume coil. This permitted parallel MR imaging which allowed for MEMRI of high resolution and short imaging times.

Task 1.1. MRI Imaging of Macrophage Infiltration using Iron Oxide (FeOx) Particles as a Contrast Agent.

Iron oxide (IO) contrast agents can be quickly and preferentially uptaken by the reticulo-endothelial system depending on their size and particle composition. Therefore, an increase in negative contrast observed in the brain by MRI, could signify that peripheral macrophages loaded with IO nanoparticles had traveled from the periphery after the blast. On the other hand, if these particles show affinity to be endocytosed by other tissues such as brain, their first destination might instead be resident brain macrophages. In order to provide information regarding inflammation and macrophage infiltration related to the site of blast injury, iron oxide contrast agent was injected intravenously and animals were imaged. We anticipated that the contrast agent would undergo specific uptake by macrophages. Moreover, we predicted that the opening of the BBB would preclude exclusion of the FeOx particles from the brain, and an area of negative (i.e., darkening) T2-weighted MRI contrast would be evident in NP mice.

FeOx particles of various sizes (10-30 nm hydrodynamic diameter), composition (e.g., P904 has a glucose derivative coating designed for macrophage imaging applications), and concentrations (500 to 1000 µmol iron/kg body weight) were injected intravenously at various time points before and after blast exposure. Post-blast injection of the Feraspin XS FeOx particles (18 nm mean hydrodynamic diameter) resulted in FeOx being taken up by the reticuloendothelial system

primarily. We next obtained P904 FeOx particles (Guerbet Research, France) coated with an amino alcohol derivative of glucose that favored macrophage uptake with the expectation that these would have longer circulation times allowing their uptake by macrophages present in tissues which are less accessible (i.e., brain) than well-vascularized tissues such as the liver or spleen.

When using the P904 FeOx particles (18 nm mean hydrodynamic diameter), we observed areas of negative contrast that was not evident in the pre-injection image (Figure 1). However, enhancement was non-specific with contrast present in both normal and injured animals. Thus, these iron particles can cross the BBB and enter the brain without being taken up by macrophages. To differentiate between infiltrating FeOxladen peripheral macrophages and resident macrophages that take up FeOx, animals were imaged over a period of days (several half-lives past FeOx blood resident time). Signal enhancement was detected early as expected and persisted for 24hr. There was no appearance of newly generated signal (i.e., FeOx laden infiltrating macrophages) after 24hr. Significant in vitro and in vivo work will need to be done to further elucidate the mechanisms of FeOx transport and to subsequently optimize imaging parameters, which is beyond the scope of this proposal.

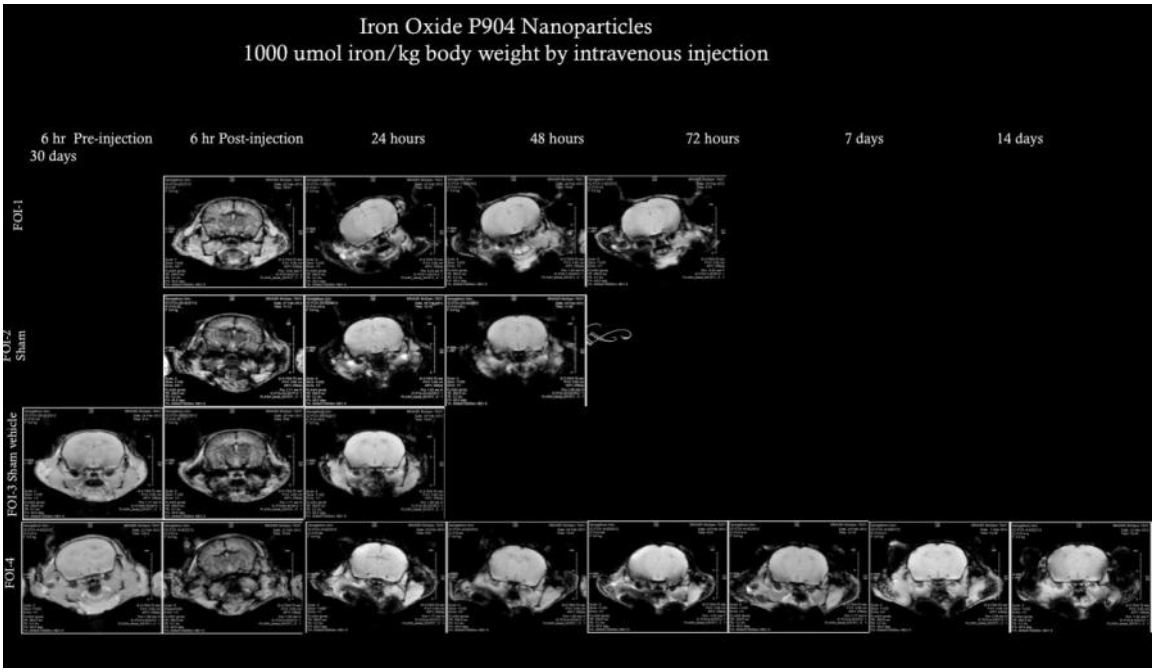

Figure 1. Representative P904 FeOx enhanced MRI imaging. Passive diffusion of P904 was observed throughout the brain at 6hr post-injection. No obvious difference in signal enhancement was observed between injured and sham animals. Moderate blast injured brains (FOI-1, FOI-4). Sham brains (FOI-2S, FOI-3S). FLASH (fast low angle shot) imaging protocol was used with TR: 350 ms, TE: 3.2 ms, FOV: 3 cm, MTX: 256 and, 8 averages.

Task 1.2. MRI Imaging of BBB Disturbance using Gadofluorine M Contrast Agent. *Gadofluorine was not available and Gadolinium-DTPA (Gd-DTPI Magnevist®) was used as contrast in experiments intended to evaluate the BBB.*

Multiple mice (Figures 2, 3, and 4) were subjected to blast-induced neurotrauma and imaged 6hr later using T1-weighted MRI to obtain a Gd-DTPI image baseline. Immediately after imaging, an intraperitoneal (IP) injection of 0.6 mL/kg Gd-DTPI was administered. Mice were imaged at 6hr (pre-Gd) and 6hr, 24hr, 72hr, 7d, 14d, and 28d post-Gd injection and blast.

Initial imaging experiments indicated there was a brightening of the brain in all scanned animals after the contrast administration (Figures 2, 3). While there was some day-to-day variability and variability between NP animals they all seemed to trend toward increased brightening in the brain while sham treated animals had less contrast-uptake. These preliminary results were interpreted as the result of a compromised BBB. However, to confirm this finding, signal would have to be normalized to eliminate day-to-day variability in signal intensity.

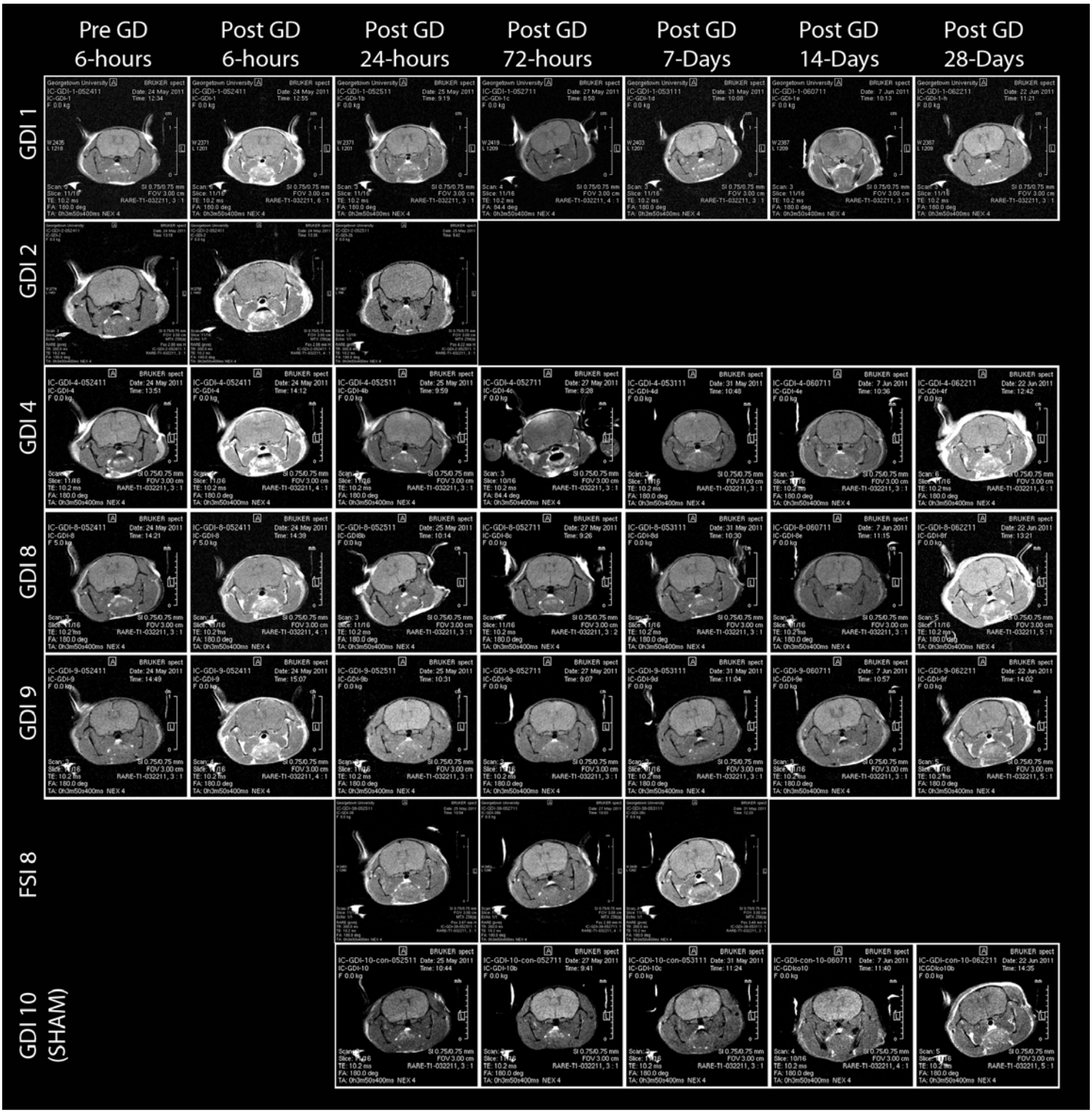

Figure 2. Gadolinium T1 MRI Imaging: BBB disturbance. Animals imaged (NP =GDI 1, 2, 4, 8, 9, and FSI 8; Sham = GD1-10). The imaging protocol is: T1-weighted RARE with TR: 300 ms, TE: 10.2 ms, FOV: 3 cm, MTX: 256, averages: 4.

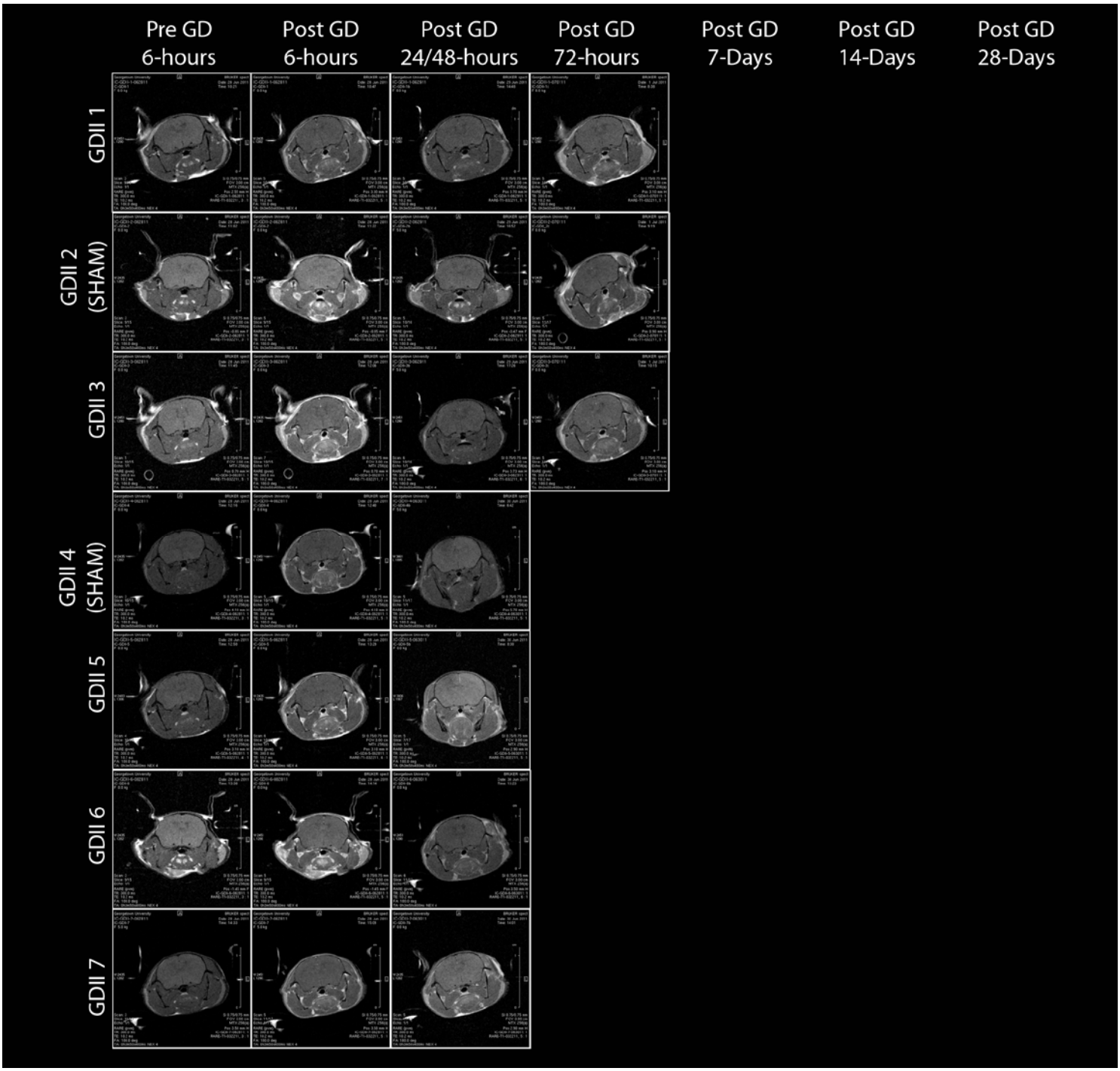

Figure 3. Gadolinium T1 Imaging: BBB disturbance. Animals imaged (NP =GDII-1, 3, 5, 6, and 7; Sham mice GDII-2 and GDII-4). The imaging protocol is: T1-weighted RARE with TR: 300 ms, TE: 10.2 ms, FOV: 3 cm, MTX: 256, averages: 4.

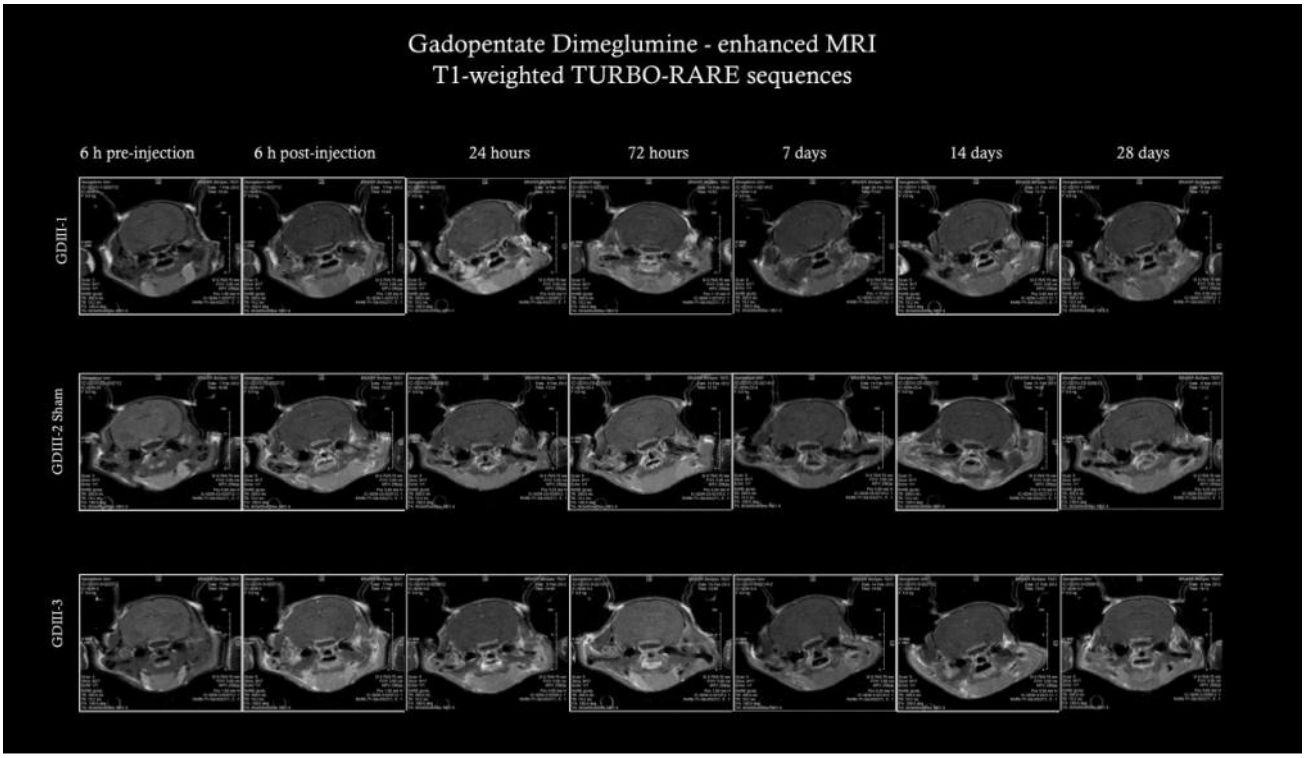

Figure 4. Gadolinium T1 MRI Imaging: BBB disturbance. Animals imaged (NP = GDIII-1, and GDIII-3; Sham = GDIII-2S). The imaging protocol is: T1-weighted RARE with TR: 300 ms, TE: 10.2 ms, FOV: 3 cm, MTX: 256, averages: 4.

With continued gadolinium-enhanced T1-weighted MR imaging, we were not able to reproduce the original findings (see Figure 4 for example). We concluded that the signal enhancement occurs at or near the 'noise' level making interpretation difficult. Given that this contrast agent doesn't appear to be consistently enhancing signal in mild/moderate blast exposed animals we proposed to discontinue GD-DTPI imaging in our July 2012 quarterly report.

Task 1.3. MR Imaging of Reactive Gliosis using $MnCl_2$-Enhanced MRI (MEMRI)

Multiple animals were injected with the $MnCl_2$ contrast agent 24hr prior to BINT and were imaged with T1-weighted MRI (Figure 5-6). MnCl2-induced signal enhancement was manifested by 48hr and in some cases was followed by a gradual increase in signal in the area of the BINT.

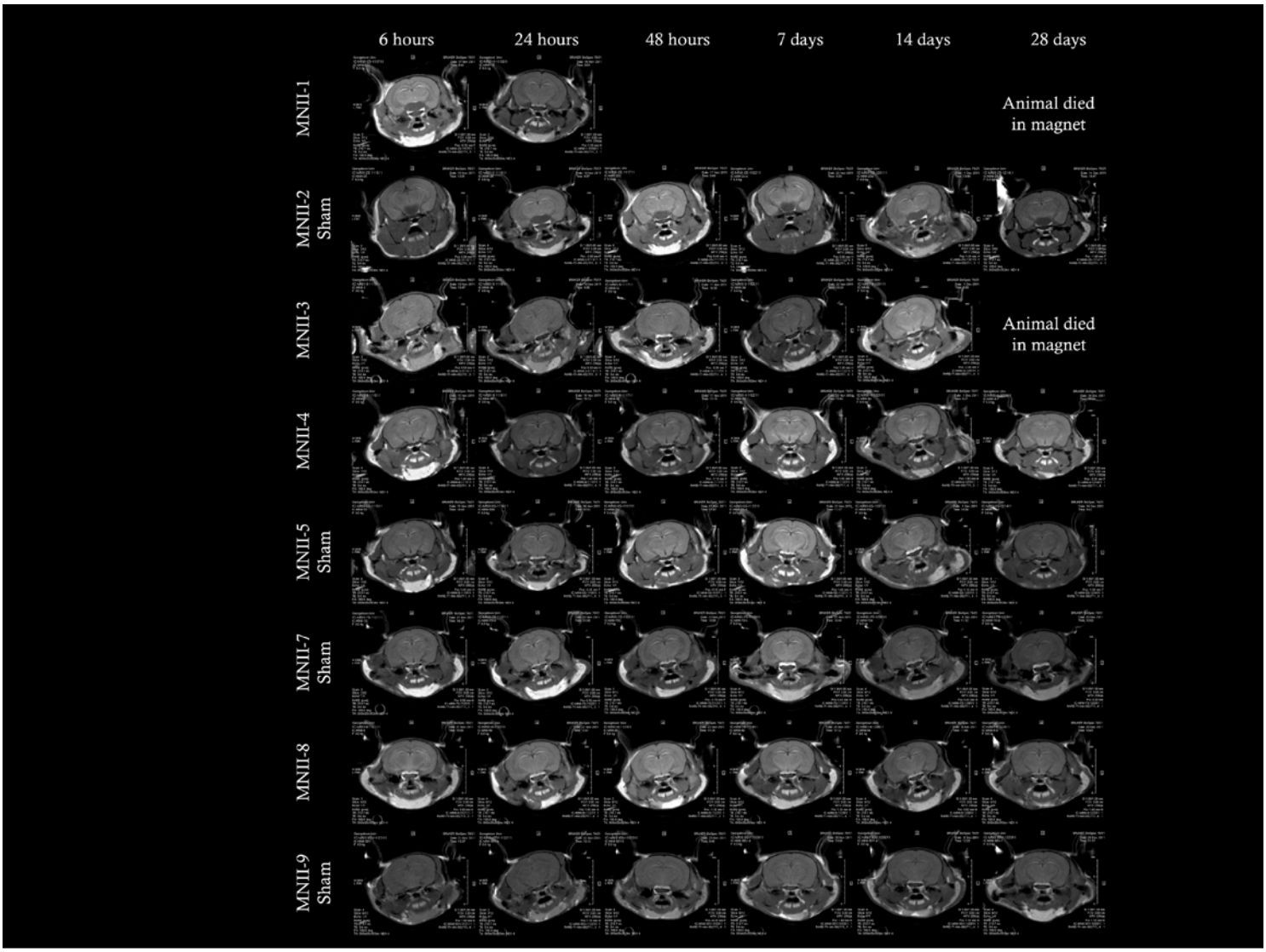

Figure 5. $MnCl_2$-enhanced T1-weighted MRI: reactive gliosis. Animals (NP = MNII 1, 3, 4, 6, 8; Sham = MNII 2, 5, 7, 9). T1-weighted RARE (rapid acquisition with rapid enhancement) two-dimensional sequence with the following parameters: Matrix: 256, TR: 218.7 msec, TE: 9.4 msec, number of averages: 4, Rare factor: 1, FOV: 3.0 x 3.0 cm, number of slices: 12, slice thickness: 1 mm.

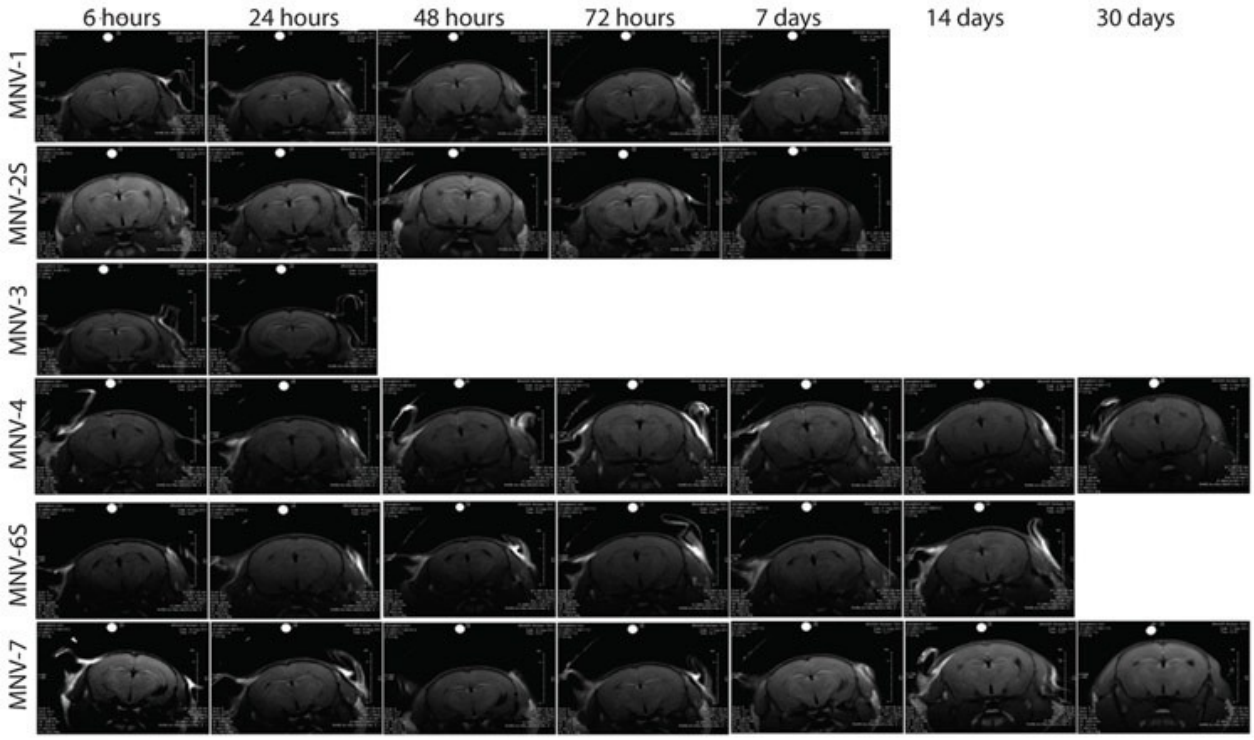

Figure 6. $MnCl_2$-enhanced T1 MRI: reactive gliosis. Animals (NP = MNV-1, 3, 4, 7; Sham = MNV-2S, 6S) Imaging Sequence, T1-weighted RARE (rapid acquisition with rapid enhancement) two-dimensional sequence with the following parameters: Matrix: 256, TR: 218.7 msec, TE: 9.4 msec, number of averages: 4, Rare factor: 1, FOV: 3.0 x 3.0 cm, number of slices: 12, slice thickness: 1 mm.

In summary, we chose to move forward with and optimize MnCl2-enhanced T1-weighted MRI (see Aim 4).

$MnCl_2$-T2 Imaging Control for Edema/Infarct

The purpose of the T2-weighted MRI in MnCl2-injected animals was to identify the presence of edema and hemorrhagic infarct. In all cases the animals were unremarkable and didn't show edema or infarcts (Figure 7).

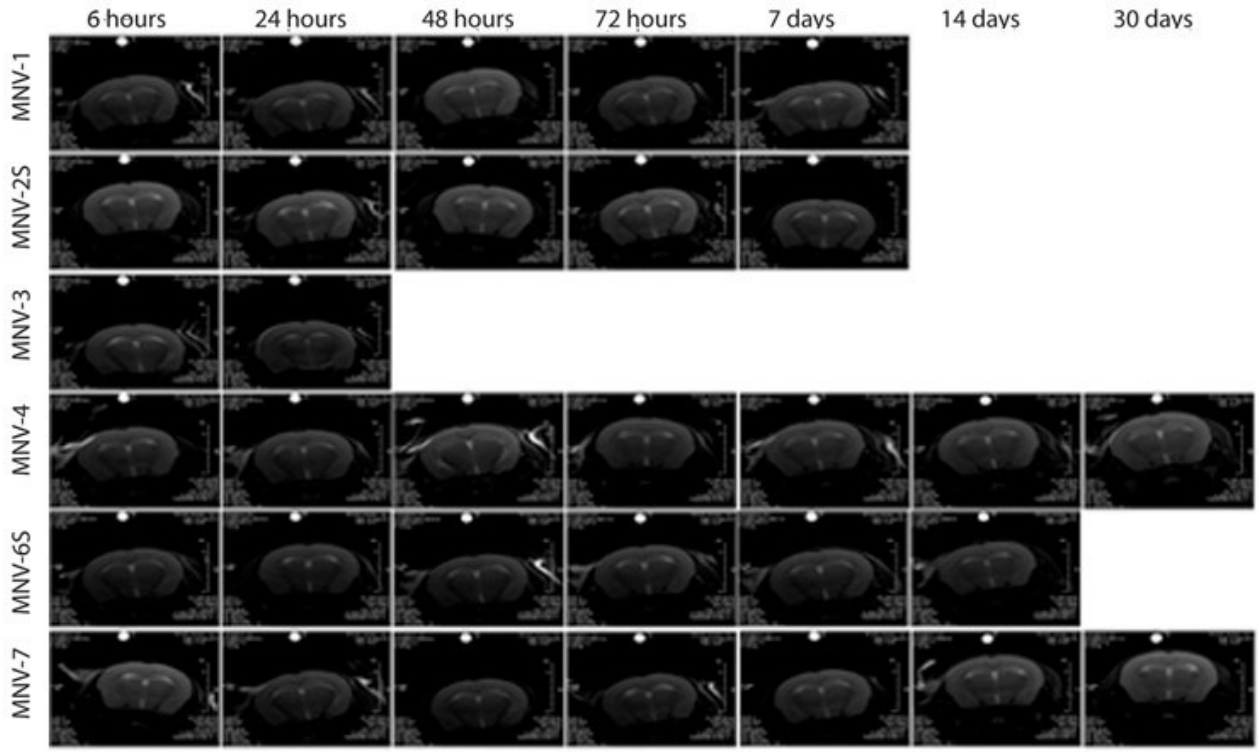

Figure 7. Representative $MnCl_2$-enhanced T2-Weighted MRI: Imaging Edema and Hemorrhagic Infarct. Animals (NP = MNV-1, 4, 7; Sham MNV-2S, 6S). Imaging Sequence, T2-weighted RARE (rapid acquisition with rapid enhancement) two-dimensional sequence with the following parameters: Matrix: 256, TR: 4200 msec, TE: 12 msec, number of averages: 1, Rare factor: 8, FOV: 3.0 x 3.0 cm, number of slices: 12, slice thickness: 1 mm, and without respiratory gating to account for breathing movement.

Task 1.4. In Vivo Bioluminescence Imaging of Activated Astrocytes using GFAP-Luciferase Reporter Mice.

Twelve GFAP-luciferase reporter mice were imaged via the IVIS Spectrum camera at assigned time points (1, 3, 7, 14, 21, and 30 days) post-blast exposure (Figure 8-10). The bioluminescent images were collected, standardized, normalized, and quantified. To ensure standardization and normalization of the luciferase bioluminescence, region of interests (ROI) were defined for both ventral (left) and dorsal (right) images. The exposed skin of these transgenic GFAP reporter animals produced some natural low-level bioluminescence, and so the defined ROI included the head and excluded the ears and nose, removing significant artifactual bioluminescence. This ROI also removed radiance created from other exposed regions (e.g. foot pads, tail) and from the Luciferin intraperitoneal injection itself (contrast visible on the abdomen of animal). For images of the ventral side of the animal, a region of interest (ROI) of 80 pixels by 80 pixels, at an angle of 45 to form a diamond shape was used. For images of the dorsal side of the animal, a region of interest (ROI) of 65 pixels by 65 pixels, at an angle of 45 to form a diamond shape was used.

Overall, the luciferase bioluminescence suggests an astrocytic response is highest in NP animals at the 24hr time point and falls off rapidly by day 3 and continues to decline until reaching sham

levels between days 7 and 14. IVIS image series of quantitative bioluminescence (radiance flux –photons/second) emitted from the dorsal side of GFAP-Luc animals at specific time points (1, 3, 7, 14, 21, and 30 days). Most artifactual regions of bioluminescence from transgenic animals (auto-bioluminescence in ears, foot-pads, tail) are removed, along with those from the Luciferin intraperitoneal injection (abdominal region). Autobioluminescence in these transgenic animals from the nose is not removed. Bioluminescence levels suggests that astrocytic response is highest at the 24hr time point, falls off rapidly at days 3 and 7, and is comparable to sham bioluminescence levels at day 14 and after (Figure 10).

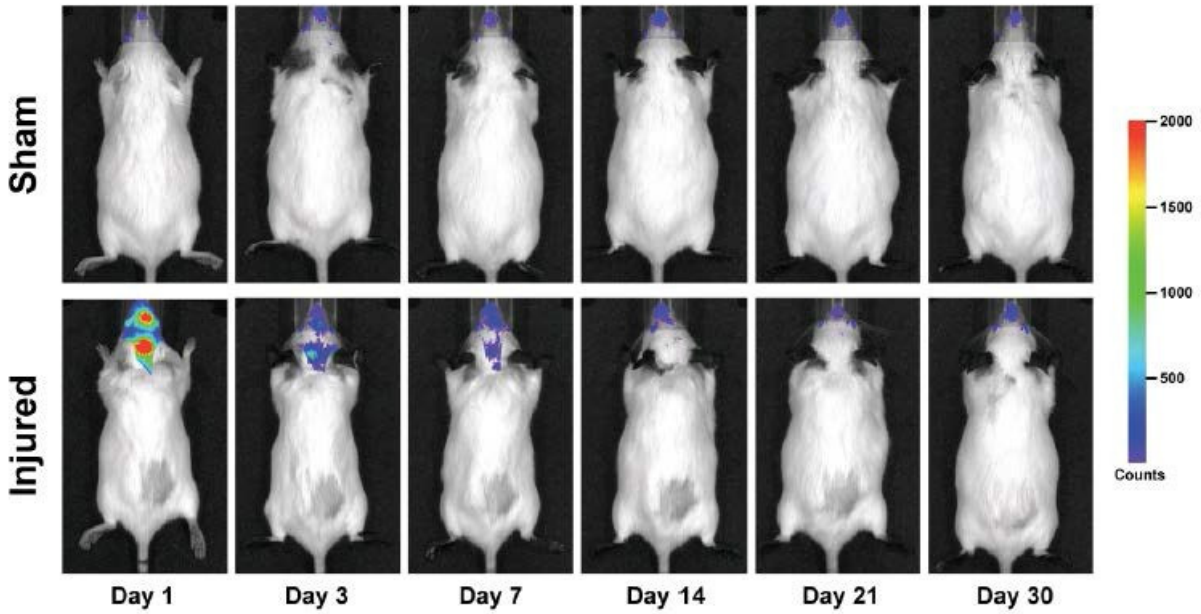

Figure 8. IVIS Imaging of luciferase bioluminescence in GFAP-luc transgenic mice – dorsal view. Sham and blast-exposed animal imaged (1, 3, 7, 14, 21, 30 days)

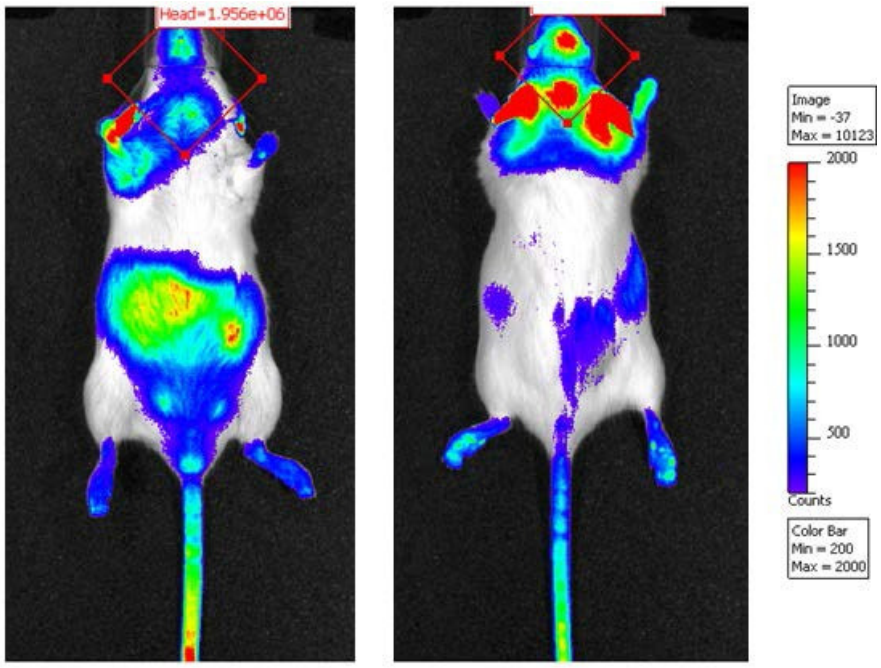

Figure 9. IVIS Imaging of Luciferase Bioluminescence – Region of interest definition ventral (left) and dorsal

(right) images demonstrating the consistent definition of region of interest (ROI) summating the luciferase bioluminescence. Ventral and dorsal images were taken from injured animal at day 1 (open-field emission filter, 5 minutes).

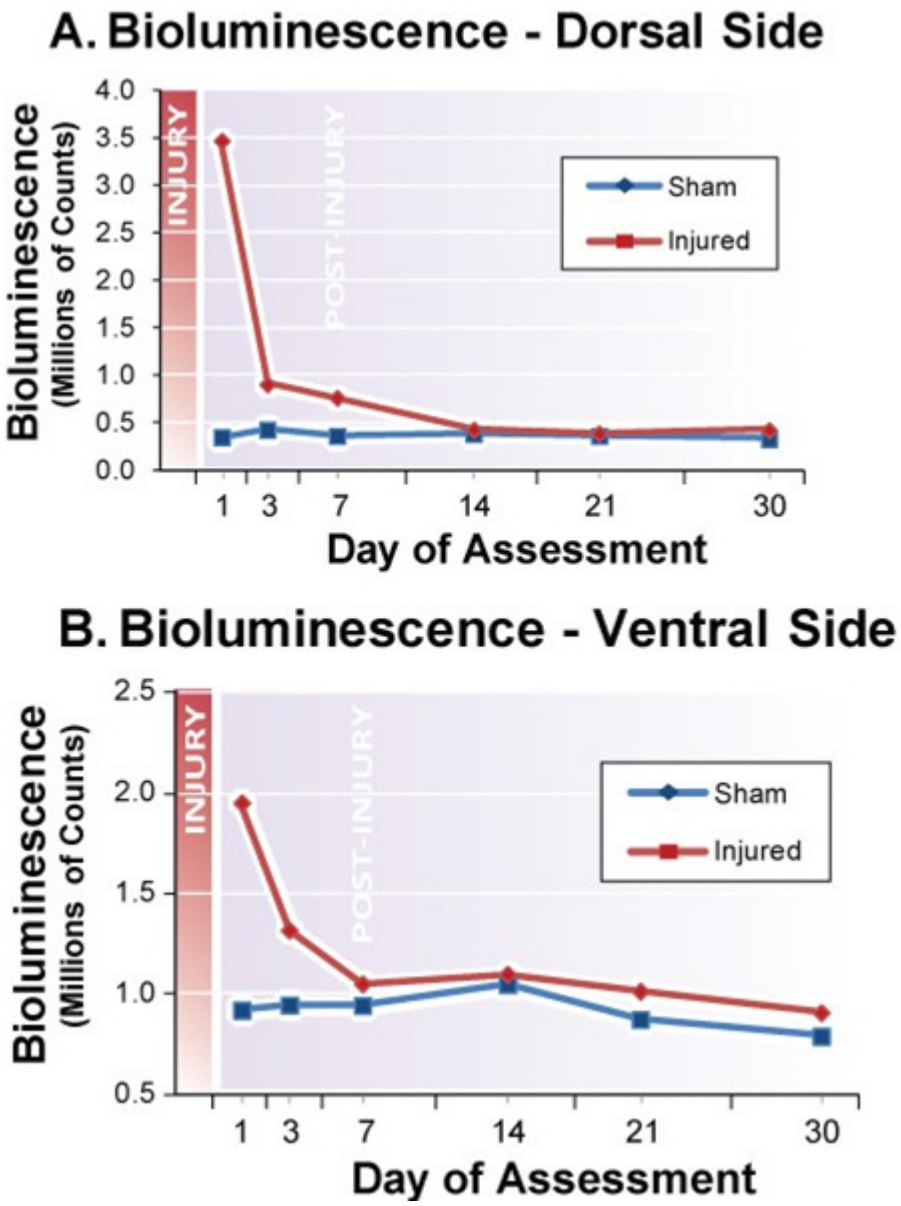

Figure 10. Quantitative luciferase bioluminescence captured in the ROI for dorsal (A) and ventral (B) images (total photon count summated at each pixel over 5 minute bioluminescence imaging period with no emission filter) of GFAP-Luc animals at specific time points (1, 3, 7, 14, 21, 30, days; Sham n=1, NP n=1).

<u>Aim 2 (24 months – April 1, 2011 to March 31, 2013)</u> Validation of imaging results by methods of neuropathology and molecular biology, and characterization of neurogenic inflammation due to blast.

Tasks 2.1. Neuropathology

Two preliminary surveys, hemotoxylin and eosin (H&E) and Fluorojade staining, were performed to assess neurodegeneration in the brains of mice post mild/moderate blast. Rare events were detected in a variety of brain regions at 7 and 14 days post blast. H&E showed a slight increase (~4x) in eosinophilic degenerating neurons in the anterior portion of the brain (including cingulate cortex, caudate putamen, and preoptic area of the hypothalamus). A slight increase in Fluorojade-C staining was observed in the fimbria and cingulum.

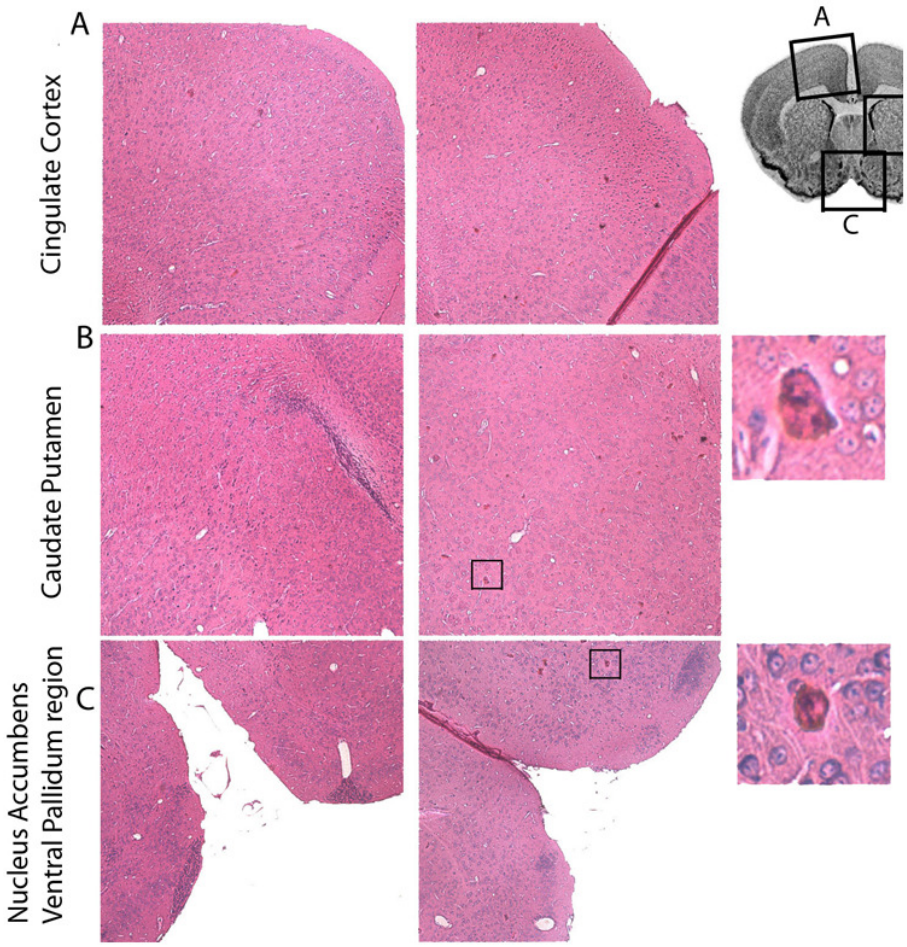

Figure 11. H&E Staining showing injury-induced degeneration in the brain: A) Cingulate cortex, B) Caudate putamen, and C) Nucleus accumbens and ventral pallidum region. Cartoon on right showing the locations of the regions sampled. Small black boxes indicate the location of the zoomed in images shown on the far right.

Hematoxylin and Eosin Staining (H&E)

Four mice (two shams and two 7 day post mild/moderate blast) were stained with H&E to evaluate the presence of degenerating neurons. We observed a 4-5x increase in eosinophilic degenerating

neurons in the anterior portion of the brain (including cingulate cortex, caudate putamen, and the preoptic area of the hypothalamus (Figure 11).

Fluorojade-C

Three mice (one sham and two 14 day-post moderate blast) were stained with Fluorojade-C to look for degenerating neurons (Figure 12). We observed an increase in Fluorojade-C signal in the cingulum and fimbria.

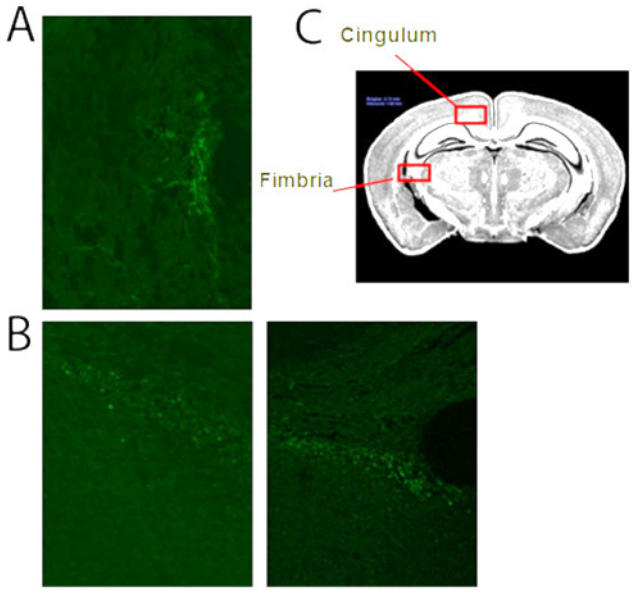

Figure 12. Fluorojade C staining signifying dying neurons in the brain: A) Cingulum, B) Fimbria, and C) Cartoon showing the locations of the regions sampled. Fibers of dying neurons are visualized in A (green). Cell bodies and fibers of dying neurons are visualized in B.

Task 2.2. Characterization of Neurogenic Inflammation using Immunohistochemistry

A number of immunohistochemical assessments were performed to evaluate the expression of signature brain trauma markers (GFAP), the various activation states of microglia (Iba1, CD86), and demyelination within the optic track (Luxol Fast Blue) in experimental groups that included sham (Sham), non-protected blast-exposed (NP), and torso-protected blast-exposed (TP) animals.

Preliminary Cortical, Subcortical, and Brainstem Immunocytochemistry

Preliminary immunohistochemical assessments were performed in the cortical, subcortical, and brain stem regions in NP and Sham animals to inform subsequent histological analyses that expanded on the number of regions and variety of assessments.

Glial Fibrillary Acidic Protein (GFAP)

Immunostaining analysis for glial fibrillary acidic protein (GFAP), a marker of astrocyte

activation and inflammation in the brain, was performed over a variety of time points after blast. Following blast exposure, an increased GFAP immunosignal can be observed in the brainstem, with a peak of activation at 7 days after blast when comparing 7, 14, and 30-day post injury animals (Figure 13). This activation diminished over time and plateaued at a level slightly higher than in uninjured animals.

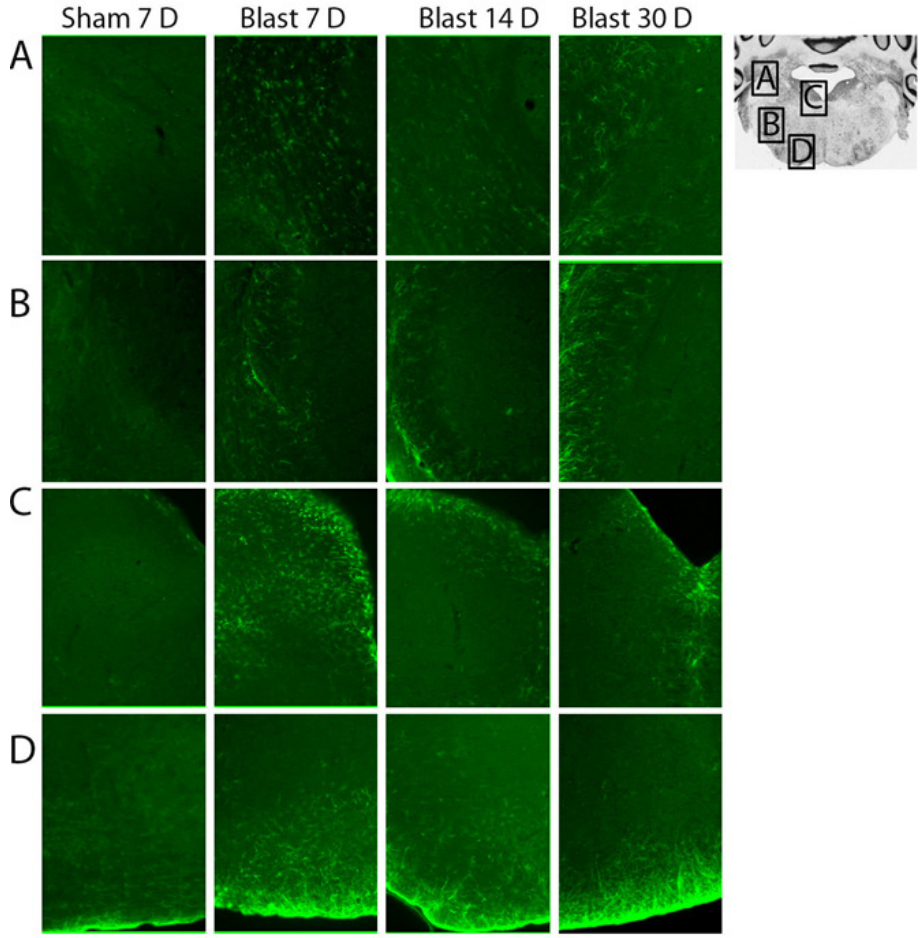

Figure 13. Injury-induced inflammation as demonstrated by activation of astrocytes with corresponding upregulation of glial fibrillary acidic protein (GFAP) in the brainstem of mice. The cartoon to the right shows the location of the sections in the brain: A) lateral lemniscus, B) trigeminal nuclei, C) dorsal raphe nucleus, and D) periolivary nuclei. Note the increased levels of GFAP immunosignal at each time point after blast. The highest levels of GFAP immunosignal are present at 7 days after blast and gradually diminish over time.

Ionized Calcium-Binding Adapter Molecule 1 (Iba1)

Immunostaining for Iba1, a marker of microglia activation and inflammation in the brain, over a variety of time points after blast were performed. Following blast exposure, preliminary analysis shows an increased Iba1 immunosignal in the hippocampus at 6hr. and 14 days post-blast (Figure 14).

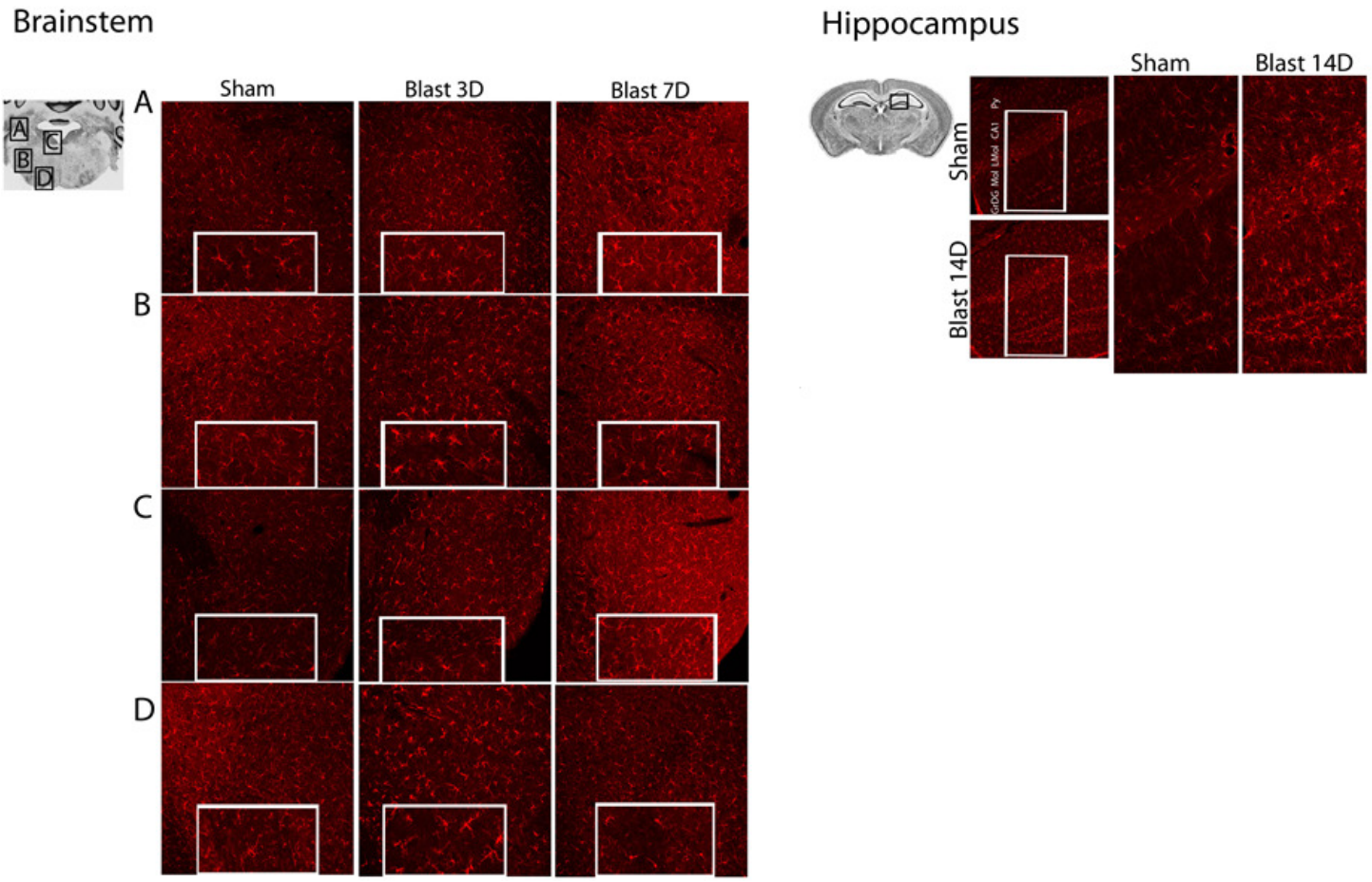

Figure 14. Injury-induced inflammation as demonstrated by activation of microglia with corresponding upregulation of Iba1 in the brainstem and hippocampus of mice. The cartoons to the left show the location of the sections in the brain. GrDG, Granule layer of the dentate gyrus. Mol, Molecular layer of the hippocampus. LMol, Lacunosum Moleculare. CA1, CA1 region of the hippocampus. Py, Pyramidal layer. Note the cellular hypertrophy observed at each time point after blast.

Markers for Microglial and Astrocytic Activation (IBA-1, CD68, GFAP)

In order to validate categorization of activated microglial cells based on morphological appearance, hemotoxylin counterstaining was done on CD68 or IBA-1 immunohistochemistry (IHC) stained sections. Microscopy showed that most large bushy IBA-1 (+) microglia are actually made composed of 2-5 small de-ramified IBA-1 (+) microglia (Figure 15). Many other stained regions are single cells. Microscopy with CD 68 staining produced the same scenario (i.e., 2-5 CD 68(+) microglia cluster appearing to be one large cell).

Therefore, two counting paradigms were employed for evaluating clusters of activated microglia in various regions of the brain. Originally, large areas of stain (either single cells or cluster of cells) were counted as one single cell because of difficulty with visually differentiating single cells from cluster of cells without counterstaining for cell nucleus. From sub-population sampling of these clusters with counter-stain, it was determined that the numbers of cells range from 2-5. Thus, to adjust for this quantification issue in the data analysis (both CD 68 and IBA-1 staining), a second

set of data with a 3x multiplicative correction factor was produced for these clusters. Statistical re-analysis did not show any changes in statistical significance (histograms) for comparisons across experimental groups, and new significance was not generated. In the histograms, numbers before and after correction are included together to show changes. The columns with colors are generated with the numbers after correction.

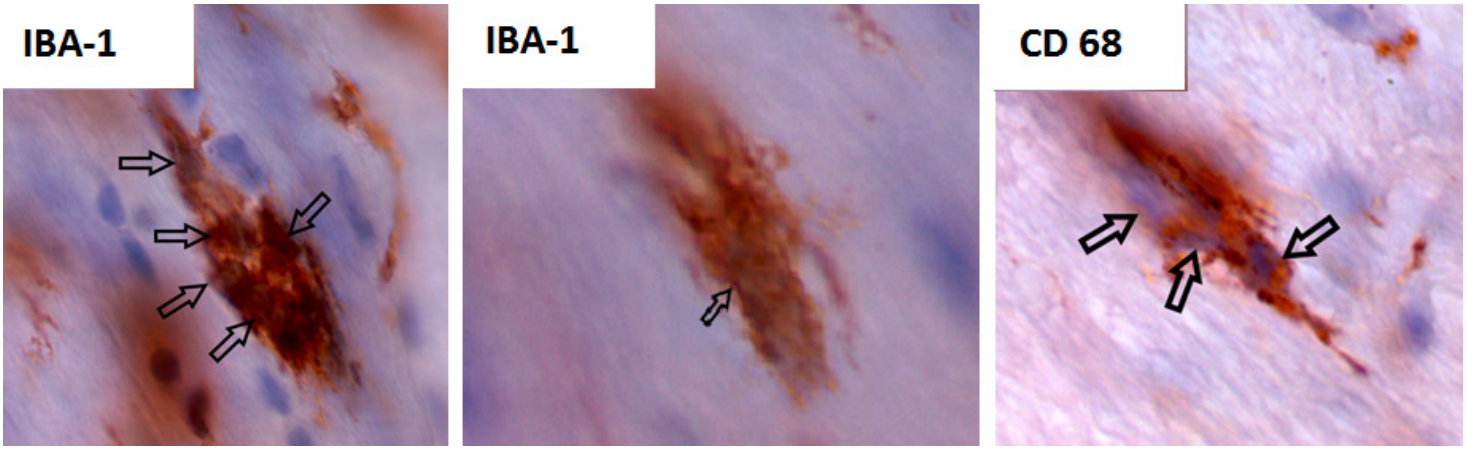

Figure 15. Depiction with IBA-1 and CD 68 staining of microglial clusters, which can contain multiple cells, compared to single cell.

Fifty three mice (NP; n=28, Sham; n=22, TP; n=3) were euthanized at various time points (1, 3, 7, 14, and 30 days after exposure to blast), brains sectioned (40 µm) (Figure 16), and stored in a cryoprotectant solution in -20° C for further processing. Microglia and astrocytes were labeled with an immunoperoxidase-DAB method using CD68 and IBA-1 antibodies for microglial labeling and GFAP for astrocyte labeling. Every 24th section starting from rostral end of the cortex to the caudal edge of the cerebellum was selected and processed as described (Sheng, Bora et al., 2003).

The presence of microglial profiles including hypertrophied and bushy microglia (Figure 17) were counted in histological sections of the optic tract. Figure 16 demonstrates the counting methodology in the visual system: optic tract is depicted in red and starting and ending planes of counting are in orange. Cerebellum was not included in stereological counting because of a common focal pattern of injury in this area. In these counts, resting microglial cells present as ramified IBA-1(+) structures, whereas activated microglial cells present with enlarged cell bodies (hypertrophied) or numerous processes (bushy). The optical fractionator probe was applied with the aid of a motorized-stage Axioplan microscope (Zeiss, www.zeiss.de) equipped with the Stereo Investigator V hardware and software (MicroBrightField [http://www. mbfbioscience.com/]).

Contours of optic tract were outlined at 5x by a blinded investigator, and cells were counted using a 40x objective. A 125x125 µm counting frame was used with a 125 µm x125 µm grid in the outlined area. Counting depth (optical dissector height) was 8–13 µm depending on average section

thickness. A guard volume of 1.0 µm was used to avoid sectioning artifacts such as lost caps and uneven section surfaces.

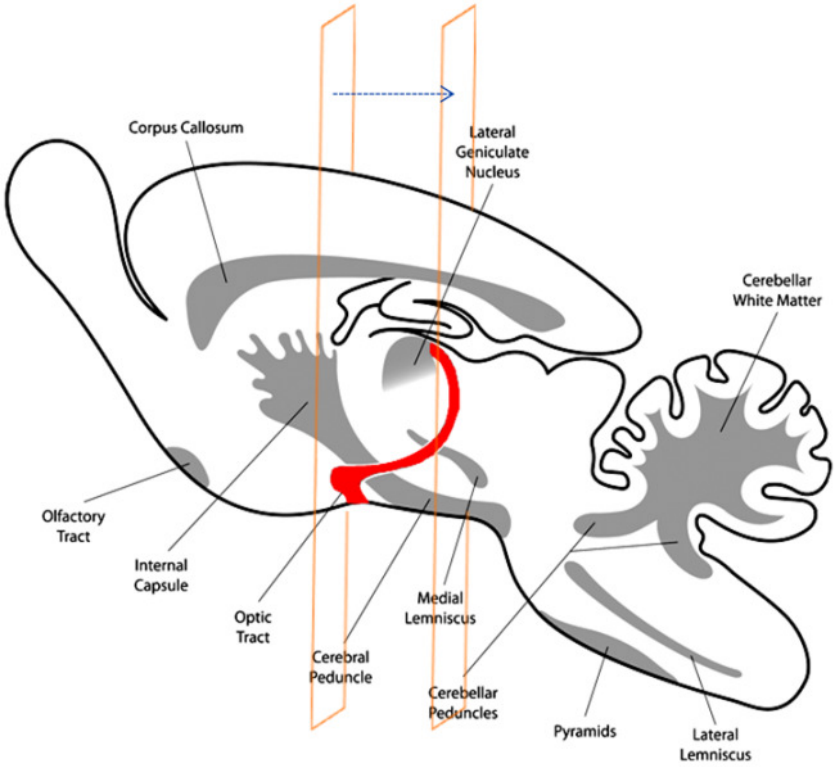

Figure 16. Schematic showing the region of the optic tract assessed by histology with various glial markers.

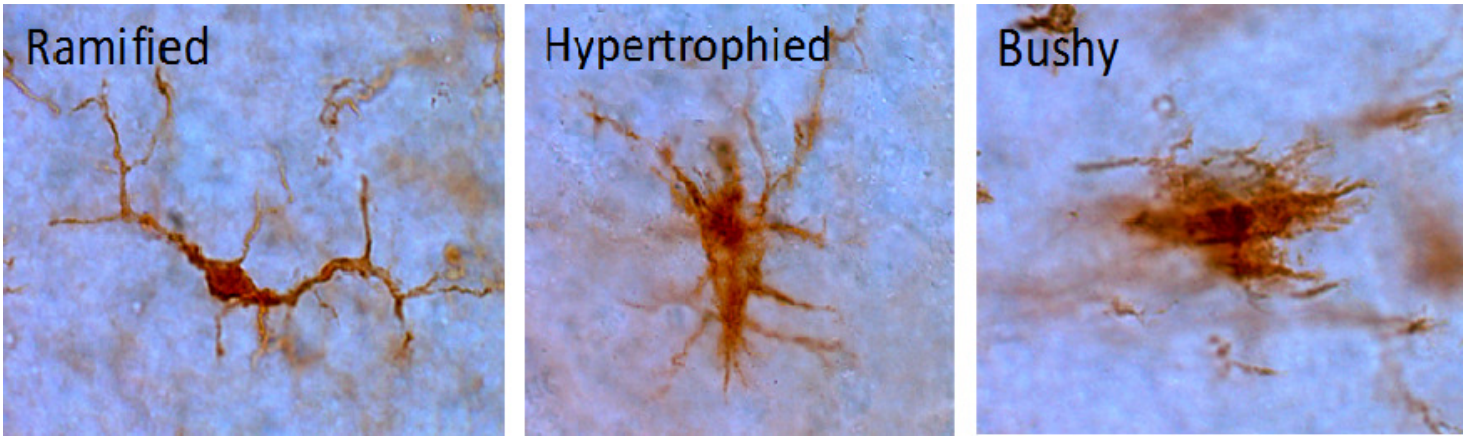

Figure 17. Microglial morphology for multiple states of microglial activation, including ramified, hypertrophied, and bushy.

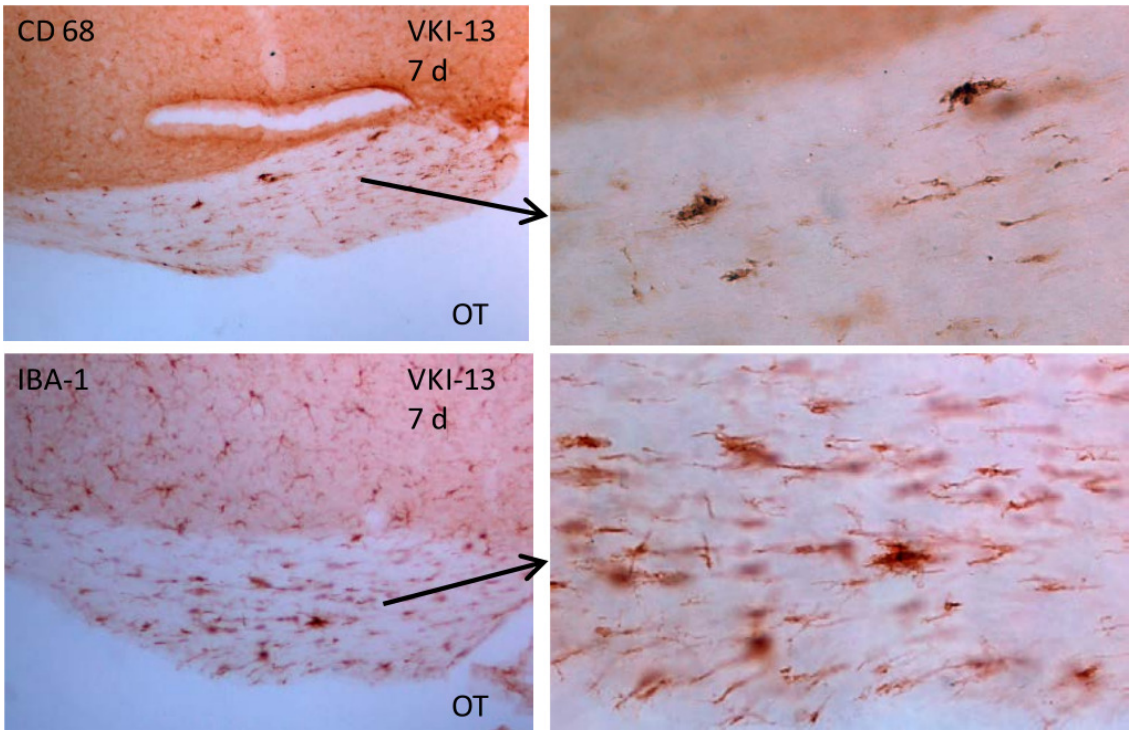

Figure 18. Subject euthanized 7d after mild-moderate blast injury (VKI-13), microglia/macrophages are activated in the optic tract, as evidenced by CD 68 (left upper panel) and IBA-1 (left lower panel) immunoreactivity on adjacent sections. Right panels are magnified to depict cellular detail.

Table 1. Density of Activated Microglia/Macrophages in Various Brain Areas Based on CD68 and IBA-1 Immunoreactivity

		Frnx		Optic		LL		Hipp		Crbl folia		SuC		LG	
number	Time	CD68	IBA-1	CD68	IBA-1	CD68	IBA-1	CD68	IBA-1	CD68	IBA-1	CD68	IBA-1	CD68	IBA-1
VKI-24	24 hr	+	+					+							
VKI-19	24 hr							±	?						
VKI-9	72 hr			+	?	+						+++	+++	+++	?
VKI-20	72 hr														
VKI-19 (2)	7 day							+	±						
VKI-13	7 day			++	++					++	?				
VKI-28	30 day			+	+					+	+		±		
VKI-26	30 day			+	+					+	±				
VKI-22	30 day			+	+					±					

Abbreviations: Frnx, fornix; Optic, optic tract; LL, lateral lemniscus; Crbl folia, cerebellar folia; Hipp, hippocampus; SC, superior colliculus; LG, lateral geniculate neucleus Note: Highlighted subject is the subject with contusion.

Immunocytochemistry with CD68 and IBA-1 antibodies demonstrates that mild-moderate blast injury causes microglial activation in various gray and white matter regions at each time point after blast. However, location of microglial activation varies among cases and time points. Densities of CD68 (+) and IBA- 1 (+) microglia were estimated at these locations. CD68 and IBA-1(+) immunoreactivity in activated microglia overlapped substantially, a pattern confirming the

presence of focal neuroinflammation in these areas (Table 1, Figure 18). The visual system (optic tract, superior colliculus) and cerebellar folia were the regions that were most frequently involved, a pattern suggesting that mild- moderate blast injury in mice has a propensity to affect the visual system and cerebellum (Table 1). Except in the case of the optic tract in some subjects, GFAP immunocytochemistry did not demonstrate substantial astrocytic activation in injured mice (Figure 19). A contusion in the frontal cortex was present in two cases (VK1-9 and L3). The contusion area was strongly positive for all three markers used (CD68, IBA- 1 and GFAP) (Figure 20).

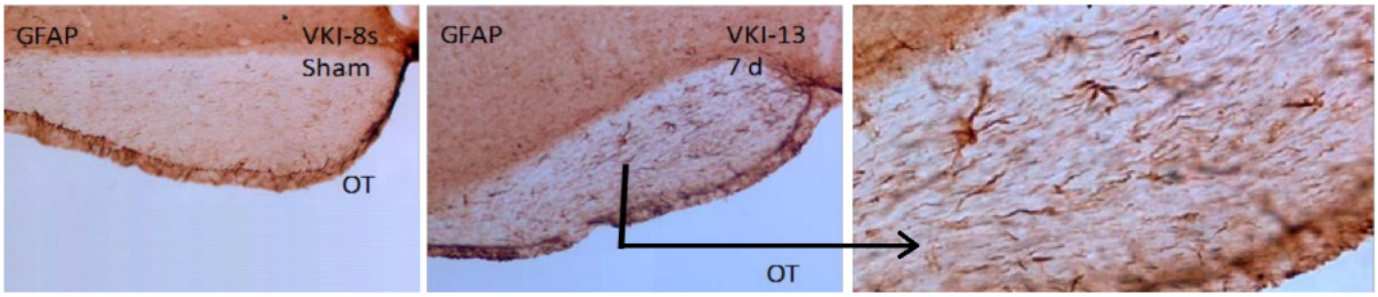

Figure 19. In this case 7d after mild-moderate blast injury (VKI- 13), there was astrocytic activation in the optic tract based on GFAP immunoreactivity (compare experimental subject in middle panel with sham control [VKI-8s] on top). Bottom panel is an enlargement of indicated region in middle panel to show cytological detail.

These findings suggest that mild-moderate blast exposure can cause focal neuroinflammation. However, the temporal and spatial dynamics of neuroinflammation are unclear because of the variance in density and location of activated microglia at various time points after blast injury. In addition, the role and type of microglia/macrophages in this type of neuroinflammation needs to be ascertained.

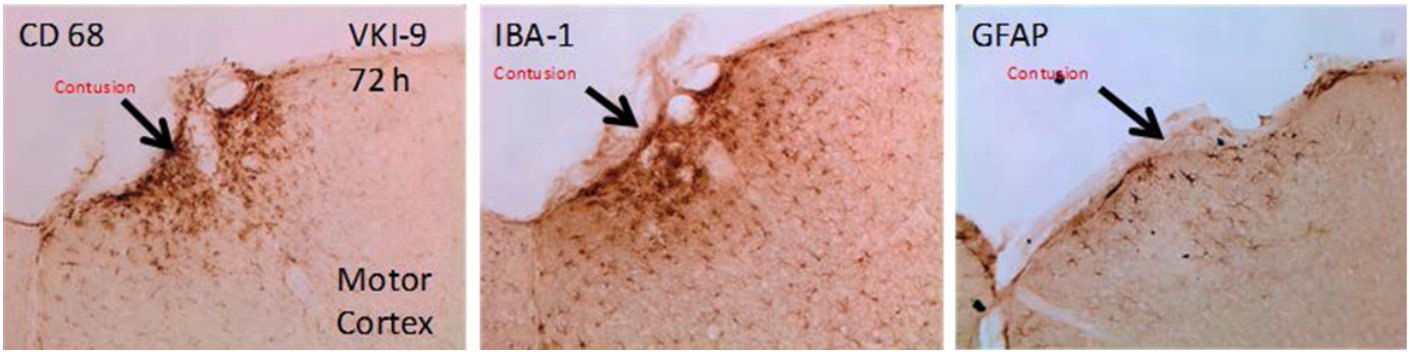

Figure 20. In this case of a subject sacrificed 72hr after mild/moderate blast injury (VKI-9), microglia is activated in the contusion area of motor cortex (arrow). Right panel depicts intensely GFAP-immunoreactive astrocytes in the same area.

IBA-1 (+) profiles showed activation in the lower corpus callosum and immediately adjacent to sub-callosal regions (Figure 21, Table 2).

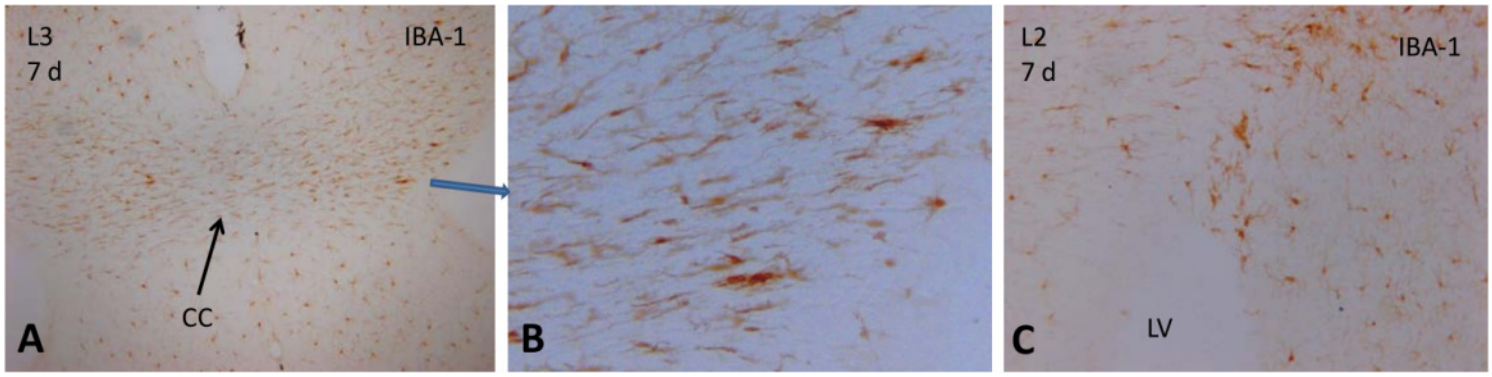

Figure 21. Microglia/macrophages are activated in the corpus callosum area (A and B) and corpus callosal sub-region (C) after mild-moderate blast injury (L2 and L3), evidenced by IBA-1-immunoreactivity.

Immunocytochemistry with IBA-1 antibody demonstrates that mild/moderate blast injury at 2 weeks causes microglial activation in the gray and white matter in patterns resembling other time points mentioned above (Figure 22). Densities of activated microglia (hypertrophic or bushy IBA1(+) morphologies) were estimated at several locations. The visual system (optic tract, superior colliculus) and cerebellar folia were the region's most frequently involved, a pattern suggesting that mild/moderate blast injury in mice has a propensity to primarily affect the visual system and cerebellum (Table 2).

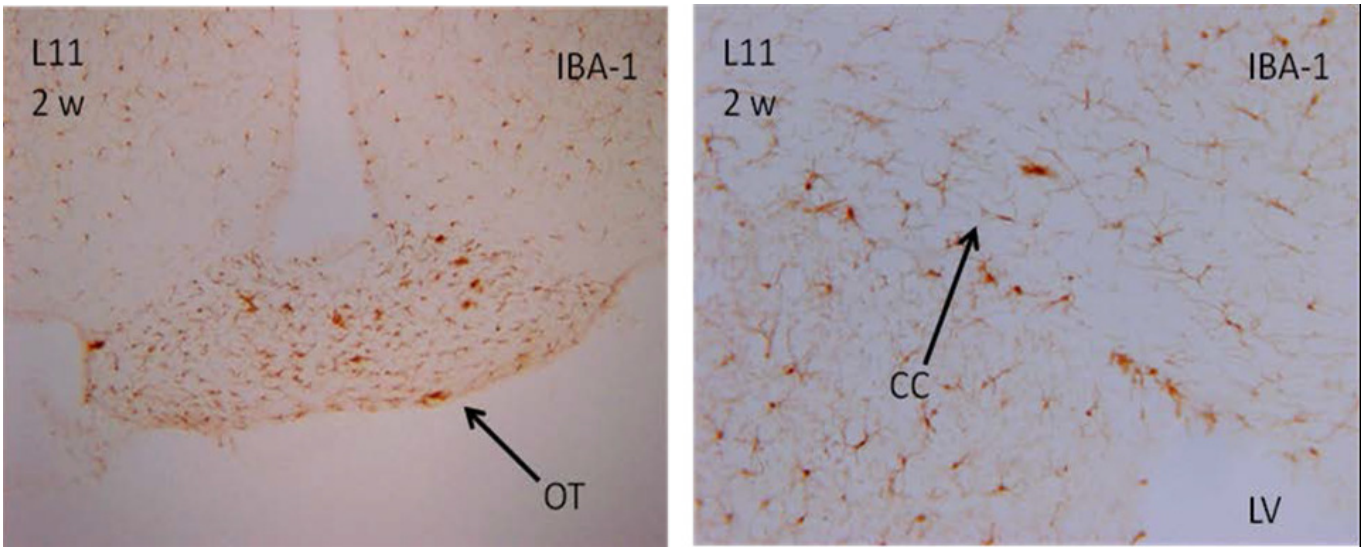

Figure 22. In this case of a subject euthanized 2 weeks after mild-moderate blast injury (L11), microglia/macrophages are activated in the optic tract (chiasm) and corpus callosum, as evidenced by IBA-1 immunoreactivity.

Activated IBA-1(+) microglial profiles in the optic tract were quantified with stereology. Results show that neuroinflammation in the optic tract gradually increased from 24hr to 2 weeks and then decreased at 30d after mild-moderate blast injury. These findings suggest that mild-moderate blast exposure causes focal neuroinflammation in the visual system and cerebellum. Significant differences between injury and sham-injured groups at the 7d and 2 week times points for total

IBA-1 (Figure 23) and activated IBA-1 (Figure 24) and at the 3d and 7d time points for CD68 (Figure 25) were identified, a pattern indicating recruitment or proliferation of microglia prior to or around these time points.

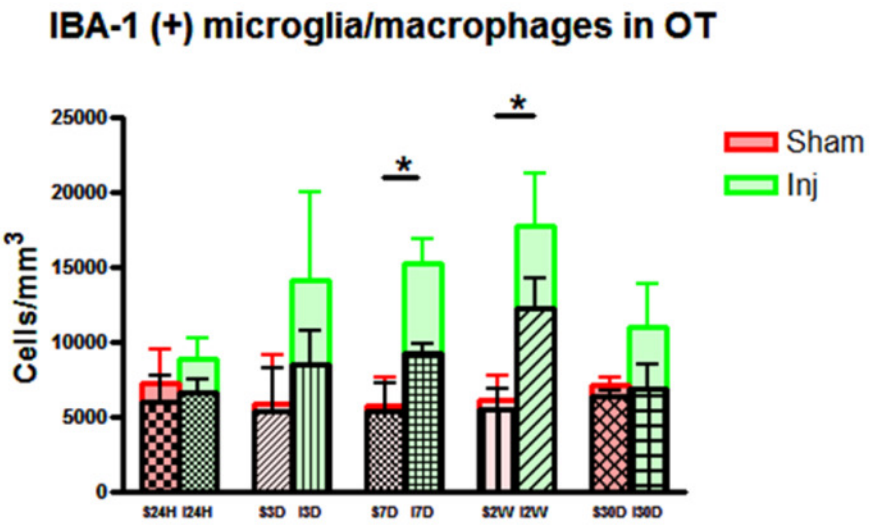

Figure 23. Temporal profile of IBA-1 stained *total* microglia/macrophages in the olfactory tract (1d, 3d, 7d, 2w, 1m) for NP and Sham conditions. The colored bars show the cell counts with the multiplication factor applied to found clusters, and black patterned bars show cells counts with each cluster equaling one cell. One asterisk $p < 0.05$. Two asterisks $p < 0.01$.

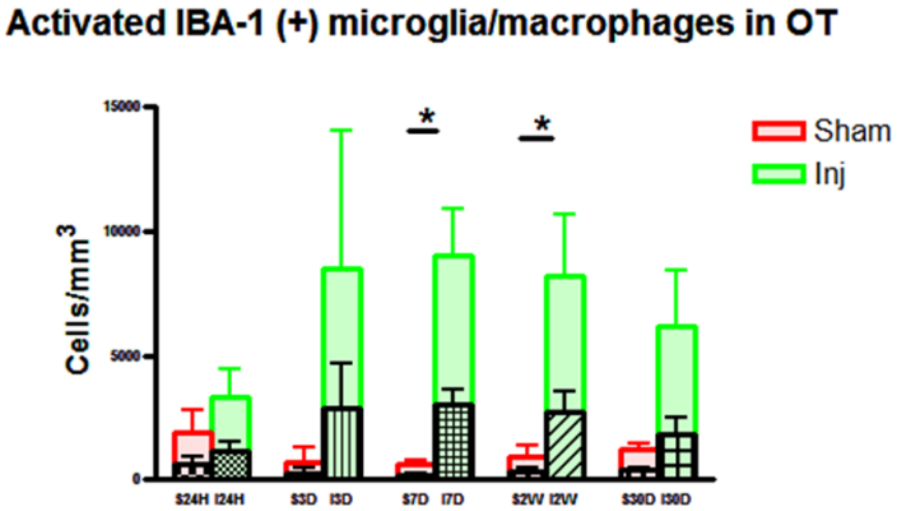

Figure 24. Temporal profile of IBA-1 stained *activated* microglia/macrophages in the olfactory tract (1d, 3d, 7d, 2w, 1m) for NP and Sham conditions. The colored bars show the cell counts with the multiplication factor applied to found clusters, and black patterned bars show cells counts with each cluster equaling one cell. One asterisk $p < 0.05$. Two asterisks $p < 0.01$.

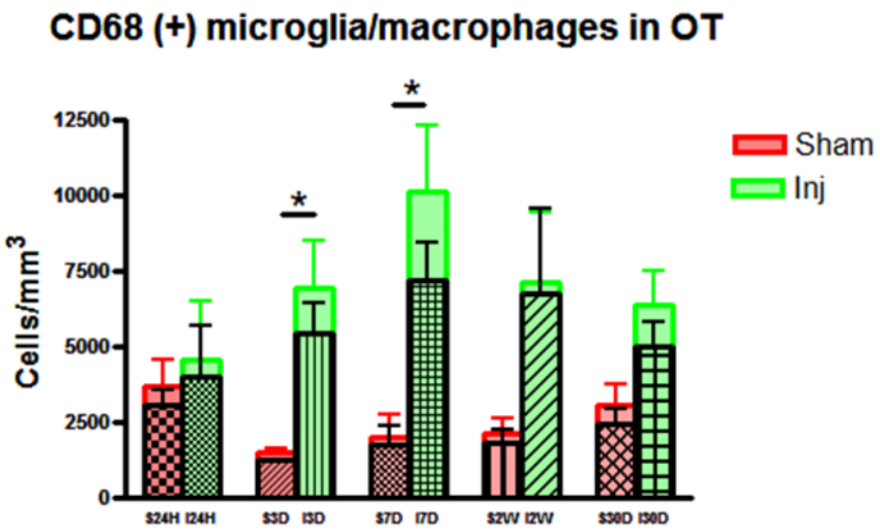

Figure 25. Temporal profile of CD68 stained *activated* microglia/macrophages in the olfactory tract (1d, 3d, 7d, 2w, 1m) for NP and Sham conditions. The colored bars show the cell counts with the multiplication factor applied to found clusters, and black patterned bars show cells counts with each cluster equaling one cell. One asterisk $p < 0.05$. Two asterisks $p < 0.01$.

To explore if torso protection with an armor-like shield can eliminate or alleviate neuroinflammation, brain sections were processed for IHC with IBA-1 and CD68 antibodies and stereological counting was then performed. Significant differences were found between NP, TP, and Sham at the 7-day times point for total IBA-1 (Figure 26) and activated IBA-1 (Figure 27), and at the 7-day time point for CD68 (Figure 28).

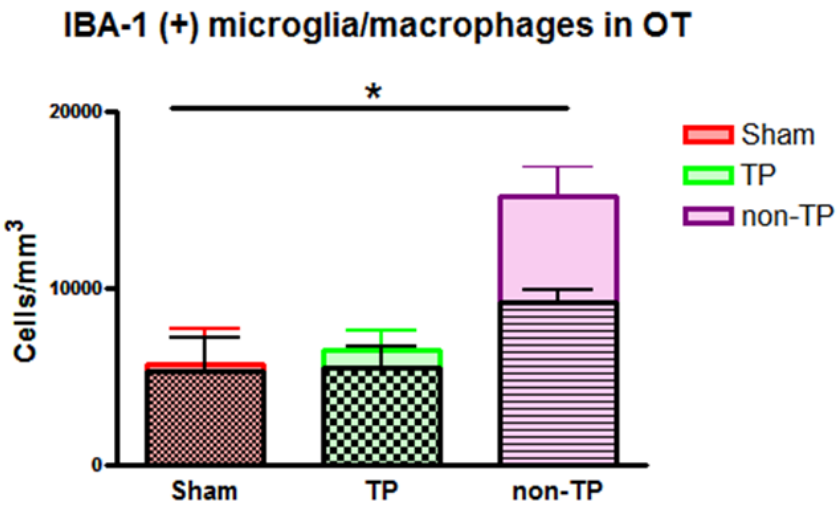

Figure 26. Temporal profile of IBA-1 stained *total* microglia/macrophages in the olfactory tract (7d) for NP (non-TP), TP, and Sham conditions. The colored bars show the cell counts with the multiplication factor applied to found clusters, and black patterned bars show cells counts with each cluster equaling one cell. One asterisk $p < 0.05$. Two asterisks $p < 0.01$.

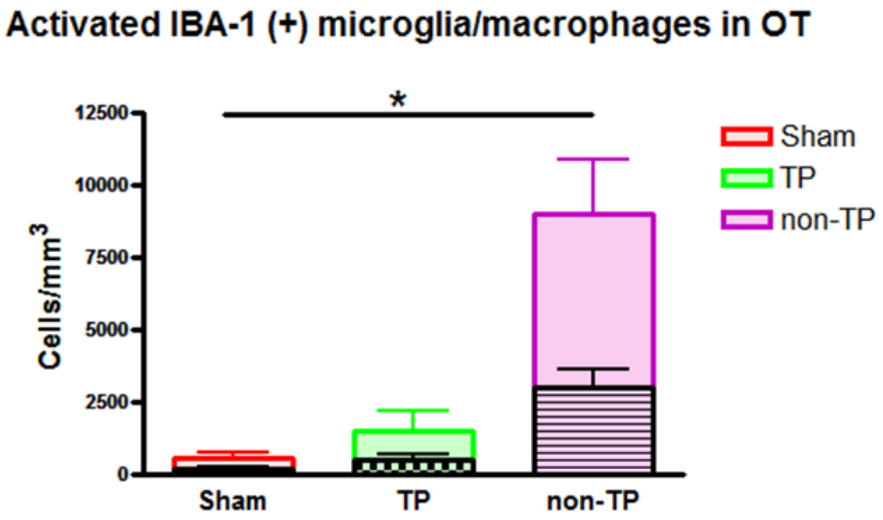

Figure 27. Temporal profile of IBA-1 stained *activated* microglia/macrophages in the olfactory tract (7d) for NP (non-TP), TP, and Sham conditions. The colored bars show the cell counts with the multiplication factor applied to found clusters, and black patterned bars show cells counts with each cluster equaling one cell. One asterisk $p < 0.05$. Two asterisks $p < 0.01$.

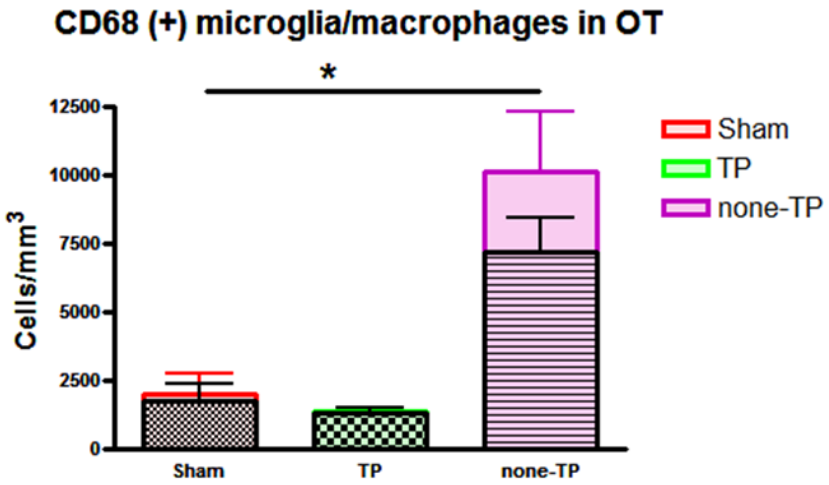

Figure 28. Temporal profile of CD68 stained *activated* microglia/macrophages in the olfactory tract (7d) for NP (none-TP), TP, and Sham conditions. The colored bars show the cell counts with the multiplication factor applied to found clusters, and black patterned bars show cells counts with each cluster equaling one cell. One asterisk $p < 0.05$. Two asterisks $p < 0.01$.

Numbers of IBA-1 (+) and CD68 (+) activated microglia in the optic tract of torso-protected animals are significantly lower compared with unprotected animals. There is no significant difference between sham-injured and torso-protected animals. Torso protection appears to have effectively prevented axonal degeneration in the optic tract, and stereological counts show that in the optic tract, torso -protected animals do not have significant neuroinflammation, which is consistent with the absence of axonal injury in this area.

Neurotoxic Microglial Presence (Kv1.3)

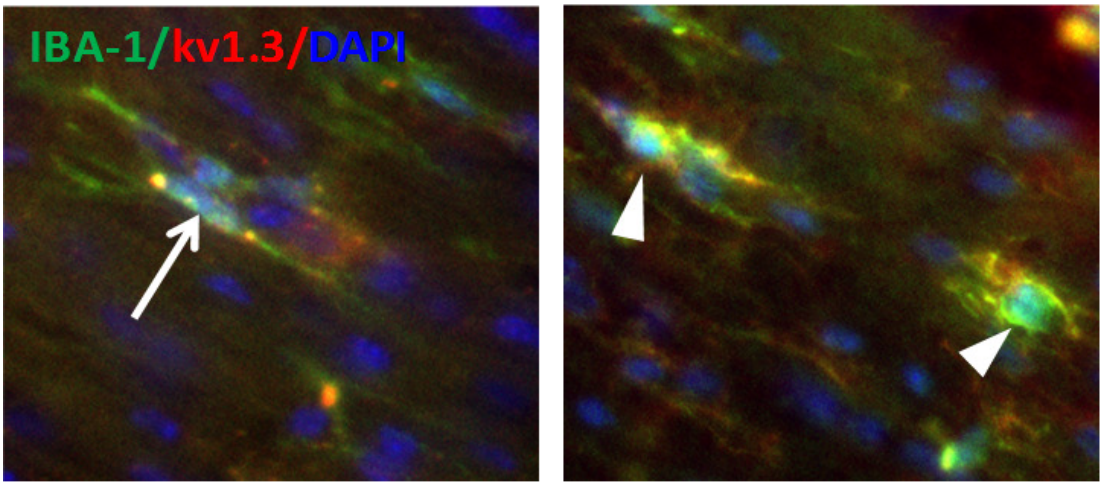

Figure 29. Dual immuno-staining of microglia with IBA-1 (green) and Kv1.3 (red) in blast –injured mouse brain sections. Small ramified (arrow, upper panel) and bushy (arrow heads, lower panel) microglia are positively labeled with IBA-1 and Kv1.3.

Expression of voltage-gated potassium channel 1.3 (Kv1.3) was identified in activated microglia (Figure 29). When small ramified microglia express high levels of Kv1.3, these microglial cells have neurotoxic properties (Yamada et al., 2013). Using Kv1.3 to label activated microglia, we saw only sporadic cases of Kv1.3 (+) microglia in the optic tract and stereological counts in optic tract did not show significant differences between injury and sham-injured groups at 2 weeks and 30 days post-injury. These findings suggest that mild blast injury causes neuroinflammation in the visual circuitry in the brain. Although one-way ANOVA did not show significant difference at any time point in the 30-day period after injury because of a large standard deviation, when compared with sham-injured group, neuroinflammation was increased significantly from 3 days to 2 weeks and then returned to normal level at 30 days. At least based on Kv1.3 IHC, conversion to a neurotoxic state of activated microglia was not evident at 14 and 30 days after injury.

Luxol Fast Blue Staining for Demyelination in the Optic Track

To explore if demyelination events occurred following exposure to blast, Luxol fast blue staining was performed at 2 weeks and 30 days after blast injury. These staining results did not show evidence of patchy demyelination in the optic tract or other areas (Figure 30).

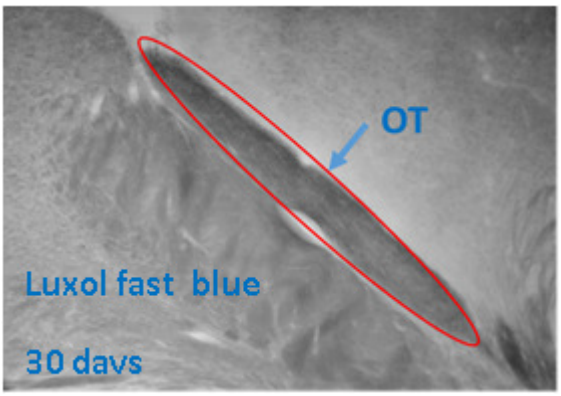

Figure 30. Luxol fast blue staining (grey mode). Area delineated with red circle is optic tract.

Table 2. Density of Activated Microglia/Macrophages in Various Brain Areas based on IBA-1 Immunoreactivity

		Frnx	OT	CC	Hipp	Crbl	SuC	LG	SN	PY
L2	7 d		++	+	±	+	±		+	
L3	7 d		++	++		+	++	+		
L4	7 d		++	++	+		+	++		
L5	2 w		+						+	
L7	2 w	±	+			+				+
L9	2 w			±		+				+
L11	2 w		+++	+			±	+		
LXU2-1	30 d					±				

Abbreviations: Frnx, fornix; Optic, optic tract; LL, lateral lemniscus; Crbl folia, cerebellar folia; Hipp, hippocampus; SuC, supper colliculus; LG, lateral geniculate body; SN, septal nucleus; PY, pyramidal tract
Note: Highlighted subject is the subject with contusion.

Task 2.3 Characterization of Neurogenic Inflammation using Western Immunoblots.

This task was not attempted. Western immunoblot characterization was replaced with additional enzyme immunoassay characterization.

Task 2.4 Characterization of Neurogenic Inflammation using Real-Time PCR

Results of this task have been published (see Figure 9-11 in Cernak, Merkle et al., 2011).

Task 2.5 Measuring Cytokine and Chemokine Protein Expression using Immunoassays.

It is generally believed that primary blast shock waves can result in neuroinflammation in the brain. During the acute phase response, immune cells secrete pro-inflammatory cytokines (e.g., TNF-α, IL1-β, IFNγ, IL-6) which further recruit hematogenous immune cells. The response is

propagated by release of chemokines which further recruit more immune cells to the area. As a result of this massive immune infiltration, large amounts of cytotoxic cytokines are produced which prolong injury. In addition, there is a complex interaction between the gut and brain. After injury, systemic immune cells, chemicals (e.g., cytokines and chemokines), and vagus nerve stimulation can have an effect on the brain. Previous results from our laboratory showed that shielding of the torso (but not head protection) dramatically reduces inflammation in the gut and brain (Cernak 2010) and ameliorates axonal injury and behavioral deficits (Koliatsos, Cernak et al., 2011). These results suggest a robust influence of the gut immune and vagus nervous system on the brain following blast trauma to the torso.

Tissues from these mice have been assessed for: 1) BBB disruption, 2) calcium mobilization, 3) neutrophil infiltration (NE), 4) oligodendrogenesis (Tcf4), and, in general, 5) inflammation. For these assessments, we have compared expression of a variety of cytokines (TNF-α, IL1-β, IFNγ, IL-6, IL-10), chemokines (CXCL1/GRO-α, G-CSF, MCP-1), growth factors (VEGF), and structural and membrane proteins (GFAP, CXCR2, CaSR, MBP) in dissected brain tissue, blood (Figures 31-50), and spleen in blast- exposed animals with and without torso shielding. While statistically significant signals were found for MBP across multiple groups in the cerebellum and serum and for NE in the cerebellum, and apparent trends were evident for a number of structural/membrane proteins and chemokines, fewer differences in signal between injured groups and sham groups were detected in growth factors (VEGF-A) and many cytokines (TNF-α, IL1-β, and IL-10).

In the following sections we provide detailed analysis of the various signals as compared across experimental groups.

Chemokine Ligand 1 (CXCL1, previously known in literature as GRO-α)

Notably, in all samples tested we see a large difference in CXCL1 expression between torso protected animals and head protected or shams at the 30 day post trauma period (chronic period; see Figure 31). CXCL1, a small cytokine expressed by neurons, macrophages, neutrophils, and endothelial cells, has been shown to have neuroprotective functions and can induce proliferation and inhibit migration of oligodendrocytes. Importantly, CXCL1 has been shown to attenuate microglial activation and maintain them in a quiescent state (Lyons, 2009). Future investigations could explore whether shielding of torso and thus increased CXCL1 levels modulates microglial activation state.

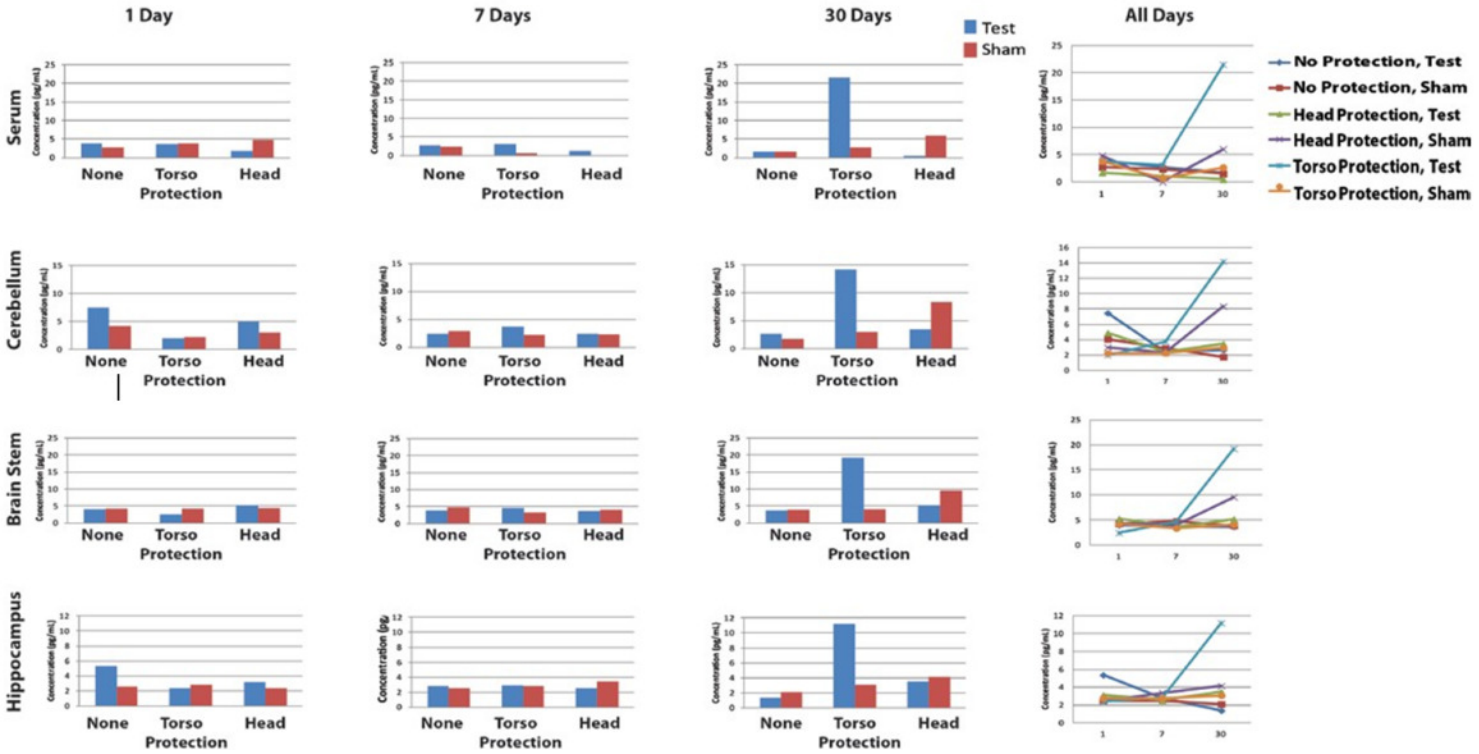

Figure 31. Temporal protein expression levels of CXCL1 (Gro-α) in mice with and without torso protection and exposure to blast. Individual sample types are plotted in rows (serum, cerebellum, brain stem, and hippocampus). The time post injury is plotted in columns (1, 7, and 30 days post-blast). The blue bars represent the injured animals and the red bars are the sham controls. The last column is depicting the evolving data over the 30-day period. The y-axis represents the concentration in pg/ml.

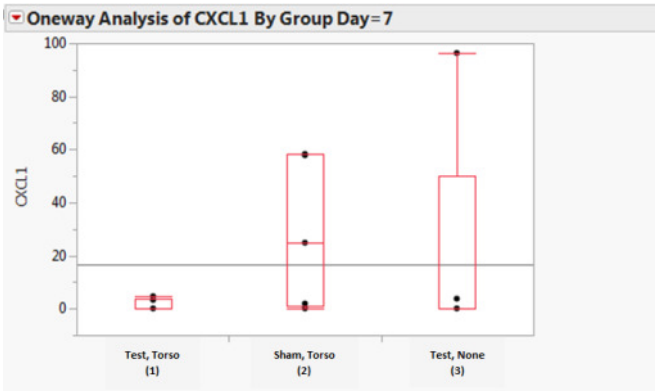

Nonparametric Comparisons For Each Pair Using Wilcoxon Method

q*	Alpha
1.95996	0.05

Level	- Level	Score Mean Difference	Std Err Dif	Z	p-Value	Hodges-Lehmann	Lower CL	Upper CL
2	1	2.60000	1.855921	1.40092	0.1612	24.6990	-3.1250	58.50300
3	1	0.20000	1.699673	0.11767	0.9063	0.0000	-4.8150	96.28400
3	2	-1.40000	1.855921	-0.75434	0.4506	-1.6900	-58.5030	94.59400

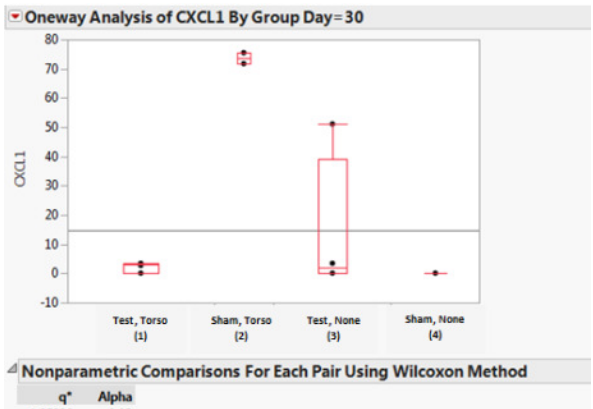

Nonparametric Comparisons For Each Pair Using Wilcoxon Method

q*	Alpha
1.95996	0.05

Level	- Level	Score Mean Difference	Std Err Dif	Z	p-Value	Hodges-Lehmann	Lower CL	Upper CL
2	1	3.15000	1.741647	1.80863	0.0705	71.7190	.	.
3	1	0.90000	1.668645	0.53936	0.5896	0.0000	-3.67900	51.11700
4	1	-1.33333	1.366260	-0.97590	0.3291	0.0000	.	.
4	3	-1.45833	1.322876	-1.10240	0.2703	-1.8395	.	.
4	2	-2.08333	1.290994	-1.61374	0.1066	-73.5585	.	.
3	2	-2.62500	1.596872	-1.64384	0.1002	-71.5700	.	.

Figure 32. CXCL1 Expression in cerebellum of TP, TP-Sham, NP, and Sham groups by day (7, 30) showing individual values, mean, and standard deviation. Statistical values of significance are displayed for each grouping.

Glial Fibrillary Acidic Protein (GFAP)

The CNS protein, GFAP, is an intermediate filament protein that is expressed by numerous cell types within the central nervous system (CNS) including astrocytes and ependymal cells. GFAP is upregulated in response to brain injury. The presence of GFAP in the serum is an indicator of BBB disruption since this protein is not normally present outside of the CNS.

The level of GFAP in the serum is greater in unprotected 7d post-blast exposed animals than shams or torso shielded mice (Figure 13). This result suggests that torso shielding reduces disruption of the BBB after blast exposure. It is unclear why there is expression in the sham animals but presumably it is due to something intrinsic (e.g., cross-reactivity with another protein) to the specific ELISA kit.

Differences between NP and Sham as well as NP and TP are evident (Figure 33). This fascinating result provides strong evidence that torso-shielding significantly attenuates BBB disruption from blast. Interestingly, torso-shielding may even abrogate BBB disruption as suggested by the lack of significant difference between TP and Sham. This result indicates that low-level blast exposure to head only does not disrupt the BBB. This highlights an important systemic contribution to brain injury. The exact nature of the systemic contribution to brain injury remains to be determined.

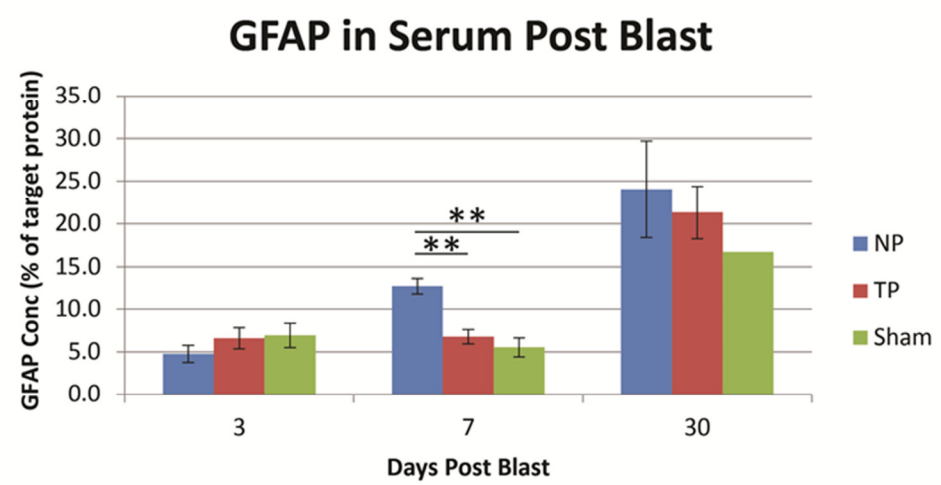

Figure 33. GFAP expression in serum. Standard error is shown. One asterisk p <0.05. Two asterisks p <0.01.

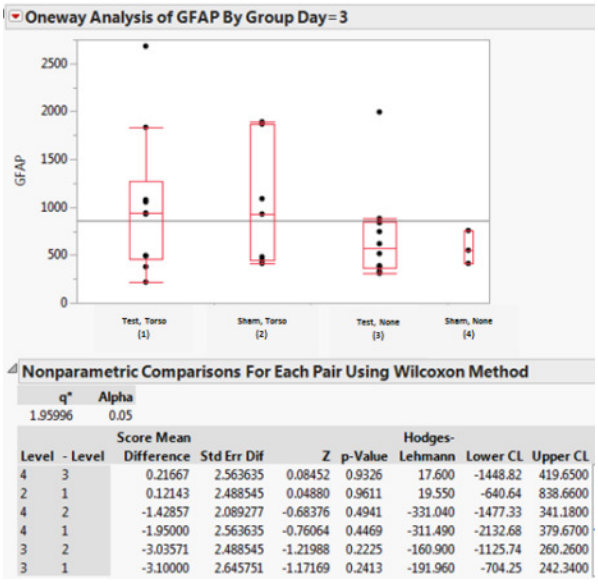

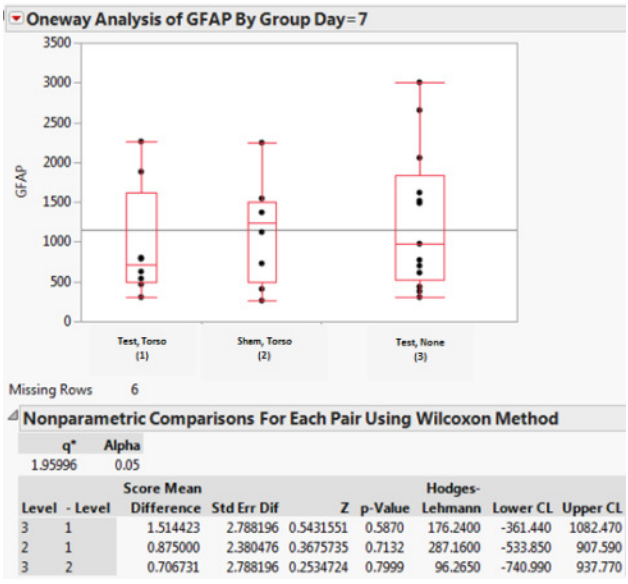

Figure 34. GFAP expression in serum of TP, TP-Sham, Sham, and NP groups by day (3, 7) showing individual values, mean, and standard deviation. Statistical values of significance are displayed for each grouping.

Calcium Sensing Receptor (CaSR)

CaSR is a G-protein coupled receptor which senses extracellular levels of calcium ion. Increased extracellular calcium binding produces a conformational change in the receptor, which activates the intracellular phospholipase C pathway, presumably through a G protein, which ultimately increases intracellular concentration of calcium, which inhibits vesicle fusion and the cAMP dependent pathway. CaSR is widely expressed and co-localized with GABA-B-R1 and R2 in brain regions involved in memory, cognition, motor reflexes, thirst, growth, and energy homeostasis (Yano et al., 2004). In cultured hippocampal neurons, the CaSR activates non-selective cation channels and Ca2+-dependent K channels and depolarizes their membrane potentials (Chattopadhyay et al., 1999). Overexpression/over-activity of CaSR in a controlled cortical impact injury model promoted injury response and pharmacological blockade reduced motor impairment. Specifically, CaSR upregulation has been shown to be closely associated with neuronal death in culture (Chang et al., 2008). Although the mechanisms responsible for overexpression of CaSR are not fully worked out, it is known that interleukin 1 beta (IL-1-β) can upregulate CaSR mRNA (Nielsen et al., 1997). Blast injury activates macrophages which increase expression of IL-1-β and may stimulate upregulation of the CaSR which in turn promotes injury response by activating a variety of signaling pathways, depolarizing neuron membrane potentials, and ultimately causing cell death.

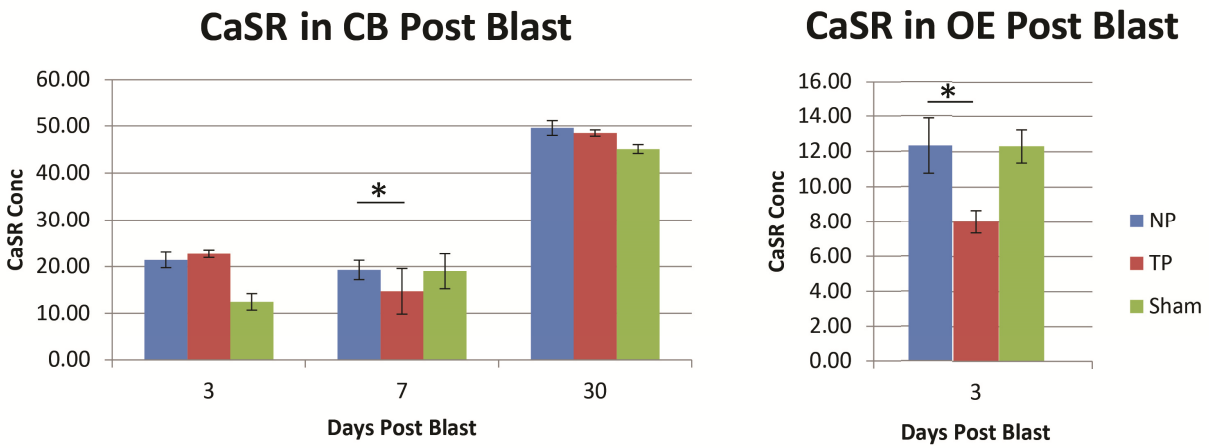

Figure 35. CaSR expression in the cerebellum and olfactory epithelium.

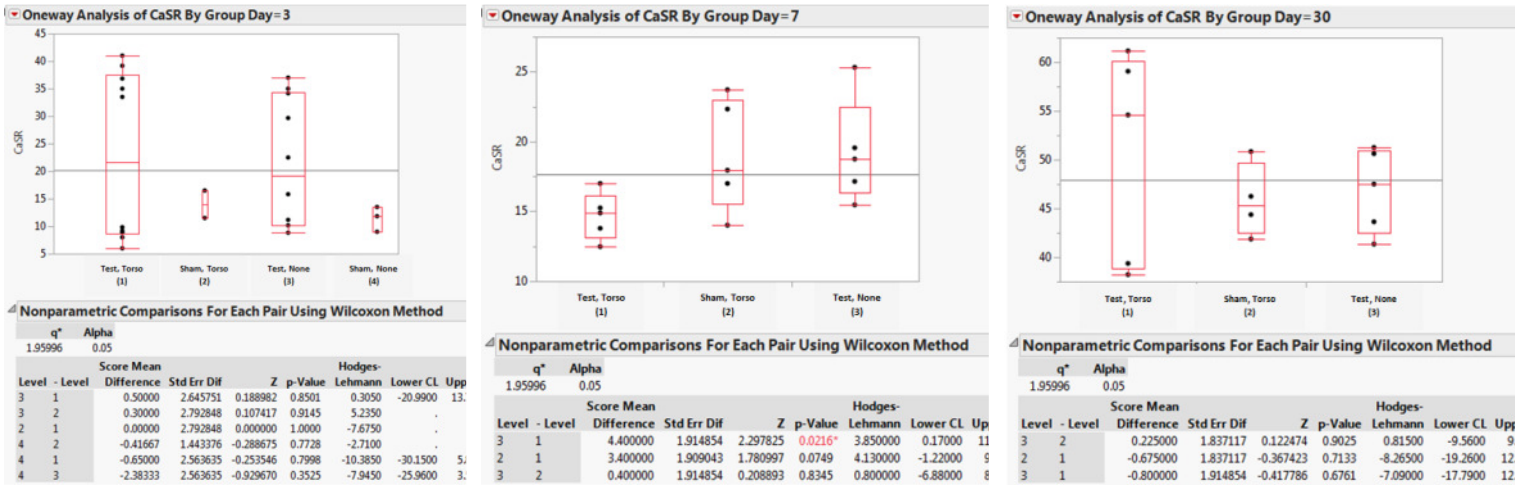

Figure 36. CaSR Expression in cerebellum of TP, TP-Sham, NP, and Sham groups by day (3, 7, 30) showing

individual values, mean, and standard deviation. Statistical values of significance are displayed for each group. Statistical significance with a p value of 0.0216 was found when comparing TP and NP animals at day 7.

Increased positive contrast by MEMRI has been shown to correlate with overexpression/over-activity of CaSR since manganese is an analogue of calcium and can utilize the same channels calcium. We hypothesized that since we see an increase in MEMRI contrast after blast exposure and this increase is reduced with torso shielding, this might also be reflected in CaSR expression levels. Here we tested this hypothesis in cerebellum and olfactory epithelium from mice after blast with and without torso shielding (Figure 36). We included olfactory epithelium because if differences between injured and sham animals were observed, the olfactory epithelium biopsy could be used as a relatively non-invasive biomarker of injury. We did not detect a significant difference in the expression of CaSR between NP, TP, and Sham animals at 3-days post-blast. Since microglia/macrophages exhibit peak activation at 7-14 days post blast injury, we reasoned that the subsequent increased release of IL-1-β may upregulate CaSR during this period (Nielsen et al., 1997). Even at these later time points (7 and 30 days post-blast) we are still not detecting significant differences between NP and Sham. It should be noted that we might still be missing the time-point that would show a difference. It is curious that there seems to be a reduction of CaSR in TP animals at 7-days post-blast in both CB and OE. Perhaps the torso-shielding is protecting the body from blast-induced tissue damage while the blast to the unprotected head may activate the anti-inflammatory efferent arm of the inflammatory reflex (see Figure 37).

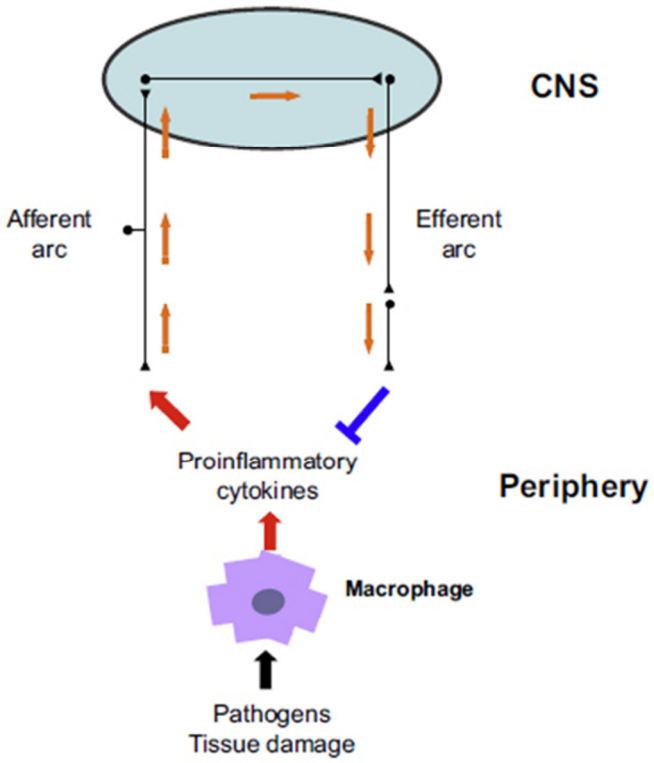

Figure 37. The inflammatory reflex (Rosas-Ballina and Tracey, 2009).

Activation of this anti-inflammatory cholinergic pathway may result in a decrease in circulating pro-inflammatory cytokine concentrations including IL-1-β (Huston, 2012). The resulting decrease in circulating pro-inflammatory cytokines in the absence of systemic tissue damage and thus a lack of activation of the pro-inflammatory response may offer protection from the immune-

related insult to the brain (less cytotoxic cytokines generated and less neutrophil/macrophage infiltration or glial activation in the brain).

Myelin Basic Protein (MBP)

Evaluating signal changes in MBP, a structural protein involved with myelination of nerves, can give information regarding demyelination when measured in brain tissue, and about BBB disruption when measured in serum. At 7d we did not detect any differences in brain MBP levels between NP, TP, or Sham animals indicating there is no detectable demyelination (Figure 38). This result along with the Luxol blue staining (Figure 30) is further proof of a lack of demyelination. We did detect a significant difference in serum MBP levels between NP and TP and between NP and Sham mice. This result suggests that low-level blast exposure to head disrupts the BBB while not affecting brain myelination levels.

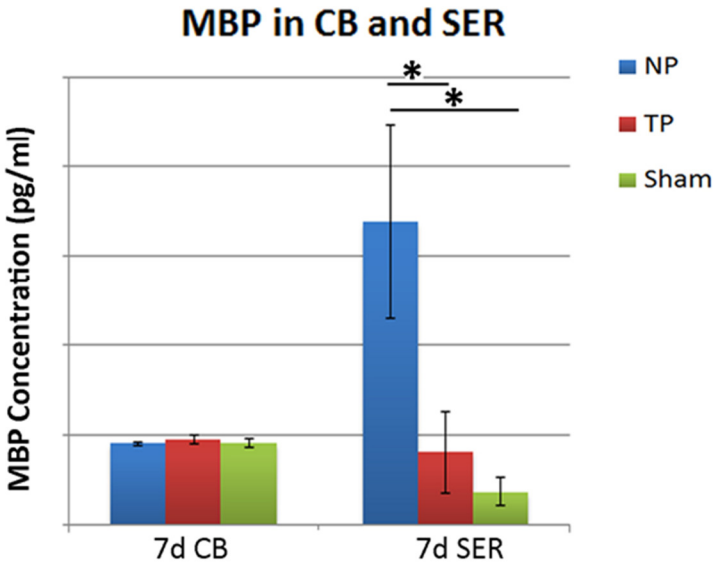

Figure 38. MBP expression in the cerebellum and serum

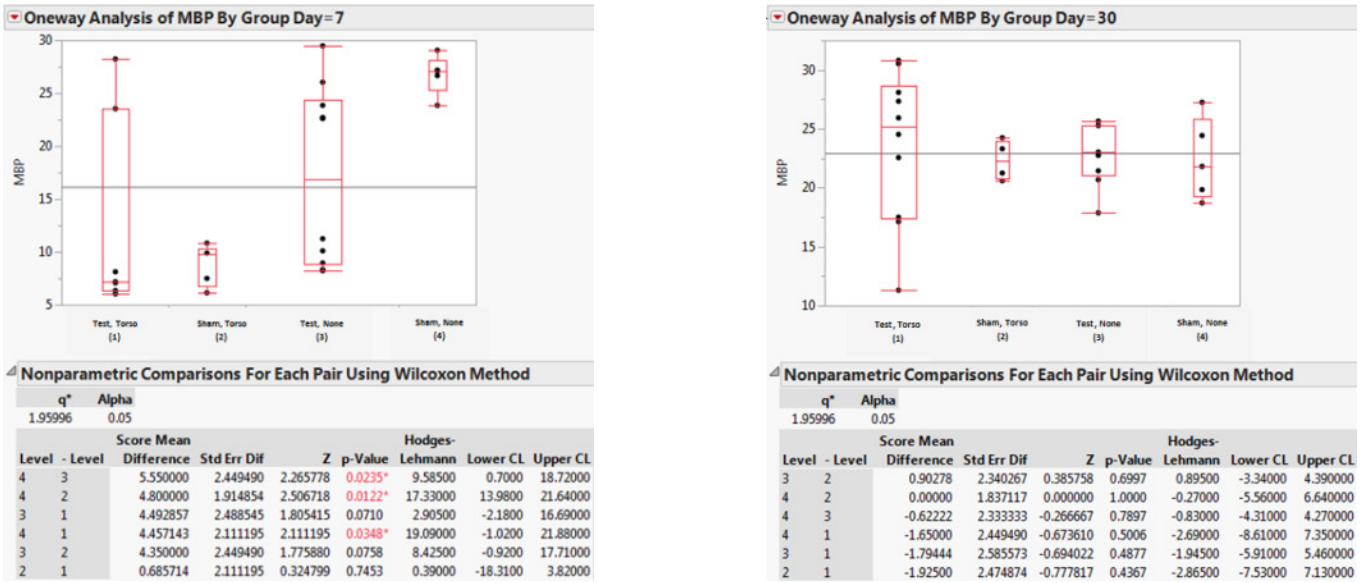

Figure 39. MBP expression in cerebellum of TP, TP-Sham, NP, and Sham groups by day (7, 30) showing individual values, mean, and standard deviation. Statistical values of significance are displayed for each grouping. Statistical significance with a p value of 0.0235 was found when comparing NP and Sham animals, p=0.0122 when comparing TP-Sham and Sham, and p=0.0348 when comparing TP and NP all at day 7.

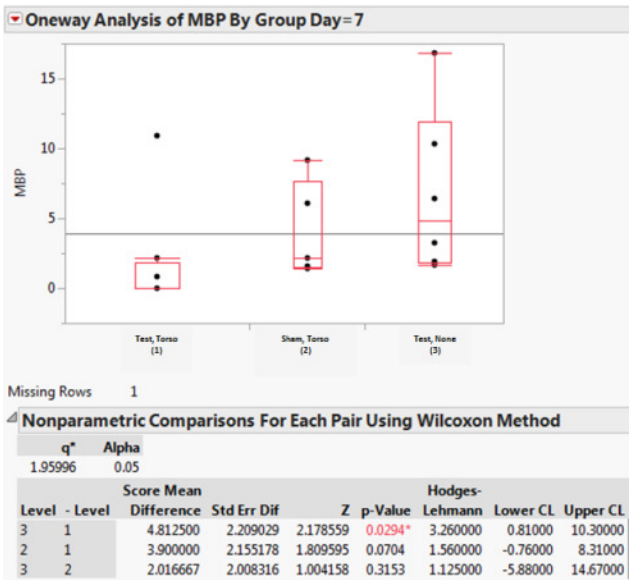

Figure 40. MBP expression in serum of TP, TP-Sham, and NP groups by day (7) showing individual values, mean, and standard deviation. Statistical values of significance are displayed for each grouping. Statistical significance with a p value of 0.0294 was found when comparing Torso protected blast-exposed animals and non-torso blast-exposed protected animals.

Neutrophil Elastase (NE)

NE is a serine proteinase secreted by neutrophils and macrophages during inflammation that destroys bacteria and host tissue. NE is being used here as a marker of activated neutrophils/macrophages. The early infiltration of neutrophils from the peripheral circulation has been repeatedly reported in experimental models of focal TBI. The production of proteases, matrix metalloproteinases, cytokines, and reactive oxygen species by neutrophils is implicated in secondary injury mechanisms triggered by TBI, including oxidative stress, increased BBB permeability, and neuronal loss. We hypothesized that neutrophil infiltration would occur soon after blast and that torso shielding would attenuate infiltration and reduce injury. However, in our previous report at 7d post-blast we did not detect a difference. We looked at an earlier time point but although we see a trend of higher neutrophil infiltration in unprotected animals versus sham it wasn't significantly different (Figure 41). Interestingly, we see a reduction in neutrophil infiltration in torso shielded animals exposed to blast compared with both NP and Sham. We propose this reduction is due to activation of the efferent anti-inflammatory arm of the inflammatory reflex which results in fewer infiltrating neutrophils. This has been seen in studies using vagus nerve stimulation and cholinergic agonists where they significantly inhibit neutrophil trafficking to sites of inflammation (Saeed et al., 2005 and Huston 2012).

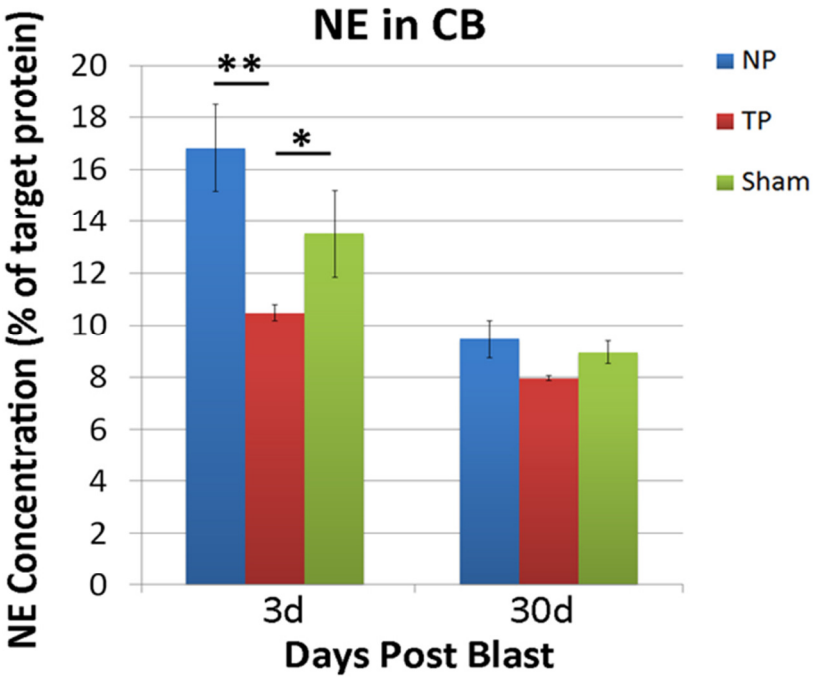

Figure 41. NE expression in the cerebellum. One asterisk $p<0.05$ two asterisks $p<0.01$.

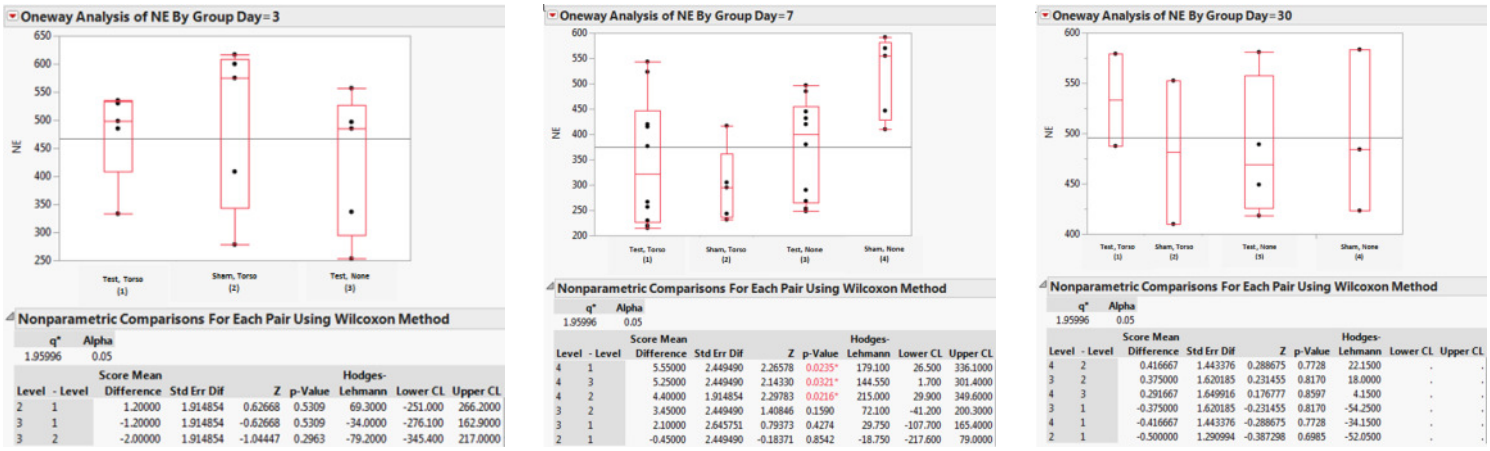

Figure 42. NE expression in cerebellum of TP, TP-Sham, NP, and Sham groups by day (3, 7, 30) showing individual values, mean, and standard deviation. Statistical values of significance are displayed for each grouping. Statistical significance with a p value of 0.0235 was found when comparing TP and Sham animals, p=0.0321 when comparing NP and Sham, and p=0.0216 when comparing Sham-Torso and Sham all at day 7.

Granulocyte Colony-Stimulating Factor (G-CSF)

G-CSF is a growth factor and cytokine that can act on neuronal cells as a neurotrophic factor. The G-CSF induces neurogenesis in the CNS, increases neuroplasticity and counteracts apoptosis. These properties are currently under investigation for the development of treatment of neurological diseases such as cerebral ischemia. We see approximately 4-fold higher levels of G-CSF in the serum of TP animals (Figure 43).

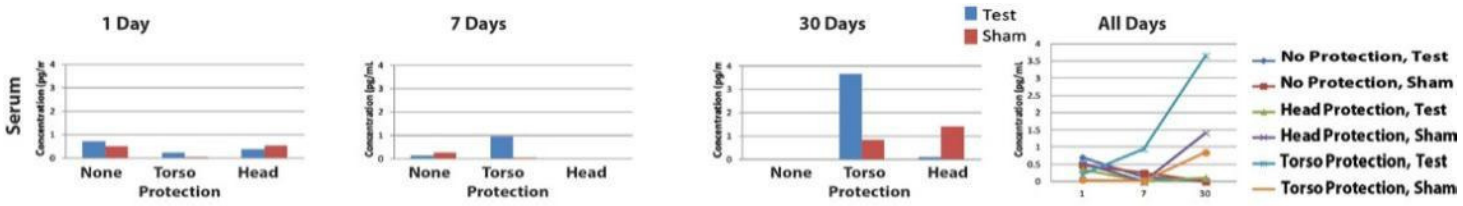

Figure 43. Temporal protein expression levels of G-CSF in mice with and without protective wear and exposure to blast. Individual sample types are plotted in rows (serum, cerebellum, brain stem, and hippocampus). The time post injury is plotted in columns (1, 7, and 30 days post-blast). The blue bars represent the injured animals and the red bars are the sham controls. The last column is depicting the evolving data over the 30-day period. The y-axis represents the concentration in pg/mL.

Interleukin-6 (IL-6)

IL-6, an interleukin that is induced by CXCL1 (Gro-α), is upregulated across several tissue samples, specifically at 30 days post-injury in the serum and spleen in TP animals (Figure 44). IL-6 acts as both a pro-inflammatory and anti- inflammatory cytokine. Its role as an anti-inflammatory cytokine is mediated through its inhibitory effects on TNF-α and IL-1, and activation of IL-1ra and IL-10. IL-6 is capable of crossing the blood brain barrier (as are many cytokines and chemokines).

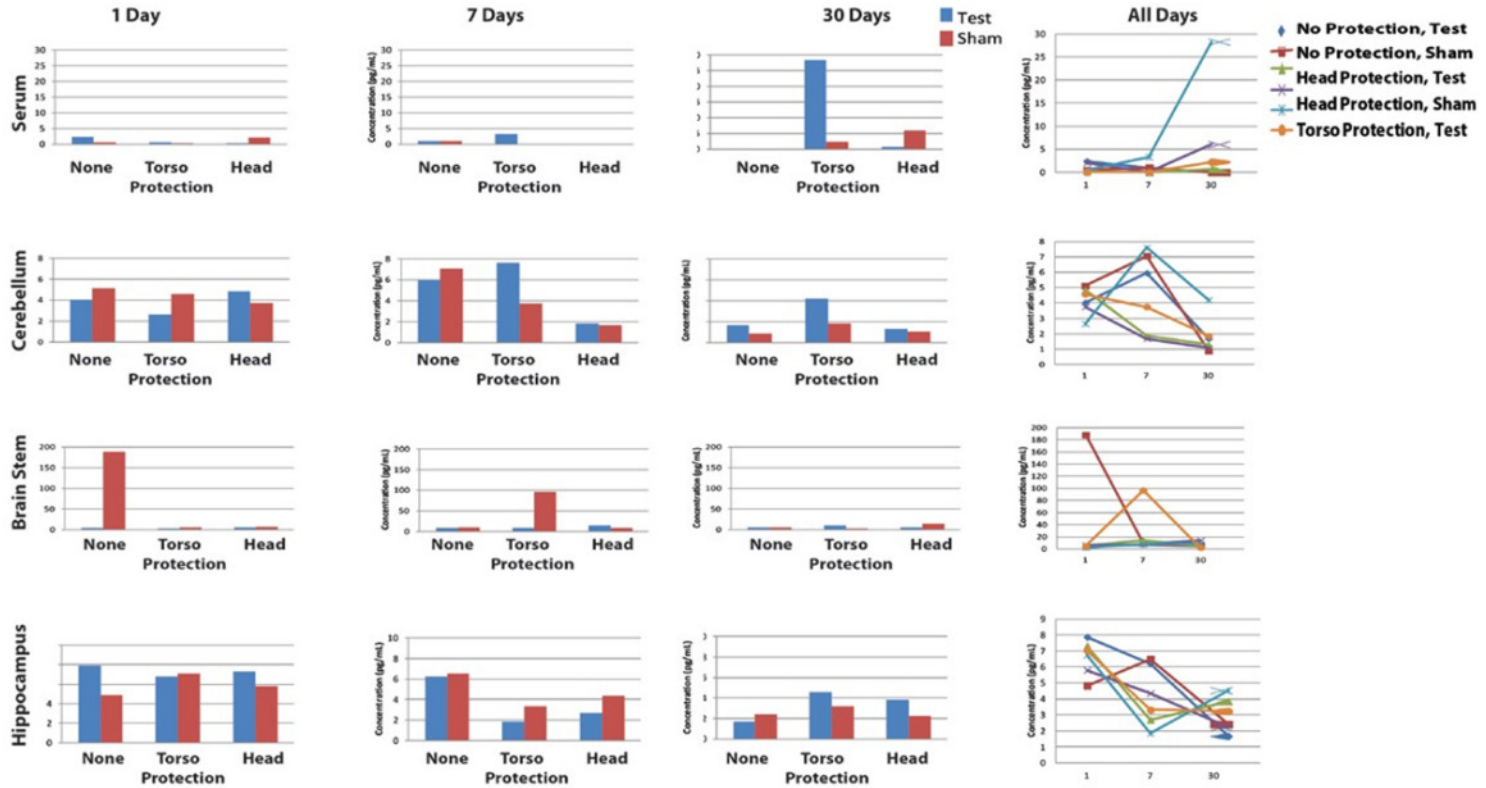

Figure 44. Temporal protein expression levels of IL-6 in mice with and without protective wear and exposure to blast. Individual sample types are plotted in rows (serum, cerebellum, brain stem, and hippocampus). The time post injury is plotted in columns (1, 7, and 30 days post-blast). The blue bars represent the injured animals and the red bars are the sham controls. The last column is depicting the evolving data over the 30-day period. The y-axis represents the concentration in pg/ml.

Vascular Endothelial Growth Factor-A (VEGF-A)

VEGF-A has been shown to be expressed by inflammatory cells (e.g., polymorphonuclear leukocytes) and astrocytes. It can be stimulated by hypoxic conditions and inhibited by edema and necrosis (Nag, Eskandarian et al., 2002). It mediates vascular permeability (vasodilator), induces angiogenesis, vasculogenesis, endothelial cell growth, cell migration, and can inhibit apoptosis. Importantly, VEGF, a HIF-1α target gene is known to play a critical role in the early phases following brain injury by causing BBB disruption leading to cerebral edema (Nag, Takahashi et al., 1997; Zhang, Zhang et al., 2000; Fagan, Hess et al., 2004; Jadhav, Matchett et al., 2007). Following exposure to blast, VEGF-A appears slightly elevated in the serum (Figure 45).

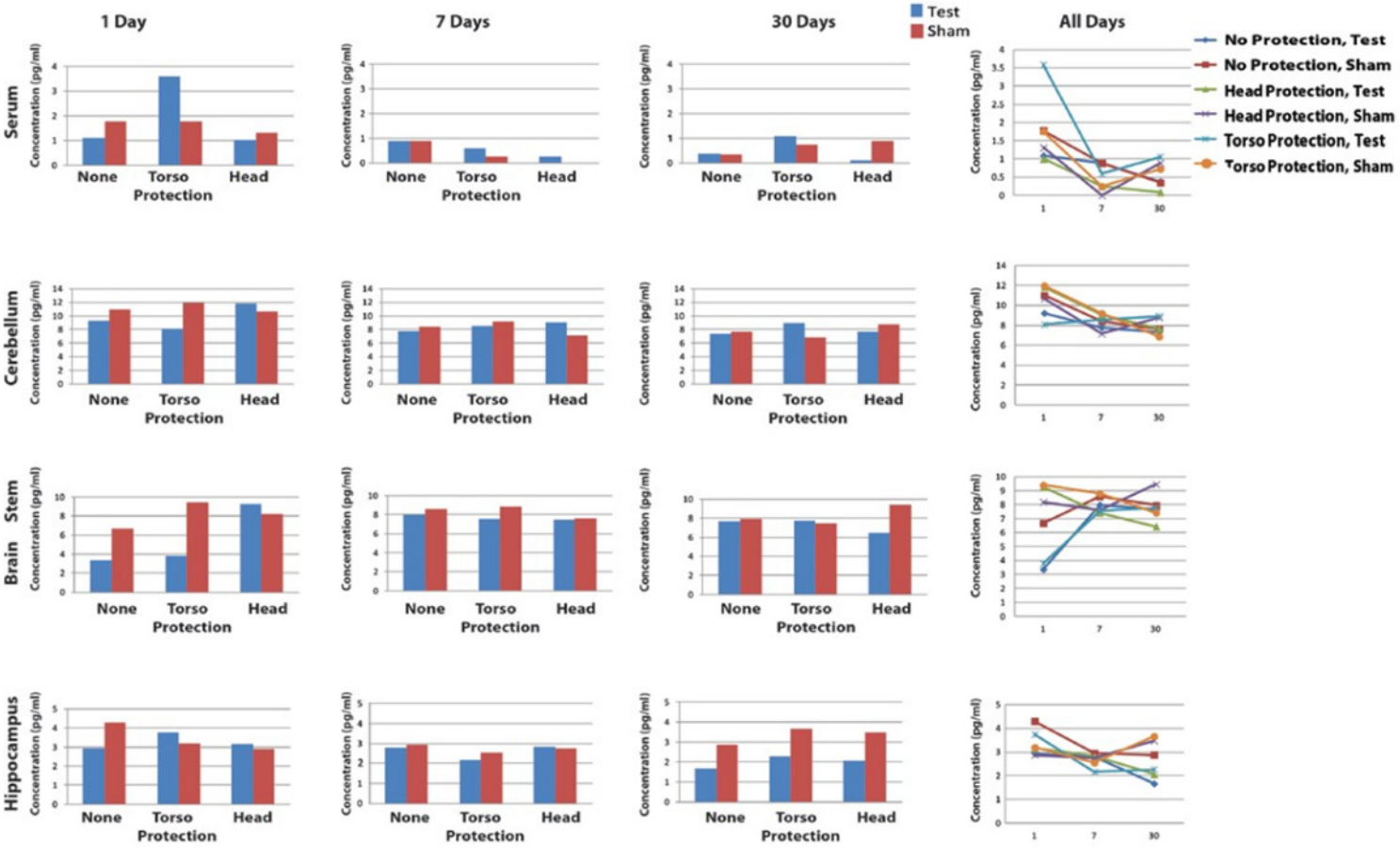

Figure 45. Temporal protein expression levels of VEGF-A in mice with and without protective wear and exposure to blast. Individual sample types are plotted in rows (serum, cerebellum, brain stem, and hippocampus). The time post injury is plotted in columns (1, 7, and 30 days post-blast). The blue bars represent the injured animals and the red bars are the sham controls. The last column is depicting the evolving data over the 30-day period. The y-axis represents the concentration in pg/ml.

Tumor Necrosis Factor-Alpha (TNF-α)

TNF-α plays a role in promoting inflammation in injured tissues, and is activated/produced by a variety of immune cells. As hypothesized and in line with imaging results, there is an increase in TNF-α in the acute phase of the injury response in the serum (Figure 46).

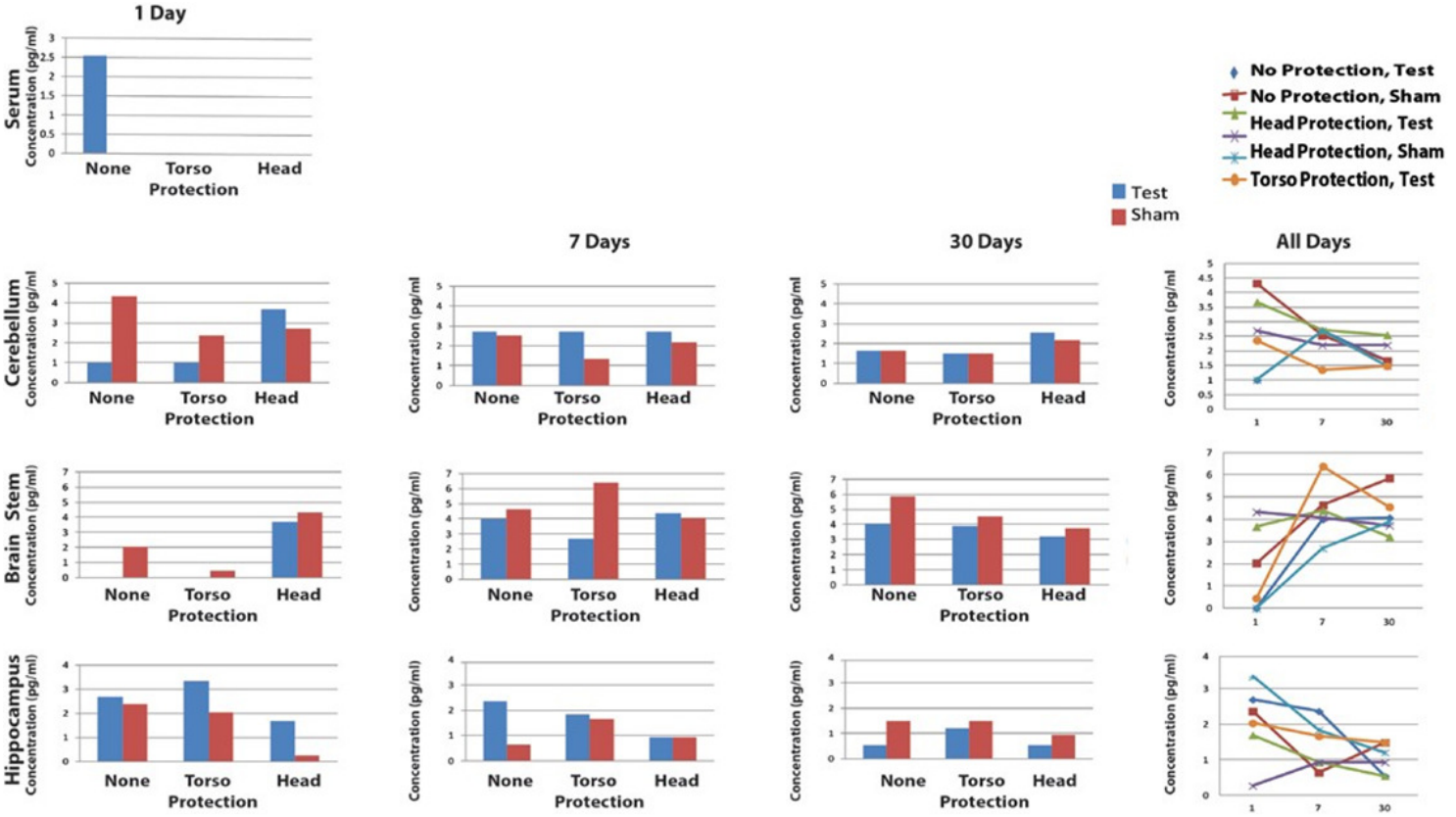

Figure 46. Temporal protein expression levels of TNF-α in mice with and without protective wear and exposure to blast. Individual sample types are plotted in rows (serum, cerebellum, brain stem, and hippocampus). The time post injury is plotted in columns (1, 7, and 30 days post-blast). The blue bars represent the injured animals and the red bars are the sham controls. The last column is depicting the evolving data over the 30-day period. The y-axis represents the concentration in pg/ml.

Interleukin 1-Beta (IL-1-β)

There appears to be an increase in IL-1-β in the cerebellum of injured mice (Figure 47). IL-1-β is a member of the interleukin 1 cytokine family produced by activated macrophages as a pro-protein, which is proteolytically processed to its active form by caspase 1 (CASP1/ICE). It is an important mediator of the inflammatory response, and is involved in a variety of cellular activities, including cell proliferation, differentiation, and apoptosis. The induction of cyclooxygenase-2 (PTGS2/COX2) by this cytokine in the central nervous system (CNS) is found to contribute to inflammatory pain hypersensitivity.

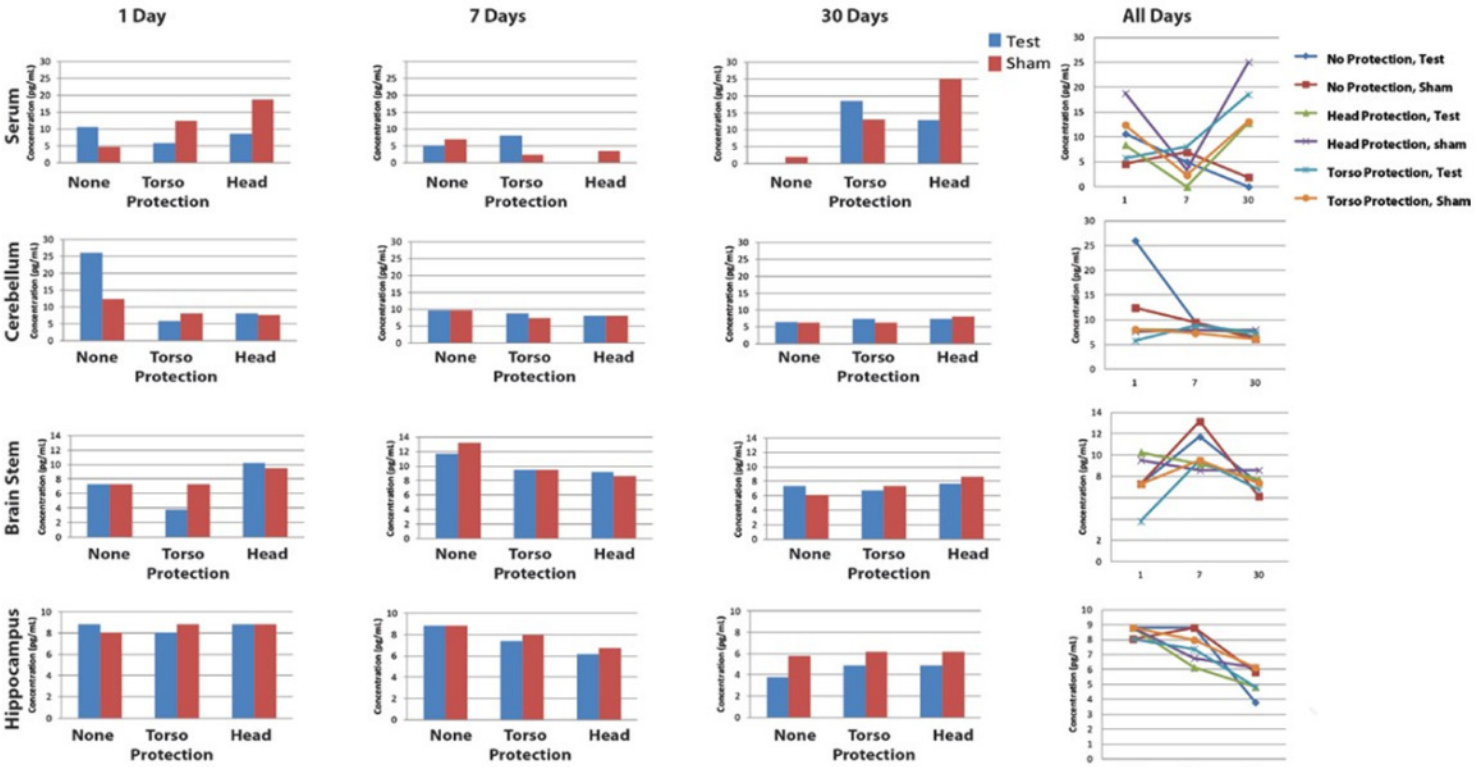

Figure 47. Temporal protein expression levels of IL1-β in mice with and without protective wear and exposure to blast. Individual sample types are plotted in rows (serum, cerebellum, brain stem, and hippocampus). The time post injury is plotted in columns (1, 7, and 30 days post-blast). The blue bars represent the injured animals and the red bars are the sham controls. The last column is depicting the evolving data over the 30-day period. The y-axis represents the concentration in pg/ml.

Interleukin10

IL-10 is an anti-inflammatory cytokine with pleiotropic effects in immunoregulation and inflammation. IL-10 can block NF-KB activity. Knockout studies in mice suggested the function of this cytokine as an essential immunoregulator in the intestinal tract; and, indeed, patients with Crohn's disease react favorably towards treatment with recombinant interleukin-10-producing bacteria, demonstrating the importance of IL-10 for counteracting the hyperactive immune response in the human body. IL-10 is capable of inhibiting synthesis of pro-inflammatory cytokines such as IFN-g, IL-2, IL-3, TNFα, and GM-CSF made by cells such as macrophages and regulatory T-cells.

IL-10 expression did not appear to be significantly different between sham and injured or any of the groups (Figure 48). It is unclear why this interleukin is expressed in both sham and injured animals acutely and then wanes over the 30-day period. It is likely this measurement is confounded by the isoflurane anesthesia used during vitals measurements and during injury induction. IL-10 is slightly increased in the spleen of all injured groups at 30-days post injury (data not shown).

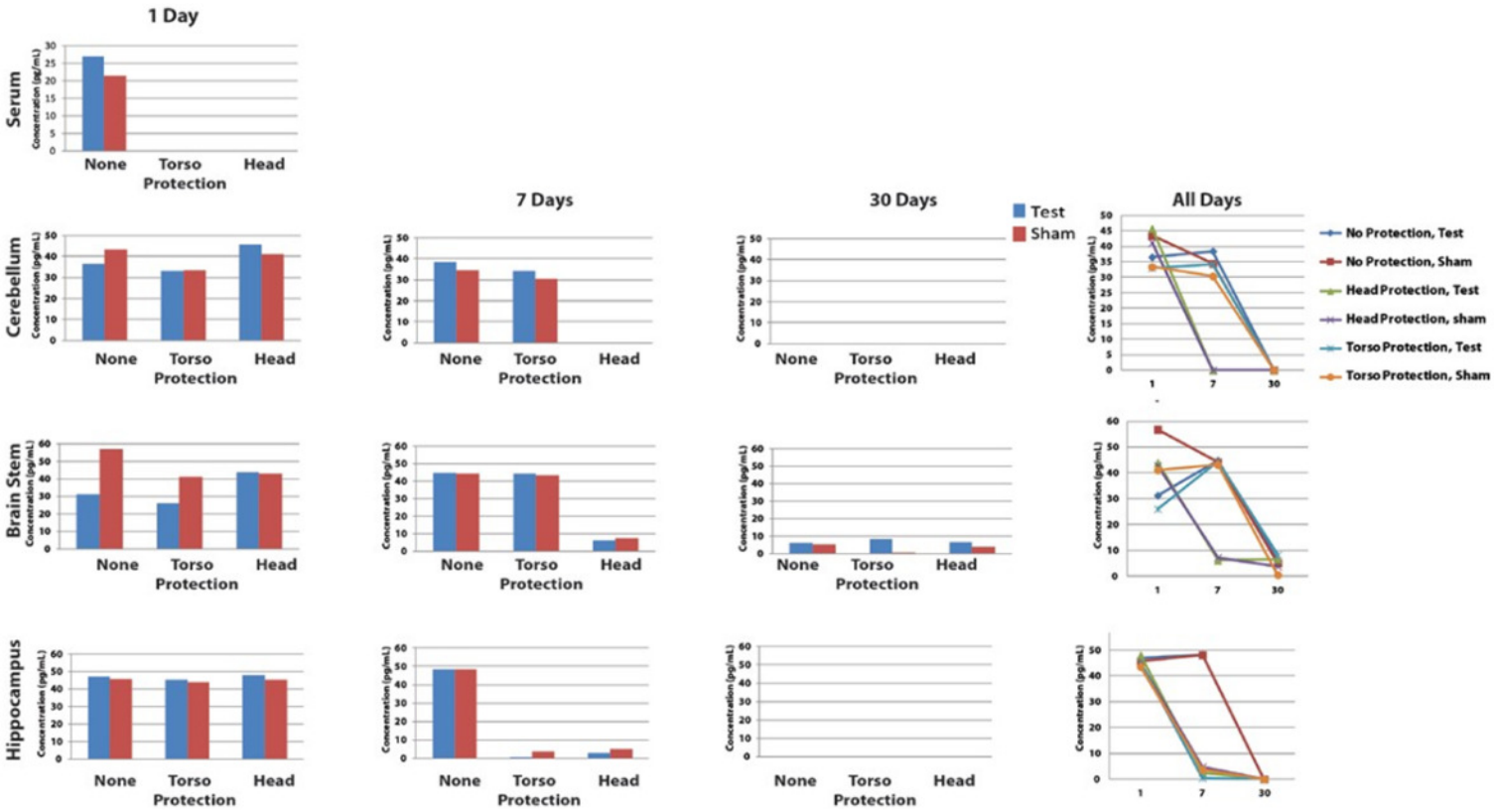

Figure 48. Temporal protein expression levels of IL-10 in mice with and without protective wear and exposure to blast. Individual sample types are plotted in rows (serum, cerebellum, brain stem, and hippocampus). The time post injury is plotted in columns (1, 7, and 30 days post-blast). The blue bars represent the injured animals and the red bars are the sham controls. The last column is depicting the evolving data over the 30-day period. The y-axis represents the concentration in pg/ml.

Monocyte Chemotactic Protein-1 (MCP-1)

MCP-1 is responsible for recruiting immune cells to inflamed or injured tissues. Along with each of the chemokines, MCP-1 appears to be upregulated in serum and spleen in the blast-exposed torso-protected group (Figure 49).

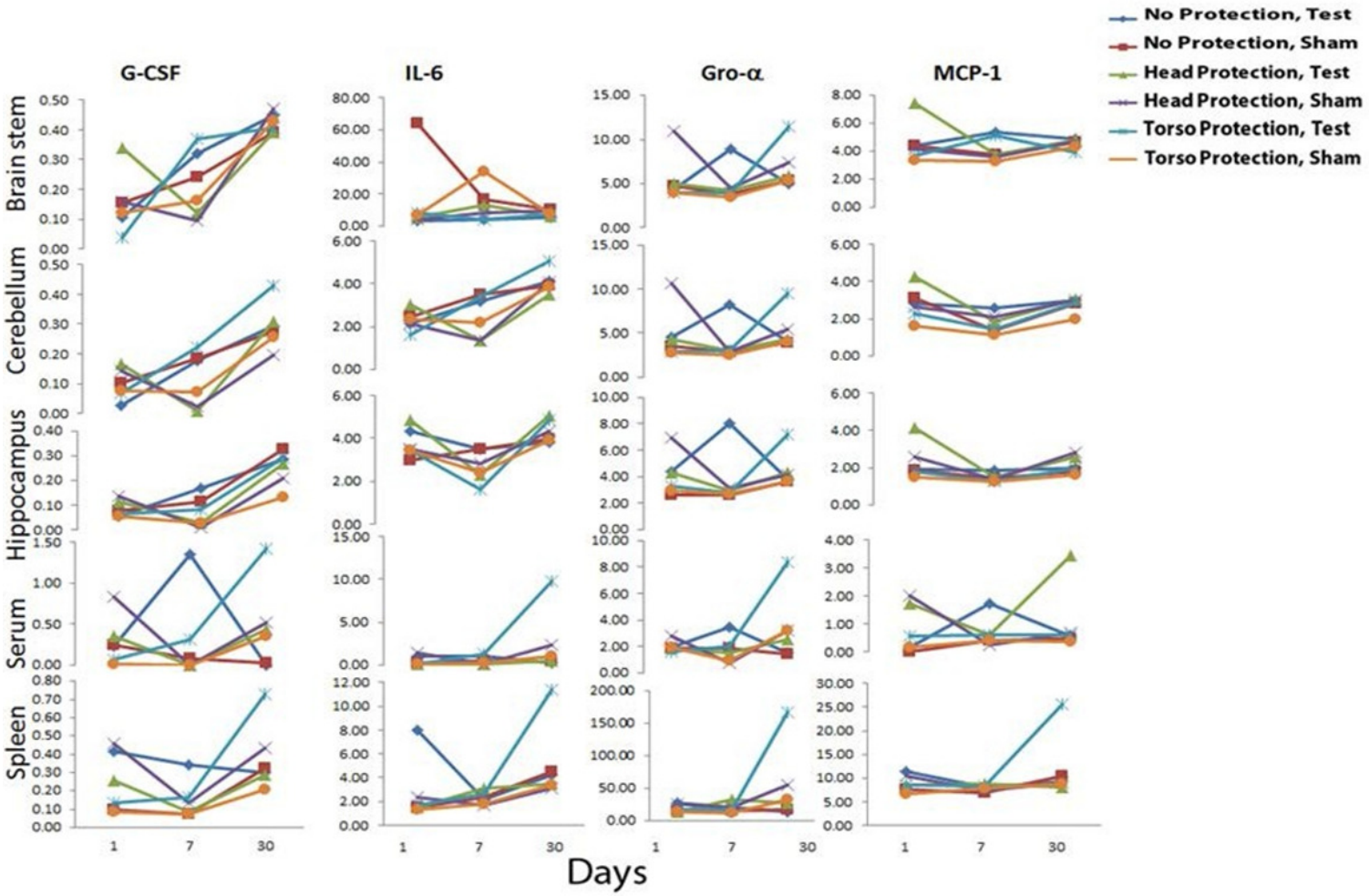

Figure 49. Temporal protein expression levels of G-CSF, IL-6, CXCL1 (Gro-α), and MCP-1 in mice with and without protective wear and exposure to blast. Individual sample types are plotted in rows brain stem, cerebellum, hippocampus, serum, and spleen). The time post injury is plotted on the x-axis (1, 7, and 30 days post-blast). These plots depict the evolving data over the 30-day period. The y-axis represents the concentration in pg/ml.

<u>Aim 3 (24 months – October 1, 2011 to March 31, 2013)</u> Characterization of functional outcomes in mice exposed to blast.

Motor Performance

To test for possible effects of exposure to mild blast on motor coordination, assessments of motor performance were performed using the Rotarod with continuously accelerating rotations. Results are shown as averages (with standard error) and assessments over 30 days are compared to baseline measurements prior to blast exposure. Baseline measures for motor performance were averaged over assessments at days 1, 2, and 3 prior to blast. NP animals were significantly impaired in the Rotarod performance when tested 1 week after exposure (Figure 50). This deficit was partially ameliorated at 3 weeks after the blast. Blast-related alterations in motor coordination and body weight were not significantly correlated between each other suggesting that deficits in motor coordination were not linked to changes in body weight following exposure to blast.

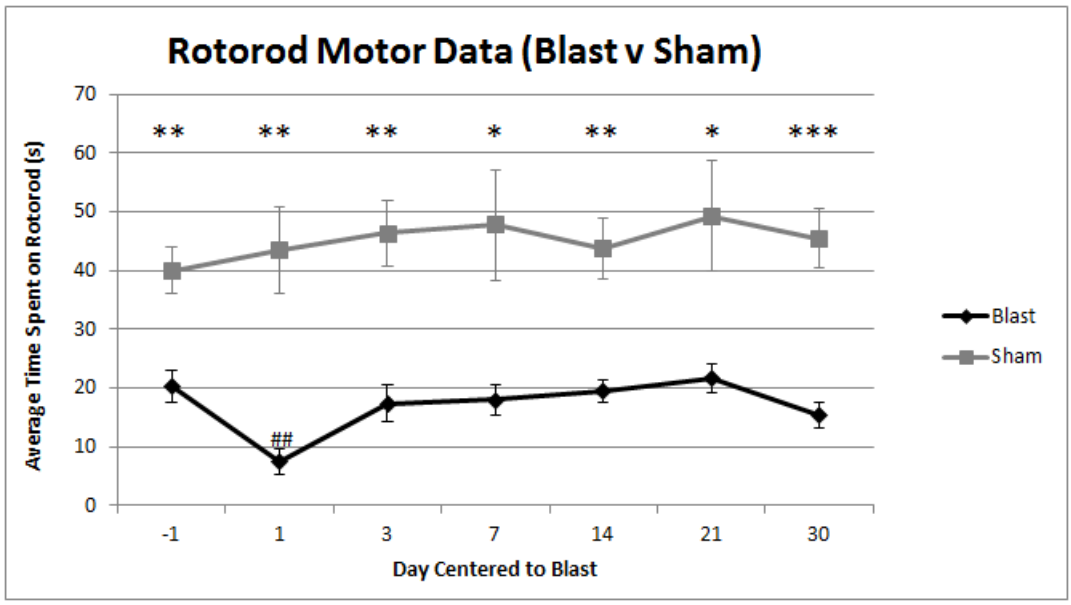

Figure 50. Motor performance in GFAP-luciferase transgenic animals exposed to mild/moderate blast with and without the surrogate outer tactical vest and sham controls. The results are shown as ± SE and measured over a 30-day post-injury period. (Unprotected blast exposed animals. N=12; Outer tactical vest animals (Kev) N=5; Sham N=8). Rotarod assessed motor outcomes in pre- trained mice. Motor performance was significantly decreased at two weeks and 30 days post trauma in unprotected and protected mice. One asterisk, $P<0.05$; two asterisks, $p<0.01$.

Similar levels of motor impairments identified in the post-blast GFAP-luciferase animals were also demonstrated previously in C57Bl6 mice by Cernak et al. (Cernak, Merkle et al., 2011).

Open-Field Behavior, Exploratory Activity

The open-field paradigm allows for simultaneous analyses of exploratory activity and levels of anxiety. To analyze anxiety levels, activity measures were broken down into peripheral and central zones. Animals across groups showed similar preferences for the periphery over central areas of the field, which can produce anxiety (Figure 51).

As had been demonstrated previously in C57Bl6 mice by Cernak et al., we are also detecting rearing impairment in the GFAP-luciferase transgenic animals (FVB/N-Tg(GFAP-luc)-Xen strain) (Cernak, Merkle et al., 2011).

We did not see a significant difference in distance traveled, freezing behavior (time immobile), or memory performance (shuttle box active avoidance assay) as had been demonstrated previously (Cernak, Merkle et al., 2011) (data not shown).

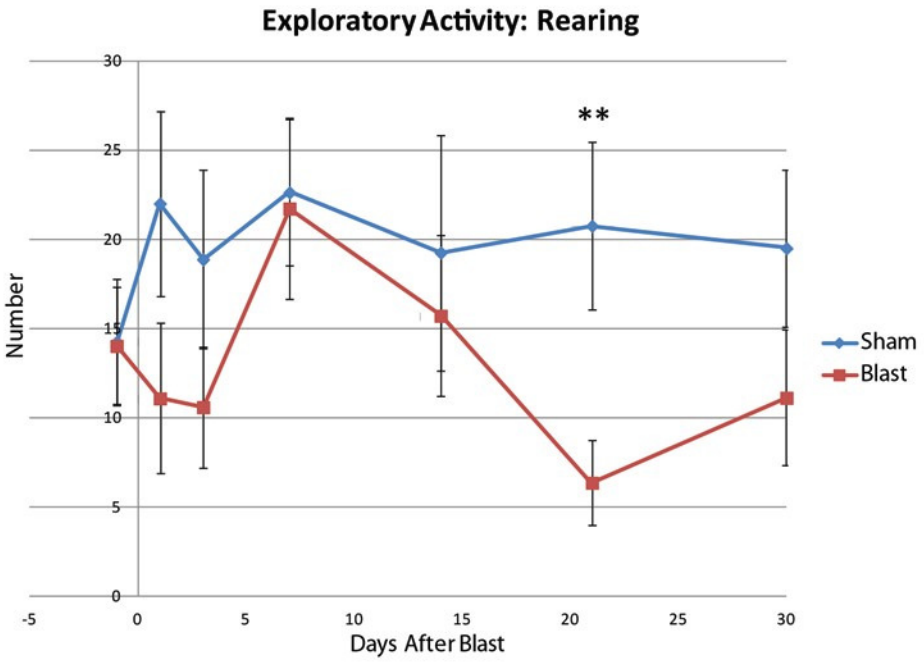

Figure 51. Exploratory activity in GFAP-luciferase transgenic animals exposed to mild/moderate blast and sham controls. The results are shown as ± SE and measured over a 30-day post-injury period. (blast exposed animals N=12; Sham N=8). Rearing was significantly decreased at three weeks in post trauma mice. One asterisk, $P<0.05$; two asterisk, $p<0.01$.

<u>Aim 4 (24 months – October 1, 2011 to September 30, 2013)</u> includes continuous correlation of imaging findings, molecular analyses, and functional data and further fine-tuning of the imaging modalities based on the validation results and correlations with outcome data.

$MnCl_2$-T1 MRI Normalization and Quantification

Phantom Development

Internal $MnCl_2$ controls (referred to as phantoms) were developed to allow normalization and quantification of $MnCl_2$-enhancedT1-weighted MRI. Phantom baseline data has been taken at various concentrations of $MnCl_2$ in solution (Figure 52). Concentrations of $MnCl_2$ in H2O were 0, 0.01, 0.02, 0.5, 1 and 2 millimolar (mM). The concentrations were designed such that running lower and higher doses is not needed since water (H2O) is zero and 1 mM is already higher than injectate /animal mass (i.e., physiological dose). Even though correlation time and other phenomena are responsible for the curves behavior (intensity versus concentration is graphed, given that there are 4 points (between 0 and 0.5mM and they were repeated three times inside the coil for reliability), in the range of physiologically possible concentrations (injectate is 1mM and this must mix with blood pool and distribute throughout the body) a more or less linear response of concentration versus intensity is evident. Hence it is believed that any noted intensity in an MRI can be linearly associated with concentration up-take of $MnCl_2$. Phantoms of 0.02 mM are placed above the head in the head radio frequency coil in every scan for calibration purposes and for concentration quantification purposes.

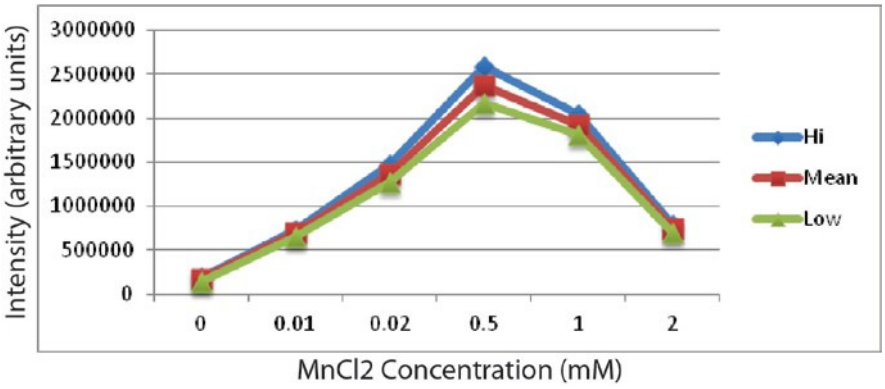

Figure 52. Phantom Intensity versus $MnCl_2$ Concentration.

Normalization with Phantom

$MnCl_2$-enhanced MR imaging of TBI mouse brains was performed in conjunction with a 0.02mM $MnCl_2$ phantom affixed to the brain coil in order to correct for variations in MRI homogeneity and imaging performance. Daily variations in phantom contrast were quantified with Paravision 5.0 Processing Software, and normalization of $MnCl_2$-contrast enhancement of brain after TBI resulted in a more accurate measure of CNS uptake.

Optimization of $MnCl_2$ Injection Protocol for Improved Signal Enhancement

In our Aim 1 Task 1.3 studies, $MnCl_2$-MRI imaging was performed by injection of $MnCl_2$ 24hr

prior to exposure to blast. As hypothesized, this resulted in a differential uptake of the contrast agent by the brain when comparing mice that had been exposed to blast versus sham animals. While this differential uptake is quantifiable, differences between groups were subtle and did not serve to provide a readily measurable response. It is known that TBI disrupts the neuronal homeostasis of calcium and subsequently $MnCl_2$ is taken up by neuronal cells through Ca2+ voltage-gated channels. We therefore predicted that if $MnCl_2$ is made available to the brain immediately following injury-induction from exposure to blast, uptake of $MnCl_2$ would increase due to the effect of the injury on these calcium channels. By changing the time cycle of availability, contrast-enhancement of the brain would be more evident by visual inspection and quantifiable by MRI.

Therefore, a new study series examined MEMRI in animals where injections were administered immediately following blast exposure (100ul of a 100mM solution of MnCl2 was injected IP five minutes post-blast). MR imaging was performed longitudinally during 30 days.

At each imaging time point following blast, uptake of MnCl2 by the mouse brain resulting from increased flux of MnCl2 through voltage-gated calcium channels was evident. For this optimization study, the MRI at 6hr post-blast showed a marked positive contrast in ventricles and peri-ventricular areas (Figure 53) when compared to Sham (Figure 54). At 24hr, positive contrast was disseminated throughout the brain and lingered for several days. At 7d and after, detectable levels for all imaged groups showed reduced values, suggesting partial clearing of the MnCl agent from the tissues under observation and excreted by the body.

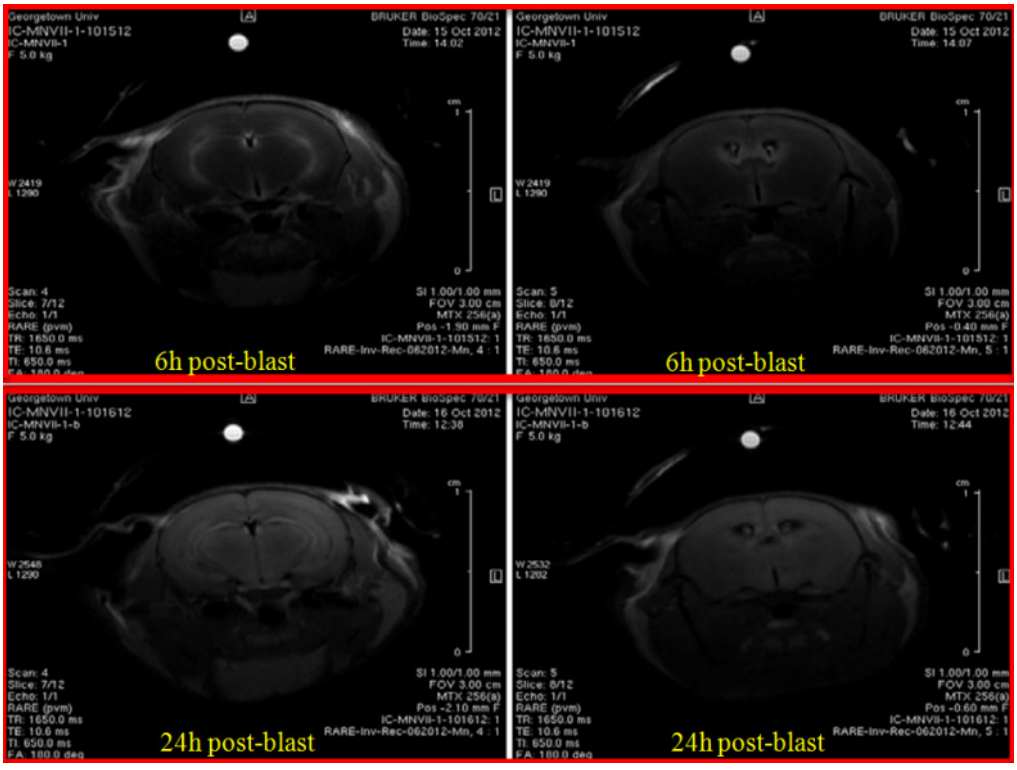

Figure 53. Representative MEMRI in blast exposed (NP) animals. MnCl2 was injected immediately after blast exposure (5 minutes). The white circle above the brain is the phantom used for normalization of image contrast.

In contrast, MR images of sham mice did not show this enhancement (Figure 28).

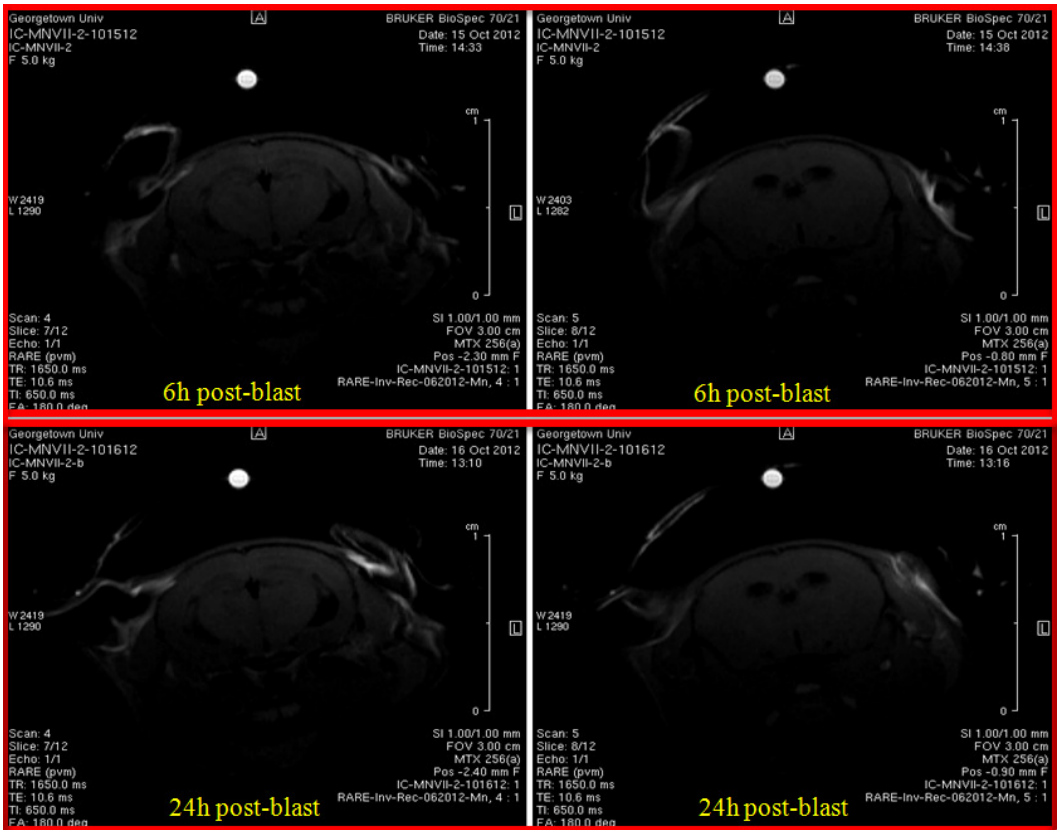

Figure 54. Representative MEMRI in sham animals. MnCl2 was injected immediately after blast exposure (5 minutes). The white circle above the brain is the phantom used for normalization of image contrast.

From the initial experiments with post-blast injections of MnCl agent, it was determined that the concentration of contrast agent administered may have resulted in morbidity and in some cases death (although causality was not established).

To reduce potential $MnCl_2$ toxicity, the dose of contrast agent was reduced for all experiments following December 2012 (50ul of a 100mM solution of $MnCl_2$ instead of 100ul). This reduced dose injected intra-peritoneally still provided sufficient contrast agent to permit adequate enhancement in MR images. In addition, this low dose reduced morbidity and mortality of the mice compared to the higher volume of 100mM solution (again, causality not established).

Quantification of Contrast in Specific Areas of the Brain using Measurements Normalized to the $MnCl_2$ Phantom

Mild neurotrauma from blast exposure followed by injection of MnCl2 results in a prominent

positive contrast enhancement in all regions of the brain as visualized by MRI in TBI mice compared to shams. Early changes in image contrast (enhancement) after exposure to low level blast start in ventricular and periventricular regions from 6hr to 2d time points. At 24hr following blast, contrast is prominent throughout the brain with the highest levels observed in the fourth ventricle, medial vestibular nucleus, principal sensory trigeminal nucleus (ventrolateral part), and the cortex. Presumably, this change is the result of increased calcium uptake and/or glial activation after exposure to shockwaves.

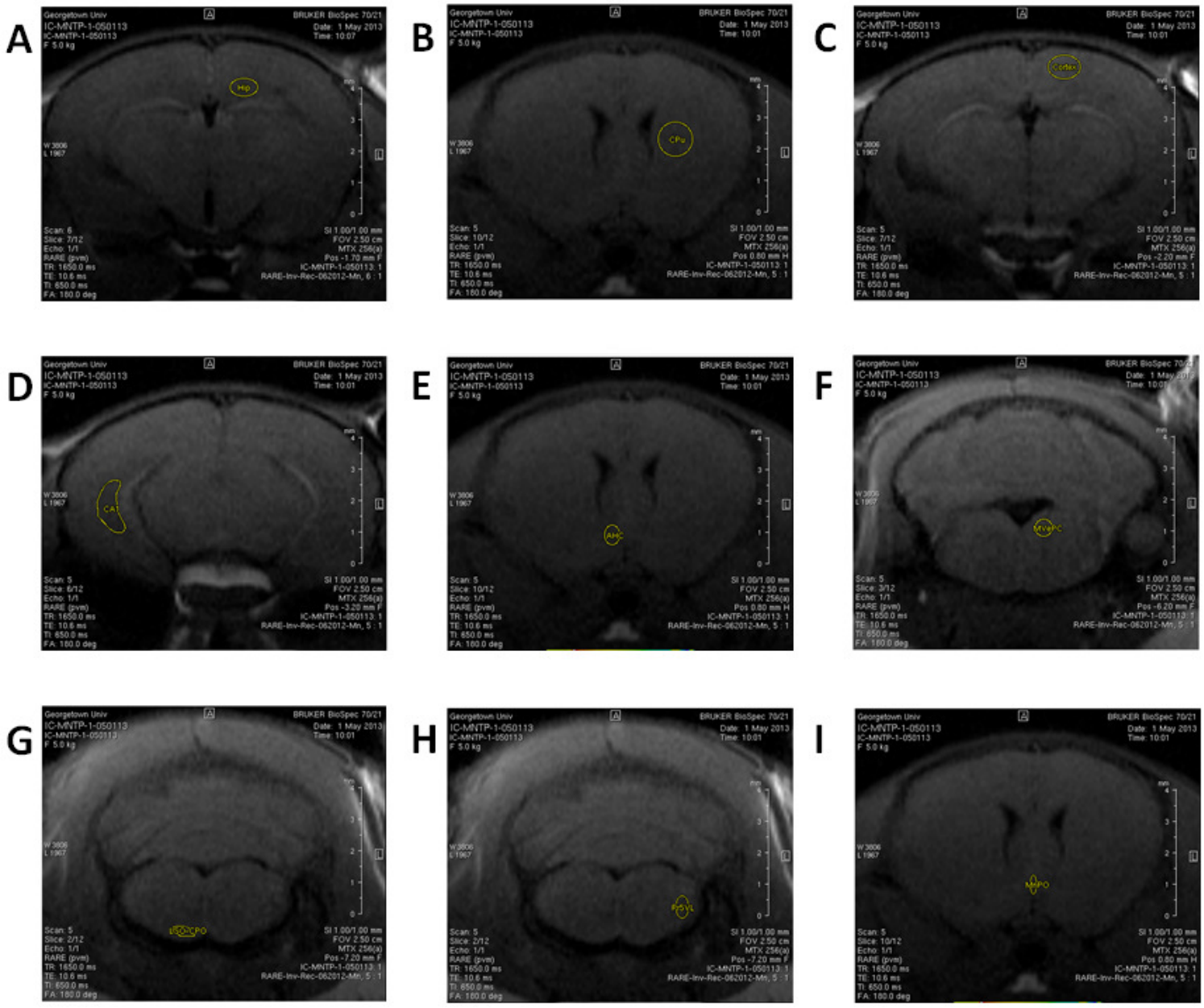

Figure 55. Regions of interest definition for various locations in the brain: A) Hippocampus (Hip), B) Caudate Putamen (CPU), C) Cortex, D) Regio Superior Hippocampus (CA1), E) Anterior Nucleus Hypothalamus (AHC), F) Medial Vestibular Nucleus (MVePC), G) Lateral Superior Olivary Nucleus Caudal Periolivary Nucleus (LSO-CPO), H) Principal Sensory Trigeminal Nucleus Ventrolateral Part (Pr5VL), and I) Median Preoptic Nucleus (MnPO), (not pictured: Cerebellum).

Several of these regions of interest (ROI) were defined for further quantitative analysis. Selected for propensity for injurious outcomes during mechanical head trauma and functional importance to cognition, memory, motor function, and behavior, these regions included the Cortex, Cerebellum, Hippocampus (Hip), Caudate Putamen (CPU), Medial Vestibular Nucleus (MVePC), Principal Sensory Trigeminal Nucleus Ventrolateral Part (Pr5VL), Lateral Superior Olivary Nucleus Caudal Periolivary Nucleus (LSO-CPO), Regio Superior Hippocampus (CA1), Anterior Nucleus Hypothalamus (AHC), and Median Preoptic Nucleus (MnPO) (Figure 55).

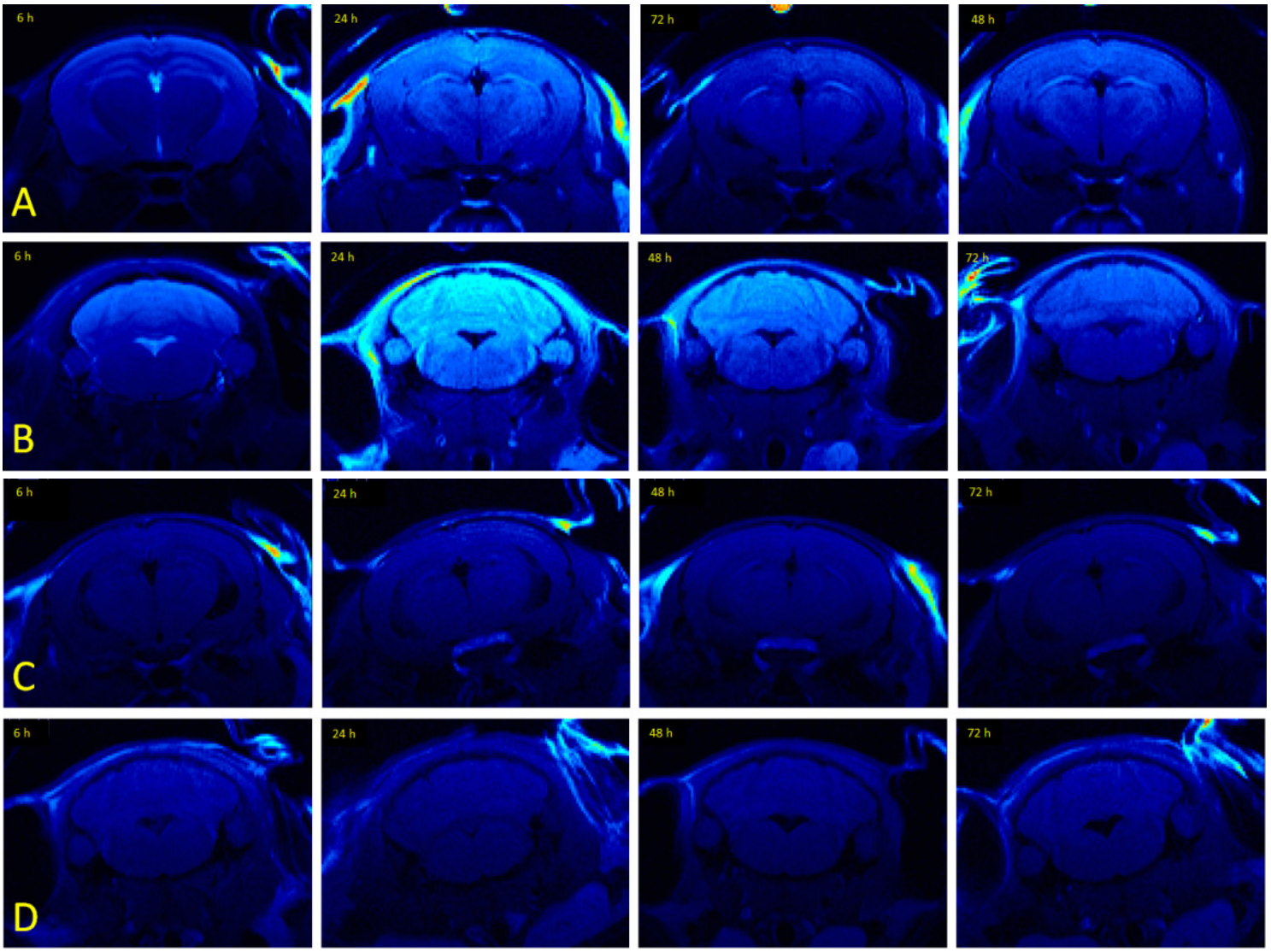

Figure 56. False color conversion of representative phantom-normalized MEMRI images at time points 6hr, 1d, 2d, and 3d from blast-exposed animals at different coronal section locations (A, B), and sham animals at the corresponding coronal section locations (C, D). False color conversion of single-color MRI provides wider color-spectrum visualization of changes in contrast.

In all brain regions considered, each NP animal has increased MEMRI intensity for at-least one or more time points collected, with contrast markedly increasing at the 24hr time point (compared to shams, Figure 56). The temporal profile of the MEMRI intensity following exposure to blast

shows the highest signal intensity at the 24 and 48hr time points (Figure 57). This elevated signal is present for several days, and by the 14d time point, both a reduction in differential signal between blast-exposed and sham animals and a general reduction in signal across all animals groups is apparent. As with previous experimental series, this may suggest clearing of the agent from the body following day 7.

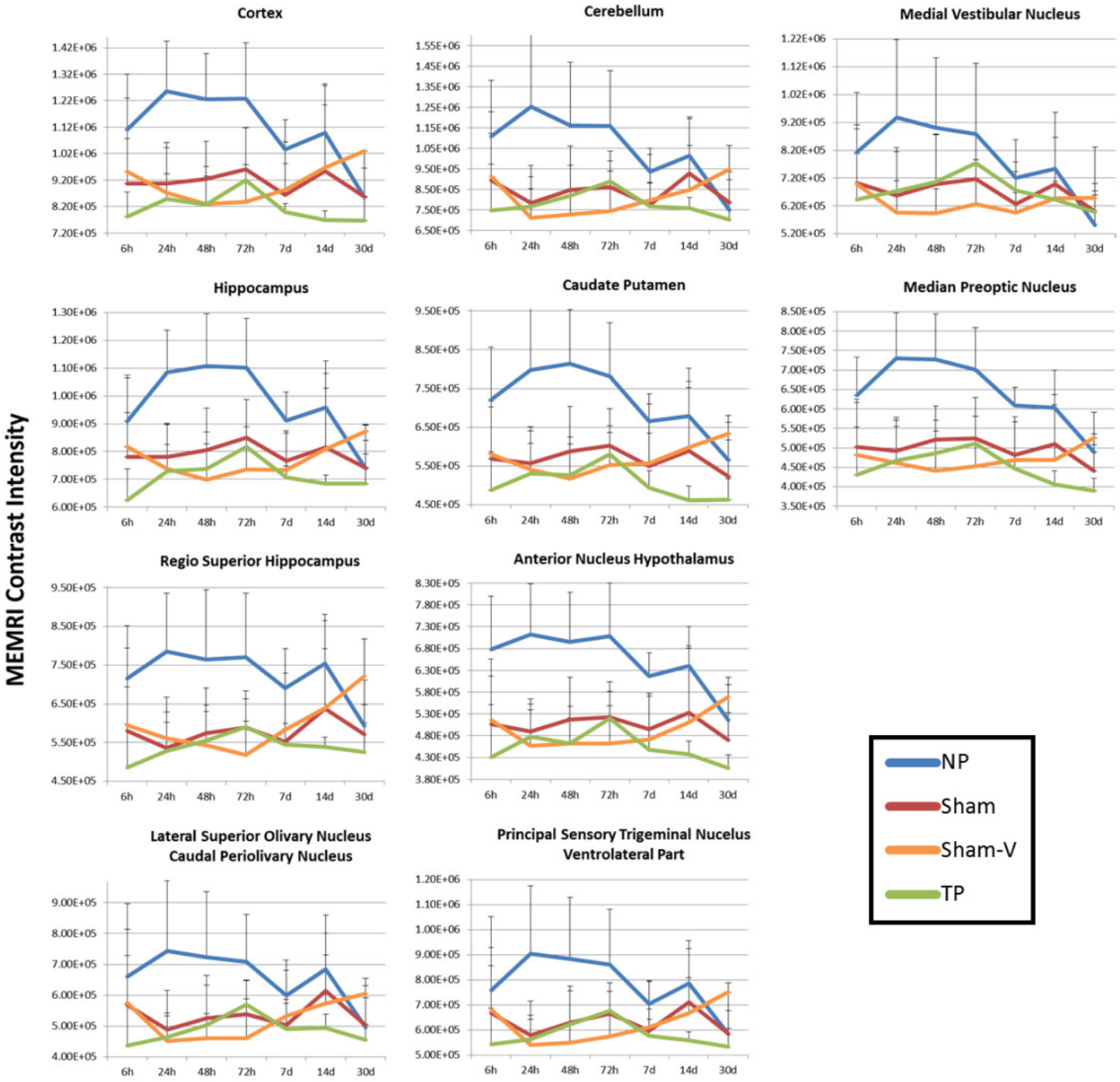

Figure 57. MnCl2-MRI contrast intensity plots with individual brain regions broken out showing mean values and standard deviation. Plots show normalized intensity (arbitrary units) over a period of 30 days post-exposure (NP=Blast with no protection; n=12, Sham=Sham; n=9, Sham-V=Sham with vehicle injection; n=4, TP=Blast with torso protection; n=5).

Figure 57 shows quantitative MnCl2-MRI contrast intensity values for each experimental condition including torso protection separated by individual brain region of interest (ROI). The general NP-response trend follows that most brain regions have highest signal intensity at 24 and 48hr. In contrast, TP animals exhibit a different MnCl2 uptake kinetics with a slow upward drift in signal enhancement between 6hr and 72hr. However, it's evident that presence of torso protection may be involved in reducing the injury response and subsequent elevations in positive signal contrast over the 24 to 48hr period.

Key Accomplishments:

Histology

- Histological collection and analysis of samples consisting of time points 1, 3, 7, 14, and 30 days post blast.
- Immunostaining and quantification for inflammation related markers (e.g., CD68, IbaI, and GFAP) was initiated under the project, but additional work is needed in these areas. Significant signal detected in the visual pathway (i.e., optic tract, superior colliculus) and cerebellum.

Immunoprofiling

- Multiplex analysis of protein expression for the following markers (i.e., Gro-α, G-CSF, IL-β, IL-10, IL-6, TNF-α, VEGF-A, IL-2, MCP-1) in different brain regions, and serum over a period of 30-days. Notable differences identified between torso shielded animals and other groups that suggest chronic alterations in chemokines in the serum and brain in torso protected animals.

MRI Imaging

- >100 MRI image datasets acquired.
- Characterized $MnCl_2$ phantom mimicking physiologically relevant contrast agent concentrations. The known concentration phantom is being compared to tissue intensity for the quantification of contrast agent uptake in brain tissue.
- The PIRL at the GUMC acquired a custom-designed stereotaxic holder to fit their new "state-of-the-art" 4-channel phased-array radiofrequency mouse brain coil and corresponding transmit volume coil to perform parallel MR imaging which allowed for MEMRI of high resolution and short imaging times.
- Optimization of $MnCl_2$ enhanced MRI (MEMRI) has yielded robust signal-differences globally throughout the brain between NP, TP, and Sham mice.

Functional Outcome

- A set of mild/moderate blast exposed GFAP-luciferase transgenic animals (FVB/N- Tg(GFAP-luc)-Xen strain) and shams tested in Rotarod, open field, and active

avoidance tasks. These animals exhibited the same trends as previously reported (Cernak, Merkle et al., 2011). No difference was detected between C57BL6J animals wearing a surrogate outer tactical vest (OTV) and those which were unprotected.

Reportable Outcomes

- Planned publication of the GFAP-luciferase IVIS imaging and functional analysis. Tentatively titled "Analysis on Neurological Outcome in Mice with Traumatic Brain Injury".
- Planned publication of manuscript describing the MnCl2-enhanced MR imaging results and time-corresponding assay results.

Conclusions

Our results support the hypothesis that there is a significant systemic influence in blast-induced neurotrauma. MRI imaging studies support the hypothesis that there is significant reactive gliosis at after blast injury. Histological analyses show temporal and spatial patterns of activated microglia in the brain after blast injury. Immunoassays reveal temporal differences in expression of cytokines and chemokines in the blood and brain.

Shock-wave exposure to the torso has a significant impact (i.e., exacerbates) on the brain's response to blast. Data from non-protected and torso-protected studies suggests that shock-wave exposure to the torso alone: 1) elicits a systemic proinflammatory response (i.e., IL-1β), 2) stimulates inflammatory response in the brain (i.e., CD68 and IBA-1 immuno), and 3) exacerbates the brains response to blast and brain injury (i.e., MEMRI). Torso shielded mice had much less pathological calcium mobilization in the brain and many physiological responses were qualitatively similar to sham (non-exposed) animals. Interestingly, we see some significant differences in expression of CXCL-1, G-CSF, IL-6 between torso-shielded and non-shielded animals suggesting an important neuroimmune interaction between the brain and systemic system. These findings suggest that blast exposure to the body elicits a significant pro-inflammatory response as a result of tissue and organ damage and that the cellular and cell secretions may cross the blood-brain barrier (BBB) and exacerbate injury response in the brain. Imaging results also demonstrate that acute/subacute enhanced calcium mobilization occurs primarily as a result of blast exposure to the torso and not necessarily to the head. This critical result highlights the importance of torso protection in armor design to protect against the negative impact of blast exposure.

Our findings may lead to new drug targets aimed to reduce the acute-subacute enhanced calcium mobilization in the brain as well as reduction in proinflammatory systemic response. Lastly,

imaging results suggest use of MEMRI as a possible diagnostic measure for blast exposure, and glial activation may be possibly exploited as an early biomarker of mild TBI.

Administrative

- Subcontract reporting from Georgetown University and Johns Hopkins University was completed coordinated by Laura Mercer, Subcontracts JHU Representative
- Bi-weekly team telecons
- Monthly reviews with Michelle Murray, Financial Manager
- List of Personnel Receiving Funding:
    - Johns Hopkins University Applied Physics Laboratory
        - Brock Wester, Principal Investigator
        - Andrew Merkle
        - Ibolja Cernak
        - Michele Schaefer
        - Nathan Boggs
        - Michele Murray
        - Raleigh Linville
        - Daniel Pham
        - Charles Schuman
        - Howard Conner
        - Quang Luong
        - Chris Bradburne
        - Ryan Murphy
        - Elaine Slujtner
        - Robert Armiger
        - Neal Bachtell
        - Thomas Baldwin
        - Donald Carey
        - Marvin Carr
        - Anthony Coakley
        - Ian Courtney
        - Kyle Cutler
        - Christopher Dooley
        - Rodney Duley
        - Henry Graham
        - Rebecca Griffiths
        - Theresa Grissom
        - Paul Gush
        - Theresa Hawkins
        - Louis Judge
        - Heather Kauffman
        - Lorayne Kauffman

- Janis Long
- Margo Mildvan
- Pamela Randolph
- Caitlyn Ryan
- Anshu Saksena
- Candece Seiling
- Michele Tranter
- Robin Walker
- Ian Wing

• Johns Hopkins University
- Vassilis Koliatsos
- Leyan Xu

• Georgetown University Medical Center
- Chris Albanese
- Olga Rodriguez
- YiChien Lee

• Children's National Medical Center
- Stanley Fricke

References

Cernak, I. (2010). "The importance of systemic response in the pathobiology of blast-induced neurotrauma." Front Neurol **1**: 151.

Cernak, I., A. C. Merkle, et al. (2011). "The pathobiology of blast injuries and blast-induced neurotrauma as identified using a new experimental model of injury in mice." Neurobiol Dis **41**(2): 538-551.

Chang et al. (2008). "The extracellular calcium-sensing receptor (CaSR) is a critical modulator or skeletal development." Science of Signals 1(35).

Chattopadhyay et al. (1999). "Evidence for extracellular calcium-sensing receptor mediated opening of an outward K+ channel in a human astrocytoma cell line (U87)." Glia 26(1): 64-72.

Effgen et al. (2012). "A multiscale approach to blast neurotrauma modeling: part II: methodology for inducing blast injury to in vitro models." Frontiers in Neurology 3(23): 1-10.

Fagan, S. C., D. C. Hess, et al. (2004). "Targets for vascular protection after acute ischemic stroke." Stroke **35**(9): 2220-2225.

Huston at al. (2012) "The Vagus Nerve and the Inflammatory Reflex: Wandering on a New Treatment Paradigm for Systemic Inflammation and Sepsis." Surgical Infections 13(4): 187-193.

Jadhav, V., G. Matchett, et al. (2007). "Inhibition of Src tyrosine kinase and effect on outcomes in a new in vivo model of surgically induced brain injury." J Neurosurg **106**(4): 680-686.

Koliatsos, V. E., I. Cernak, et al. (2011). "A mouse model of blast injury to brain: initial pathological, neuropathological, and behavioral characterization." J Neuropathol Exp Neurol **70**(5): 399-416.

Lyons, A., Lynch, A.M. et al. (2009). "Fractalkine-induced activation of the phosphatidylinositol-3 kinase pathway attenuates microglial activation in vivo and in vitro." J Neurochem 110: 1547-1556.

Nag, S., M. R. Eskandarian, et al. (2002). "Differential expression of vascular endothelial growth factor-A (VEGF-A) and VEGF-B after brain injury." J Neuropathol Exp Neurol **61**(9): 778-788.

Nag, S., J. L. Takahashi, et al. (1997). "Role of vascular endothelial growth factor in blood-brain barrier breakdown and angiogenesis in brain trauma." J Neuropathol Exp Neurol **56**(8): 912-921.

Nielsen et al. (1997) "Inhibition of PTH Secretion by Interleukin-1β in Bovine Parathyroid Glands in Vitro is associated with an Up-Regulation of the Calcium-Sensing Receptor mRNA." Biochemical and Biophysical Research Communications 238(3): 880-885.

Owens, B. D., J. F. Kragh, Jr., et al. (2008). "Combat wounds in operation Iraqi Freedom and operation Enduring Freedom." J Trauma **64**(2): 295-299.

Saeed et al. (2005) "Cholinergic stimulation blocks endothelial cell activation and leukocyte recruitment during inflammation." Journal of Experimental Medicine 201(7): 1113-1123.

Sheng, J. G., S. H. Bora, et al. (2003). "Lipopolysaccharide-induced-neuroinflammation increases intracellular accumulation of amyloid precursor protein and amyloid beta peptide in APPswe transgenic mice." Neurobiol Dis **14**(1): 133-145.

Yamada et al. (2013) "A novel objective classification of reactive microglia following hypoglossal axotomy using hierarchical cluster analysis." The Journal of Comparative Neurology 521(5): 1184-1201.

Yano et al. (2004) "Calcium-sensing in the brain." Cell Calcium 35(3): 257-264.

Zhang, Z. G., L. Zhang, et al. (2000). "VEGF enhances angiogenesis and promotes blood-brain barrier leakage in the ischemic brain." J Clin Invest **106**(7): 829-838.

Appendix – Published Papers

Cernak, I., A. C. Merkle, et al. (2011). "The pathobiology of blast injuries and blast-induced neurotrauma as identified using a new experimental model of injury in mice." Neurobiol Dis **41**(2): 538-551.

Neurobiology of Disease 41 (2011) 538–551

Contents lists available at ScienceDirect

Neurobiology of Disease

journal homepage: www.elsevier.com/locate/ynbdi

The pathobiology of blast injuries and blast-induced neurotrauma as identified using a new experimental model of injury in mice

Ibolja Cernak [a,*], Andrew C. Merkle [a], Vassilis E. Koliatsos [b], Justin M. Bilik [a], Quang T. Luong [a], Theresa M. Mahota [a], Leyan Xu [b], Nicole Slack [a], David Windle [a], Farid A. Ahmed [a]

[a] Biomedicine Business Area, National Security Technology Department, Johns Hopkins University Applied Physics Laboratory (JHU/APL), Laurel, MD, USA
[b] Department of Pathology, Johns Hopkins University School of Medicine (JHU SOM), Baltimore, MD, USA

ARTICLE INFO

Article history:
Received 5 August 2010
Revised 5 October 2010
Accepted 27 October 2010
Available online 11 November 2010

Keywords:
Blast
Blast injury
Traumatic brain injury
Blast-induced neurotrauma
Mouse
Behavior
Motor function
Cognitive function
PCR
Inflammation

ABSTRACT

Current experimental models of blast injuries used to study blast-induced neurotrauma (BINT) vary widely, which makes the comparison of the experimental results extremely challenging. Most of the blast injury models replicate the ideal Friedländer type of blast wave, without the capability to generate blast signatures with multiple shock fronts and refraction waves as seen in real-life conditions; this significantly reduces their clinical and military relevance. Here, we describe the pathophysiological consequences of graded blast injuries and BINT generated by a newly developed, highly controlled, and reproducible model using a modular, multi-chamber shock tube capable of tailoring pressure wave signatures and reproducing complex shock wave signatures seen in theater. While functional deficits due to blast exposure represent the principal health problem for today's warfighters, the majority of available blast models induces tissue destruction rather than mimic functional deficits. Thus, the main goal of our model is to reliably reproduce long-term neurological impairments caused by blast. Physiological parameters, functional (motor, cognitive, and behavioral) outcomes, and underlying molecular mechanisms involved in inflammation measured in the brain over the 30 day post-blast period showed this model is capable of reproducing major neurological changes of clinical BINT.

Introduction

The main blast effects of explosive devices are: 1) primary (caused by the blast wave itself); 2) secondary (caused by the fragments of debris propelled by the explosion); 3) tertiary (acceleration of whole or part of the body by the blast wind); and 4) quaternary (flash burns as a consequence of the transient but intense heat of the explosion (Mellor, 1988; Owen-Smith, 1981). Accumulating experimental and clinical evidence shows that blast wave can cause brain injury without inflicting penetrating wounds of the head (i.e., secondary blast effects) or "coup-countercoup" (i.e., acceleration/deceleration via tertiary blast effects) (Cernak and Noble-Haeusslein, 2010; Warden et al., 2009). While much effort has been devoted to the mitigation of other types of blast injury, it is only recently that the importance of primary blast-induced neurotrauma (BINT) has been recognized (Cernak et al., 1999; Ling et al., 2009; Martin et al., 2008; Warden et al., 2009).

One of the key prerequisites to understanding primary BINT and its sequelae is accurate characterization of the blast environment. Improvised Explosive Devices (IEDs), observed in Operation Iraqi Freedom (OIF) and Operation Enduring Freedom (OEF), vary in type and deployment with the primary source for explosive material being ordnance, particularly artillery shells. The blast generated from these IEDs is strongly governed by factors such as fill chemistry, scale, casing, shape, initiation, and immediate surroundings. Because of the range of possible blast threat scenarios, it is critical to identify a representative set of threat conditions for investigation and laboratory simulation, thus develop a military-relevant model that replicates the vital mechanisms of injury seen in theater (Cernak and Noble-Haeusslein, 2010).

Primary BINT is caused by complex mechanisms of systemic, local, and cerebral responses to blast exposure (Cernak and Noble-Haeusslein). Thus, understanding this unique pathological entity requires a holistic approach, taking into account all vital injury mechanisms, not only those induced by a direct interaction between the shock wave and the head. The current experimental models used in an attempt to study primary BINT differ widely, and include TBI models that deliver direct impact to the head without involving the other parts of the body (such as the fluid-percussion, controlled cortical impact, and air-gun-type compressed air-delivered models)

* Corresponding author. Biomedicine Business Area, Johns Hopkins University Applied Physics Laboratory, 11100 Johns Hopkins Rd., Mail Stop MP2 N108, Laurel, MD 20723, USA. Fax: +1 443 778 5889.
E-mail address: ibolja.cernak@jhuapl.edu (I. Cernak).
Available online on ScienceDirect (www.sciencedirect.com).

0969-9961/$ – see front matter © 2010 Elsevier Inc. All rights reserved.
doi:10.1016/j.nbd.2010.10.025

(Dennis et al., 2009; Dewitt and Prough, 2009), as well as those that expose the whole body to overpressure (such as the shock tube and blast tube models or the open field blast conditions) (Bauman et al., 2009; Cernak et al., 1996, 2001; Long et al., 2009; Saljo et al., 2009) (Axelsson et al., 2000; Cernak et al., 1990). The major challenge in modeling primary BINT using experimental animals is reproducing the essential components of military-relevant blast conditions while replicating pathological components or phases of clinical BINT seen in patients. Therefore, the first objectives of this study were to develop a highly controlled mouse model of blast injuries, and to establish the parameters necessary to cause reproducible mild, moderate, or severe trauma. Having established these parameters, we further characterized the pathobiology of mild and moderate BINT, the most frequent injury groups encountered in clinical practice, based on physiological and functional parameters as well as molecular mechanisms of inflammation in the brain.

Materials and methods

All protocols involving the use of animals complied with the Guide and Care and Use of Laboratory Animals published by NIH (DHEW publication NIH 85-23-2985), and were approved by the Johns Hopkins University Animal Use Committee.

The injury device

The Johns Hopkins University Applied Physics Laboratory (JHU/APL) has developed a modular, multi-chamber shock tube capable of reproducing complex shock wave signatures seen in theater and tailoring pressure wave signatures. The single-driver shock tube system generated dynamic overpressure loading conditions necessary to induce mild, moderate, and severe levels of lethality in mice. The instrumented system allowed for direct measurement and calculation of the various shock loading characteristics, including static pressure, total pressure, and overpressure impulse. The 14.6 cm (6″) diameter pneumatic shock tube system (Fig. 1) consisted of both a driver (pressurized) and a driven (ambient) section. Before each test, a diaphragm was inserted between the two sections, creating a closed volume driver section that would allow pressurization. The driver section, which initially contained ambient air, was pressurized with helium gas until the pressure differential between the driver and driven sections exceeded the material failure threshold of the diaphragm thus initiating rupture. We varied the diaphragm rupture pressure levels by selecting various combinations of Kapton and polyethylene sheets. Upon diaphragm rupture, a shock wave propagated down the length of the shock tube.

Side mounted pressure sensors, used to record the static pressure and wave propagation, were installed at five locations along the shock tube inner wall. All sensor data were collected at a frequency of 200 kHz, and the data was post-processed to remove high frequency noise components. Fig. 2 provides characteristic traces of pressure data collected from sensors located in the driver and driven sections of the shock tube, including information about the peaks' duration. The first sensor, PS1, was located in the driver section and was used to determine the initial conditions prior to diaphragm rupture. Note that the pressure did not immediately drop off after the diaphragm ruptured because pressure sensor PS1 is located 47.5 cm (18.70″) upstream from the diaphragm. As noted in Fig. 2, the pressure sensor next to the diaphragm (PS2) was used to determine the time of diaphragm rupture, whereas the pressure sensor in the middle of the driven section (PS3) measured the magnitude of the static pressure and the duration of the pressure pulse. While a side mounted pressure sensor can only measure static pressures, a pressure probe pointed into the flow can be used to measure the total pressure. The total pressure is the stagnation pressure for compressible flow where the flow is brought to rest adiabatically, and it more closely represents the pressure that the specimen experiences when facing the shock wave. To measure the total pressure for each test condition, shock tube tests were conducted with a pressure probe inserted in place of the small animal specimen. Analytical equations can provide closed form solutions for the determination of shock tube parameters, such as the static pressure and total pressure. These solutions can be used to confirm the pressure sensor results for specific test conditions and to determine pressure values in lieu of performing experiments to measure the values directly.

Due to the nature of the shock tube tests, equations for unsteady wave motion within a compressible fluid can be used to calculate shock tube parameters based on initial conditions of the shock tube

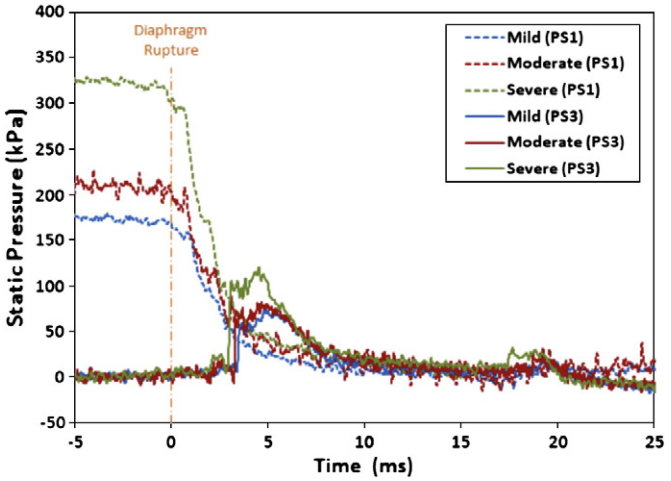

Fig. 2. Pressure data collected from shock tube tests representative of typical mild, moderate, and severe shock wave loads. The pressure traces in blue show the evacuation of air from the driver section recorded by a static pressure sensor, P1, located 47.5 cm upstream from the diaphragm. The traces in green and red show the response of static pressure sensors at two different locations in the driven section, 8.5 and 452 cm downstream from the diaphragm, respectively.

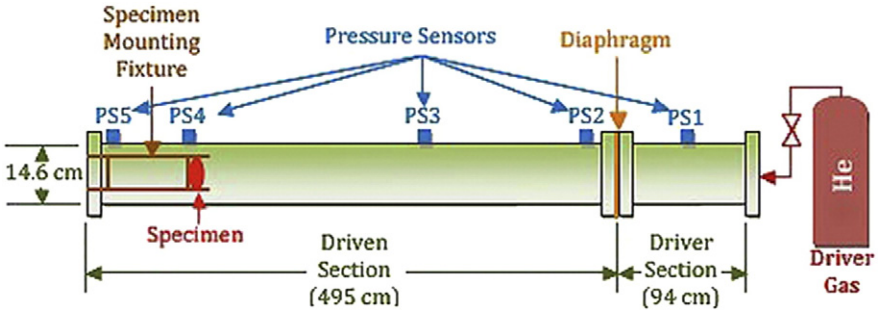

Fig. 1. Schematic representation of the shock tube system.

(Anderson, 2003; Ben-Dor et al., 2001). The total pressure for compressible fluids can be calculated from the following:

$$p_{\text{total}} = p_2\left(1 + \frac{\gamma_1 - 1}{2}M_2^2\right)\left(\frac{\gamma_1}{\gamma_1 - 1}\right) \quad (1)$$

where p_2 is the static pressure in the region immediately following the shock wave front, γ_1 is the specific heat ratio for the fluid (air) in the driven section, and M_2 is the Mach number of the induced mass motion behind the shock front.

The static pressure for (1) can be determined by solving the following equation for p_2:

$$\frac{p_4}{p_1} = \frac{p_2}{p_1}\left\{1 - \frac{(\gamma_4 - 1)\left(\frac{a_1}{a_4}\right)\left(\frac{p_2}{p_1} - 1\right)}{\sqrt{2\gamma_1\left[2\gamma_1 + (\gamma_2 + 1)\left(\frac{p_2}{p_1} - 1\right)\right]}}\right\}^{\left[\frac{-2\gamma_4}{(\gamma_4 - 1)}\right]} \quad (2)$$

where p_1 is the pressure in the driven section, p_4 is the pressure in the driver section, γ_1 is the specific heat ratio for the fluid (air) in the driven section, γ_4 is the specific heat ratio for the fluid (air-helium mixture) in the driver section, a_1 is the speed of sound through the fluid in the driven section, and a_4 is the speed of sound through the fluid in the driver section.

Induction of injury

Mice (C57/Bl6; male; 3–4 months; 25.22 ± 1.96 g; Jackson Laboratories; $n = 309$ total) had access to food and water *ad libitum*. Animals were anesthetized with 4% isoflurane evaporated in a gas mixture containing 30% oxygen/70% nitrous oxide and applied through a nose-mask. The animals were allowed to breathe spontaneously without tracheal intubation. The mouse was mounted either in supine or prone position to the animal holder, a metal mesh fixture that could be secured inside the driven section of the shock tube. The fixture positioned the specimen at 53 cm (20.87″) upstream from the driven section opening, ensuring that the only a well-formed incident shock wave loaded the animal and that potential rarefactions from the tube opening were minimized. The neck, head, torso, and abdomen of the animal were fixed to the animal holder aiming to avoid any movement, thus tertiary blast effects.

Two hundred seventy shock tube tests were conducted in this study (Table 2), and each test was categorized as causing mild, moderate, or severe levels of lethality in mice. The initial loading conditions were approximated based on the Bowen curve of blast lethality and lung damage for mice (Bowen et al., 1968b; Richmond et al., 1967) and tested in preliminary experiments (not shown). Static pressure measurements from tests within each mild, moderate, or severe category were averaged and used to determine the rupture pressure, peak static pressure, and impulse. The rupture pressures were then used to calculate the static pressure and total pressure from the analytical equations. The results from the static pressure measurements and analytical calculations are listed in Table 1. The table also includes total pressure measurements obtained from the pressure probe tests. The data in Table 1 provides insight into the shock wave parameters that cause mild, moderate, and severe levels of lethality in mice.

Groups

The animals were divided into nine groups. Table 2 summarizes the group characteristics including the number of animals assigned into each group, the task description, and the main goals of the experiments.

Table 1
Shock wave parameters determined with analytical calculations and direct measurements. The blast injury severities refer to animals in supine position.

Parameter	Units	Mild		Moderate		Severe	
		Mean	SD	Mean	SD	Mean	SD
Measured rupture pressure	psig	26.5	2.1	30.9	2.5	42.8	4.6
	kPag	183	14	213	17	295	32
Measured static pressure	psig	9.9	1.2	11.0	1.4	15.3	2.4
	kPag	68	8	76	10	105	17
Calculated static pressure	psig	11.9	N/A	13.7	N/A	18.3	N/A
	kPag	82	N/A	94	N/A	126	N/A
Measured total pressure	psig	14.9	N/A	18.0	N/A	27.6	N/A
	kPag	103	N/A	124	N/A	190	N/A
Calculated total pressure	psig	15.1	N/A	17.9	N/A	25.7	N/A
	kPag	104	N/A	123	N/A	177	N/A
Measured impulse	Psig-ms	50	5	51	21	72	17
	kPag-ms	345	34	352	145	496	117

Acute neurological evaluation, mortality, and blast injury severity

In Group I, the anesthetized animals were subjected to various levels of injury, depending on the pressure applied to the driver section of the shock tube, with the gauge pressure, i.e., the pressure relative to the local atmospheric or ambient pressure, ranging from 172 to 310 kPag (25–45 psig). Immediately following injury, anesthesia was discontinued and the animals were maintained on room air alone. No resuscitation was performed after trauma. Acute neurological recovery was assessed in all mice by recording indicators of sensorimotor function: recovery of hind paw-flexion following the

Table 2
Experimental groups used in the current study.

Group	Animal number	Description	Purpose
I	100	Supine position; exposed to shockwaves of graded intensity	Establishing mortality rates, and injury severity categories (mild, moderate, and severe)
II	100	Prone position; exposed to shockwaves of graded intensity	Establishing mortality rates, and injury severity categories (mild, moderate, and severe)
III	15	Supine position; exposed to mild intensity shockwave	Vital function and functional (motor, cognitive, and behavior) outcome measurements
IV	15	Supine position; exposed to moderate intensity shockwave	Vital function and functional (motor, cognitive, and behavior) outcome measurements
V	20	Supine position; exposed to mild intensity shockwave	Inflammatory gene response profiling in the brain measured at 1, 3, 7, 14, or 30 days after exposure ($n = 4$ per time point)
VI	20	Supine position; exposed to moderate intensity shockwave	Inflammatory gene response profiling in the brain measured at 1, 3, 7, 14, or 30 days after exposure ($n = 4$ per time point)
VII	15	Sham control mice; Supine position	Anesthetized mice placed in the animal holder were left outside adjacent to the shock tube during the detonation without being exposed to the shock wave; used as sham controls for vital function measurements and functional outcome tests
VIII	20	Sham control mice; Supine position	Anesthetized mice placed in the animal holder were left outside adjacent to the shock tube during the detonation without being exposed to the shock wave; used as sham controls for gene profiling
IX	4	Naïve mice	Anesthetized and sacrificed for inflammatory gene profiling in the brain.

gradual application of pressure and the latency to recovery of the righting reflex. The mortality rate was assessed at 24 h post-trauma.

Blast injury severity in animals with lethal outcome and in survival animals in Groups III and IV at the end of the 30-day post-exposure period was performed using a slightly modified Pathology Scoring System (PSS) for Blast Injuries according to Yelverton (1996). The elements of the Injury Score (IS) equations were defined as:

- E - extent of injury to organ or organ system components;
- G - injury grade, which includes the surface area of the lesion or the percentage of the organ traumatized or the number of fractures in the case of the skeletal system;
- ST - severity type elements, classifying the type of the worst-case lesion to an organ or system; and
- SD - severity depth elements, indicating the depth or degree of disruption of the worst-case lesion.

The PSS/ IS used as quantitative measure of blast injury severity was defined as:

$$IS = (E + G + ST) \times SD.$$

Physiological parameters

Body weight (BW) measurements were performed before, and at 3, 5, 7, 10, 14, 18, 21, 25, and 30 days post-exposure.

Multiple vital signs were measured non-invasively using the MouseOx® Pulse Oximeter (Starr Life Sciences Corp., Oakmont, PA) before injury, immediately after, and at 7, 14, 21, and 30 days post-exposure. The measured parameters included: arterial blood oxygen saturation, where the oxygen saturation of hemoglobin is reported after each heartbeat; pulse rate, i.e., heart rate (HR) with a measurement range of 90–900 beat per minute (bpm); respiratory rate (RR) reported every 1.7 s where the value reported is the result of a moving range of the rate of breathing for the 10 previous breath rate measurements; and pulse distention (PD), i.e., a measurement of the distention of the arterial blood vessels (carotid artery) between the sensors due to a cardiac pulse and used as a non-invasive indicator of a blood flow.

Neurological outcome

Motor and cognitive functions were assessed in animals assigned in Groups III, IV, or VII. Motor scoring was performed on days 1, 2, 3, 4, 5, 7, 10, 14, 21, and 30 after blast exposure using the rotarod test, which has been described as being one of the most sensitive tests to detect motor deficits in rodent brain injury (Hamm et al., 1994). Briefly, animals were placed on a rotarod device (Panlab Rota-Rods LE 8200, Harvard Apparatus, Holliston, MA). The mice were allowed to explore the rotarod for 2 min without rotation and then the drum was slowly accelerated to 14 rotations per minute (rpm). The mice were subjected to 2-minute training trials for 7 consecutive days before exposure. The rotarod test was performed by first placing the mice on the rotating drum (25 rpm) for 2 min and then measuring the length of time each animal was able to maintain its balance walking on top of the drum.

Spontaneous exploratory behavior after blast exposure was assessed using the open field test. This test was conducted in a white, opaque rectangular polypropylene arena measuring 45 cm × 45 cm × 40 cm with a lamp positioned 30 cm above the arena and providing 550 lx illumination. Each mouse was placed individually into the center of the arena and allowed to roam freely in the box. The animal's movement was recorded over a 5-min period by using a video camera on 7 consecutive days before injury, and on days 1, 2, 3, 4, 5, 7, 10, 14, 21, and 30 days post-exposure. The tracking program AnyMaze® (Stoelting, Wood Dale, IL) was used to calculate both the frequency and duration of a range of behavior. The parameters included: distance covered (m); mean speed of movement (m/s); number of rearing as a measure of exploratory activity; number of center entries; time spent in the center; and time spent immobile (s). Using MatLab Software (MathWorks, Inc., Natick, USA), the recorded information was processed to establish the pattern of the animal's exploratory activity by calculating a density map of its movement.

Cognitive outcome was measured using the active avoidance procedure, a model in which anxiety, learning, and memory play an important role in the performance of the animals (Martin et al., 2002; Trigo et al., 2008). Briefly, before injury, mice were trained to avoid an aversive stimulus associated with the presentation of a conditioned stimulus (CS) in a two-way shuttle box apparatus (Panlab/Harvard Apparatus Shuttle Box LE918; Harvard Appartus, Holliston, MA). Acquisition and performance of the active avoidance response (AAR) was carried out in the automatically operated and PC-controlled two-way shuttle box with two compartments (20 × 10 cm) connected by a 3 × 3-cm door. The AAR test began 5 min after the animal (one at a time) was placed in the shuttle box. The acquisition was achieved using daily 100-trial sessions for 6 consecutive days. A conventional AAR schedule (Trigo et al., 2008) was used where each trial began with conditioned stimulus (CS: light stimulus of approximately 40 lx, lasting 5 s) switched on in the compartment in which the mouse was placed. The CS preceded in 5 s the onset of the unconditioned stimulus (US: foot shock of 0.2 mA continuously applied to the grid of the floor) and overlapped it for 25 s. Thus, the light was presented in the compartment for 30 s (5 s alone and 25 s together with the US). At the end of the 30-s period, both CS and US were automatically turned off. A conditioned response was recorded when the animal avoided the US by changing from the compartment where the animal received the CS into the opposite compartment within the 5 s after the onset of the CS. A crossing response during the CS was considered being an AAR and terminated the CS, thus preventing US onset. Active avoidance latency (AAL; s) was defined as a period that precedes AAR. A response after US onset, i.e., escape response (ER), terminated both CS and US. Escape response latency (ERL) was defined as the period between foot shock and its termination. Between each trial session, there was an inter-trial interval of 30 s. Animals were subjected to 100-trial active avoidance sessions 7 days before injury, and on 1, 2, 3, 4, 5, 7, 14, 21, and 30 days post-exposure.

Gene expression

For molecular analysis of the brains, mice assigned to Groups V, VI, or VIII ($n = 20$; $n = 4$ per time point) were anesthetized with 2-2-2-tribromoethanol (125 mg/kg, Sigma) and euthanized at 1, 3, 7, 14, and 30 days after mild or moderate BINT. Naïve mice ($n = 4$ per strain) were killed immediately after reaching the surgical level of anesthesia.

Semi-quantitative RT-PCR

Aiming to establish a causal relationship between blast-induced neurological deficits and chronic molecular alterations, outcomes also included evaluation of activation and proliferation of astrocytes and microglia, as well as release of microglial associated inflammatory factors. The inflammatory-related gene response was analyzed based on the expression of: the glial fibrillary acidic protein (GFAP), an indicator of astrocyte reactivity associated with glial scar formation; ED1, a marker for activated microglia and macrophages; myeloid related protein 8 (MRP8, previously called Calgranulin A or S-100 calcium binding protein A8 [S100A8]) expressed in activated macrophages and microglial cells); Osteopontin (OPN), an adhesive glycoprotein acting as a chemoattractant that recruits microglia, macrophage and astrocytes in response to ischemia; and the chemokine CC ligand-2 (CCL2; formerly monocyte chemoattractant

protein-1, MCP-1) implicated in macrophage recruitment into damaged parenchyma after TBI. As a housekeeping gene, we used ribosomal protein L19 (RPL19). Our pilot study (results not shown), aimed at establishing a reliable reference gene for multi-organ response to graded blast injury, confirmed the highest level of stability of RPL19 both in the brain and in the lungs. The stability of RPL19 in comparable conditions and organs was also found in published literature (Boda et al., 2009; Chari et al., 2010; Wan et al., 2010; Zhou et al., 2010).

Total RNA was isolated from the dissected hippocampus and brainstem at different time points followed by BINT (Total RNA Miniprep kit; La Jolla, CA). Total RNA (0.5 μg) was separated by electrophoresis on a 1.2% agarose, 2.2 M formaldehyde gel to evaluate the quality of RNA samples. For cDNA synthesis, 5 μg of total RNA was reverse transcribed using Superscript (GIBCO BRL) and oligo (dT)-primer. The resulting cDNA was amplified by PCR using sense and antisense primers described in Table 3. The amount of synthesized cDNA was normalized by PCR using primer-specific RPL19. PCR reactions were performed using the Applied Biosystems Veriti® 96-well thermal cycler (Applied Biosystems Lt., Carlsbad, CA). Each PCR reaction was repeated at least twice. The thermal cycling parameters were as follows: 1 min 30 s at 94 °C followed by 30 cycles of 30 s at 94 °C, 1 min 30 s at 59 °C, 1 min at 72 °C, and final incubation for 5 min at 72 °C. PCR reaction products were analyzed by agarose gel-electrophoresis. After adjustment of cDNA concentration for each individual sample from control and experimental animals, relative abundances of mRNA for the selected genes were estimated based on the intensity of cDNA bands using Quantity One 1-D Analysis Software (BioRad, Lab., Inc. Hercules, CA). Primers for each gene were located in different exons where possible.

Statistical analysis

Statistical analysis was performed using Sigma Stat 2.03 (SPSS, Chicago, IL, USA) or SPSS 15.0 for Windows (SPSS). All continuous data are expressed as mean ± SD and were analyzed by repeated measures analysis of variance followed by individual Student-Neuman-Keuls test. Gene expression measurements were analyzed by two-way ANOVA and *p*-values for overall effects of time are reported in full to three decimal places. Tukey's post hoc test was used for comparisons between and within individual injury groups and time points, reported as $p<0.05$ or $p< 0.001$. Statistically significance was considered at the 5% level.

Results

Mortality and blast injury severity

Fig. 3 shows the mortality rates in animals at 24 h after being exposed to graded intensity shock waves. A position-dependence of mortality has been established, where the mild intensity shock wave

Table 3
Sense and antisense primer used for RT-PCR.

Name	Species	Gene bank number	Sequence
RPL19	Mouse	BC010710	GGTACTGCCAATGCTCGGAT TCCTTGGACAGAGTCTTGATGA
Osteopontin (Secreted phosphoprotein-1)	Mouse	X13986	ACATGAAGAGCGGTGAGTCTAAG CAGATACCTATCATCTTCCTTACTC
MRP8	Mouse	M83218	ATGCCGTCTGAACTGGAGAAGG CTACTCCTTGTGGCTGTCTTTG
GFAP	Mouse	NM_010277	TGTCAGAAGGCCACCTCAAGAG TCTCTACTCTGCTCATCTTTCCTC
CCL2/MCP1	Mouse	M19681	GAGCTACAAGAGGATCACCAGC CAGTCCGAGTCACACTAGTTCAC
ED1	Mouse	NM_009853	GGAGGTTGTGACGGTACCCAT GCAGCTGAGCAGCCTGTAGC

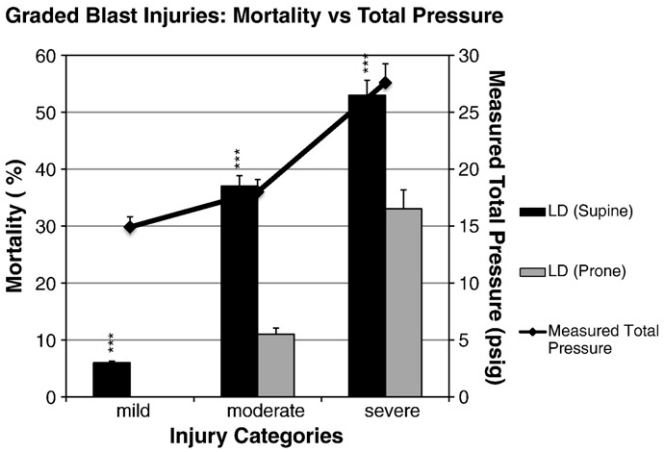

Fig. 3. Mortality rate in relation to the total pressure (expressed as psig) of the blast exposure (solid line). Results are shown as means ± SD. The lethality (LD) was measured in animals positioned either in supine or prone position in relation to the shockwave front. The mortality rate was significantly higher in all animals exposed in supine position to the shockwave, whereas the injury severity was significantly higher in animals exposed in supine position to the shockwave of moderate or severe intensity. ***$p<0.0001$ in comparison of supine vs. prone.

(measured rupture pressure: 183 ± 14 kPa, i.e., 26.5 ± 2.1 psig; measured total pressure: 103 kPa, i.e. 14.9 psig) caused 5% mortality in animals in supine position and no-lethality in animals in prone position. Moreover, after moderate or severe intensity shock exposure, the corresponding mortality rates in supinely positioned animals were 37% and 53%, whereas in prone animals there were significantly ($p<0.001$) lower, i.e., 11% and 33%. Death occurred mostly immediately due to cardiorespiratory depression or within 3 h because of extensive lung damage.

The total scores of blast injury severity (Fig. 4A) in animals in supine position were: 24.44 ± 0.50 PSS after mild intensity blast exposure, 59.27 ± 3.52 PSS in animals exposed to moderate intensity blast, and 83.67 ± 6.33 PSS in animals after severe intensity blast exposure. In comparison, animals in prone position (Fig. 4B) showed less injury severity: 21.25 ± 0.82 PSS after mild blast exposure, 32.05 ± 0.84 PSS after moderate exposure ($p<0.001$ compared to the supine position), and 62.33 ± 4.32 PSS after severe intensity blast exposure ($p<0.01$ versus supine position). The most significant damage had been observed in the lungs regardless of the body position. Heart injuries were more frequent and severe in supinely positioned animals exposed to moderate or severe intensity shock waves, as compared to the corresponding groups of animals placed in prone position (moderate: 5.90 ± 0.30 PSS versus 0; severe: 9.6 ± 0.84 PSS vs. 1.33 ± 0.07 PSS; $p<0.001$) (Fig. 4A and B). On the other side, injuries of abdominal organs, mostly liver and kidneys, were more prominent in animals in prone position vs. those supinely positioned: mild: 2.50 ± 0.01 vs. 0 PSS ($p<0.001$); moderate: 3.50 ± 0.01 vs. 2.45 ± 0.01 PSS ($p<0.05$); severe: 3.80 ± 0.02 vs. 2.38 ± 0.01 PSS ($p<0.01$) (Fig. 4A and B).

Gross pathological observation of the brains following mild blast injury showed an absence of focal lesions, contusion, or subarachnoid hemorrhage. Among the first series of mice included in Groups I and II and exposed to blast of moderate or severe intensity, only few animals, regardless of their position, showed signs of subdural and/or subarachnoid hemorrhage. We assume that these pathological changes were caused by acceleration/deceleration rather than primary blast since after improving the head restrain on the animal holder, no signs of subdural and subarachnoid bleeding were seen.

Physiological parameters

Blast exposure caused significant weight loss in both mild and moderate injury groups, although the changes in body weight were

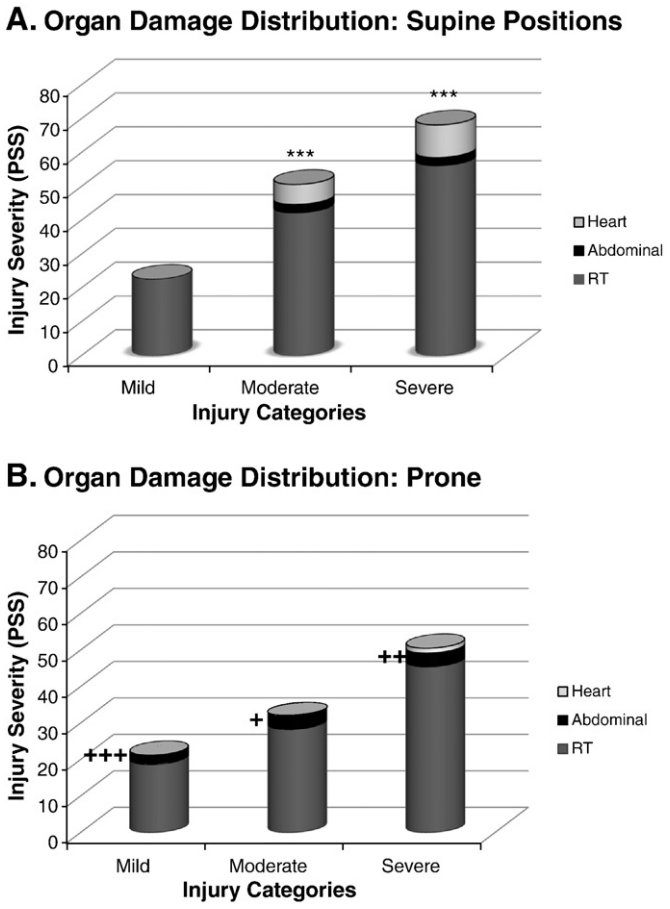

Fig. 4. Influence of the body position on organ damage distribution expressed as PSS/IS: (A) supine; (B) prone. While the damage of the respiratory tract (RT) was most prominent in all animals regardless of their position, animals exposed in supine position to the shockwave showed more heart damage (Heart) and less solid abdominal organ injury (Abdominal) as compared to the animals injured in prone position. $^{***}p<0.0001$ refers to heart damage; $+p<0.05$, $++p<0.01$, and $+++p<0.0001$ refer to abdominal damages in comparison supine vs. prone.

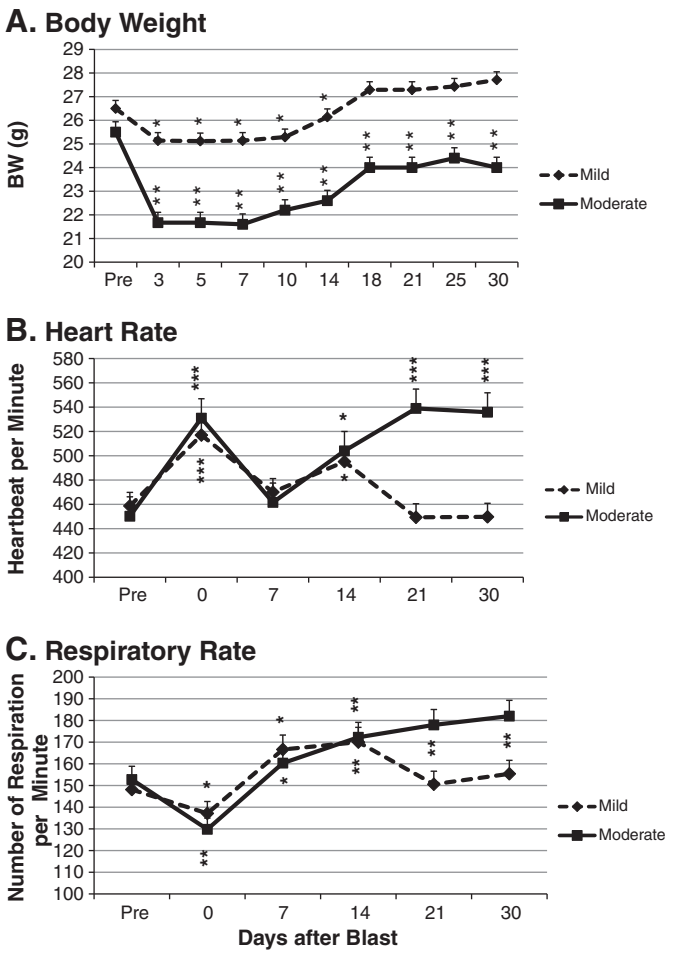

Fig. 5. Physiological changes caused by blast exposure. Results are shown as means ± SD and measured over a 30-day post-exposure period in animals before and after being exposed to mild (dashed line) or moderate (solid line) intensity shockwave. (A) Changes in the body weight (BW) expressed in grams (g). After the significant decline, the BW returned to pre-injury levels in animals with mild blast injuries, whereas it remained significantly decreased in animals with moderate blast injuries at the end of the 30-day observation period. (B) Non-invasive measurement of heart rate alterations (heartbeat per minute). The multiphase response showing significant increase immediately and 14 days after exposure ended with normalization in animals with mild injuries, and significant and persistent tachycardia in animals with moderate injuries. (C) Non-invasive measurement of respiratory rate alterations (number of respiration per minute). The multiphase response shows significant decrease immediately and increase on days 7 and 14 after exposure, and ends with normalization in animals with mild injuries and significant and persistent tachypnea in animals with moderate injuries. $^{*}p<0.05$, $^{**}p<0.01$, and $^{***}p<0.001$ compared to pre-injury levels.

more prominent in animals with moderate blast injuries (Fig. 5A). The lowest BW values were measured at day 3 post-exposure in both experimental groups (mild: 25.14 ± 0.52 g compared to pre-injury value of 26.5 ± 0.44 g; moderate: 21.67 ± 0.48 g compared to pre-injury value of 25.82 ± 0.52 g). At the end of the observation period (i.e., 30 days post-exposure), the BW was normalized in mild blast injury group, whereas it remained significantly ($p<0.01$) reduced in animals with moderate blast injuries.

Peripheral arterial O_2 saturation was significantly ($p<0.05$) reduced immediately after blast exposure (mild: 97.00% vs. 99.56% pre-injury; moderate: 95.12% vs. 99.14% pre-injury), followed by values close to pre-exposure levels. Heart rate changes showed multi-phase, injury severity-dependent dichotomy in response to shock wave exposure (Fig. 5B). In animals with mild blast injuries, the HR after an immediate significant ($p<0.001$) increase (517 ± 8 bpm vs. 459 ± 9 bpm pre-injury) showed normalization on day 7 post-exposure, increase ($p<0.05$) 14 days after injury, and finally, back to pre-injury levels at the end of observation period. On the other hand, animals with moderate blast injuries had significantly ($p<0.001$) increased HR immediately after exposure (531 ± 9 bpm vs. 450 ± 10 bpm pre-injury), and after a period of normalization on day 7, demonstrated continuous increase in HR until the end of the 30-day observation period. Interestingly, the pattern of the RR response was similar to the multi-phase, exposure intensity dependent changes of the HR (Fig. 5C). The PD alterations were comparable in both mild and moderate injury groups: after initial significant reduction of PD suggesting decreased blood flow (mild: 164.45 ± 16.54 μm vs. 284.65 ± 29.13 μm pre-injury; moderate: 125.09 ± 13.67 μm vs. 292.22 ± 23.02 μm), the values returned back to normal after day 7 post-exposure (results not shown).

Neurological outcomes

Fig. 6A shows motor performance in animals exposed to mild or moderate shock wave intensity. All animals demonstrated a significant decline in rotarod performance during the entire 30-day observation period. Animals exposed to mild intensity shock wave showed reduced motor performance starting with day 1 post-injury (23.89 ± 1.35 s compared to 48.52 ± 2.45 s pre-injury; $p<0.01$) with the lowest value measured on day 7 (18.43 ± 1.21 s) and normalization after day 14. Animals with moderate blast injuries demonstrated more prominent changes albeit with a similar trend.

After blast exposure, there was a highly significant ($p<001$) decline in AAR performance in both injury groups during the first 3 days post-exposure as compared to pre-exposure levels (mild: 65.0 ± 1.5% of total

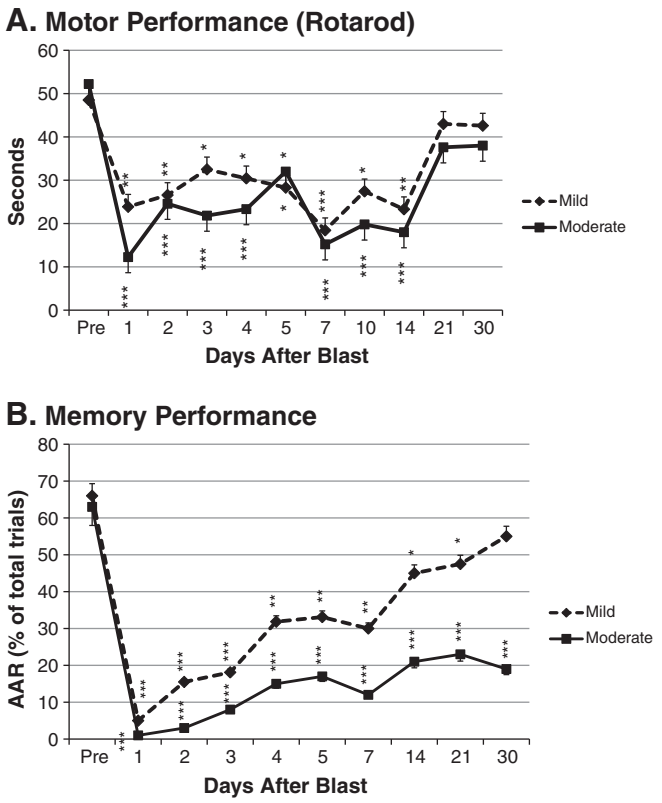

Fig. 6. Motor and cognitive performance in animals exposed to either mild (dashed line) or moderate (solid line) intensity shockwave. The results are shown as means ± SD and measured over a 30-day post-injury period. Pre-injury scores are shown at point "Pre." (A) Rotarod assessed motor outcomes in pre-trained mice. Motor performance was significantly declined in all animals in the first 2 weeks post-trauma, followed by normalization at the end of the observation period. (B) Cognitive performance assessed based on active-avoidance response (AAR) expressed as a percentage of total 100 trials. Cognitive performance was significantly declined in animals with mild injury up to day 21 post-injury and showed a trend toward normalization at the end of the observation period. Animals with moderate injury showed more profound and persistent decline in cognitive performance. $^{*}p<0.05$, $^{**}p<0.01$, and $^{***}p<0.001$ compared to pre-injury levels.

trials; and moderate: 63.0 ± 2.0% of total trials). In the moderate blast injury group, such a significant ($p<0.001$) memory deficit continued to the end of the 30-day observation period (19.0 ± 1.0% of total trials), whereas in the mild blast injury group, the AAR performance showed slow but steady improvements toward normalization (Fig. 6B).

In the open field spontaneous activity test, injury resulted in significant decline in activity in both experimental groups measured as a distance covered over a 5-min period (Fig. 7A) or speed of movement (Fig. 7B). Specifically, mice with moderate blast injury showed reduced spontaneous exploratory activity during the entire 30-day post-exposure period, without a tendency toward normalization, as compared to pre-exposure levels (15.95 ± 0.81 vs. 9.37 ± 0.52 m). The reduction in open field activity was almost identical in the mild blast injury group during the first 4 days after exposure as compared to the mild blast injury group. However, after a period of significantly decreased activity ($p<0.001$ as compared to pre-exposure levels of 16.77 ± 0.93 m), animals exposed to mild blast slowly improved their activity to the normal level at day 14 post-injury. Reduced spontaneous activity was associated with intensified freezing behavior in both mild and moderate blast groups measured as increased time spent immobile (Fig. 7C) or decreased time spent in exploring the environment by rearing (Fig. 7D). Such behavior is consistent with increased stress/anxiety and is not associated with decreased sensory or motor deficits (Larsson et al., 2002; Vallee et al., 1997). Spontaneous exploratory activity, thus interest toward environment, did not normalize in these animals over the 30-day post-exposure period, although the decline in activity and reduced interest toward environment was more prominent in the animals exposed to moderate blast than in animals with mild blast injury. Such a behavioral impairment comparable to human post-traumatic depression is well illustrated by the density map analysis of the movement patterns. Fig. 8A shows the density map of an animal's movement before being exposed to mild blast, where the animal covered and explored the entire surface of the field with a predilection toward corners. Two weeks (Fig. 8B) and even 1 month (Fig. 8C) after injury, the animal's activity was declined showing lack of interest toward exploration and sitting in one of the corners motionless.

Gene expression

Fig. 9 provides information on the expression levels of the chosen genes in the hippocampus and brainstem of naïve and sham animals (table) and summarizes the gene changes in these brain structures of mice with either mild or moderate blast injuries measured at 1, 3, 7, 14, and 30 days post-trauma. Analysis of genes playing role in inflammatory processes in the brain:

- GFAP - an indicator of astrocyte activation (Saljo et al., 2001; Salter and Fern, 2008; Zhu and Dahlstrom, 2007);
- ED1 - a marker of the presence of macrophages and activated microglia (Kaur et al., 1997; Moxon-Emre and Schlichter, 2010; Urrea et al., 2007);
- macrophage-related protein MRP8 (Nacken et al., 2003; Ziegler et al., 2009);
- osteopontin - a secreted glycoprotein that has been implicated in cellular (glia, macrophage) migration/activation and matrix remodeling after TBI (Choi et al., 2007; Wang et al., 1998); and
- CCL - formerly MCP1 with potent chemotactic capacity for monocytes, macrophages and microglia after TBI (Semple et al., 2010a) showed dose-, i.e., blast intensity-dependent changes in gene expressions (Figs. 10 and 11).

Similar to the functional outcome measures, changes in gene expressions demonstrated a multi-phase pattern; namely, after an immediate peak in activation, a period of relative decline ensued followed by a phase of increased expression. Interestingly, in general, changes in gene expressions were more pronounced in the brainstem, supporting the theory (Cernak and Noble-Haeusslein, 2010; Cernak et al., 2001) and most recent clinical findings on the brainstem's involvement in the pathobiology of BINT (Peskind et al., 2010).

Discussion

The importance of blast injury and blast-induced neurotrauma research

The creation of a reliable animal model for BINT research with direct applicability to the theater conditions that Warfighters experience is vital to Force Readiness for a number of reasons. America's Armed Forces in Iraq and Afghanistan sustain injuries from almost daily exposure to explosions or blasts with more than 73% of all U.S. military casualties caused by rocket-propelled grenades, improvised explosive devices (IEDs), and land mines (Ritenour et al., 2010, Department of Defense, Personnel and Procurement Statistics). The Defense and Veterans Brain Injury Center (DVBIC) estimated that approximately 180,000 service members were diagnosed with TBI between 2001 and 2010, with the overwhelming distribution of mild TBI (mTBI) caused by blast. Terrio et al. (2009) reported that, following deployment to Iraq, 22.8% of Soldiers from a Brigade Combat Team had clinician-confirmed TBI history. While many Warfighters with TBI reported remission of their symptoms, 38.9% endorsed at least one mild TBI-related symptom at the post-deployment health assessment. Irritability, memory and speech problems (reduced verbal fluency, working memory, and executive

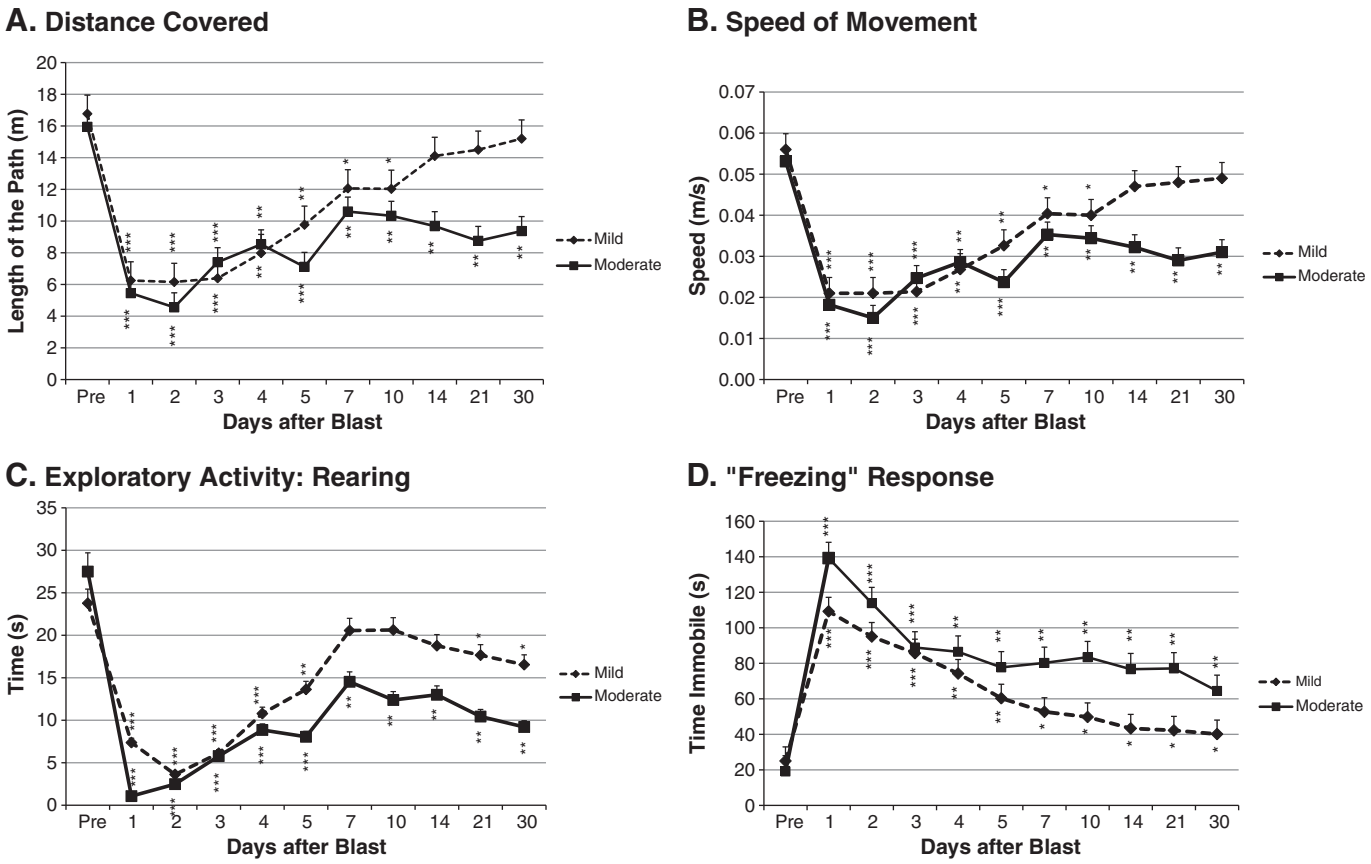

Fig. 7. Open field activity in mice subjected to either mild (dashed line) or moderate (solid line) intensity shockwave. The results are shown as means ± SD and measured over a 30-day post-injury period, and the pre-injury scores are shown at point "Pre.". (A) Distance covered during a 5-min test period and measured as a length of the path (m). (B) Speed of movement expressed as m/s. (C) Time spent in rearing used as an indicator of exploratory activity, thus interest toward the environment, expressed in seconds (s). and (D) "Freezing" response measured as time spent immobile and expressed in seconds (s). While the distance covered and speed of movement returned to pre-injury levels in animals with mild blast injury at the end of the 30-day post-injury period, their exploratory activity remained declined and the "freezing" response increased suggesting continuous disinterest toward their environment. The decline in open field activity of mice with moderate blast injury was significant and incessant. $^{*}p<0.05$, $^{**}p<0.01$, and $^{***}p<0.001$ compared to pre-injury levels.

functioning) (Nelson et al., 2009), headache, dizziness and balance problems, as well as psychological impairments such as depression and post-traumatic stress disorder were among most frequent (Peskind et al., 2010; Terrio et al., 2009). It is noteworthy that nearly half of the time these problems developed or were noted after the acute phase (Terrio et al., 2009). Thus, while explosion-induced mortality has remained low and unchanged, long-term consequences including those caused by BINT seem more frequent. TBI due to blast exposure causes significant immediate and long-term health problems in our military personnel and limits their ability to continue on active duty.

Existing methodological challenges

Accumulating clinical and experimental evidence shows that BINT is caused by complex co-occurring mechanisms of systemic, local, and cerebral responses to blast generated by explosion (Cernak and Noble-Haeusslein, 2010). While our understanding on the pathobiology of BINT mechanisms is increasing, the existing literature is disparate, with a large diapason of differing experimental models used. Often, the models are oversimplified, and fail to adequately reproduce the physical properties of the injurious environment, based on the physics of blast and military-relevant injury scenarios. This, in turn, may lead to misleading results, which, by introducing confusion into the research field, impedes research progress.

All clinically and militarily relevant BINT models should fulfill the following requirements: 1) the injurious factor of blast should be clearly defined and reproduced in controlled, reproducible, and quantifiable fashion; 2) the resulting injury should be reproducible, quantifiable, and imitate features of human BINT; 3) the injury outcome defined based on morphological, physiological, molecular, and/or functional/behavioral parameters should be in correlation with the chosen injurious factor of the blast; thus 4) the mechanical characteristics of the blast components such as intensity, complexity of blast signature or its duration, among others, should predict the outcome severity (Cernak and Noble-Haeusslein, 2010). Experimental animal models of primary blast injuries routinely employ either (1) a shock tube that use compressed air or gas to generate a shockwave or (2) blast tubes that utilize explosive charges to generate a shockwave (Nishida, 2001; Robey, 2001). In general, anesthetized animals are fixed in special holders that prevent movement of their bodies in response to blast, hence preventing tertiary blast effects. The majority of currently used experimental models reproduce the ideal Friedländer type blast wave with one overpressure peak followed by a short negative pressure phase, without the capability to replicate a non-ideal blast wave with multiple shock, expansion and refraction waves as seen in real-life conditions (Dodd et al., 1990; Long et al., 2009) (Fig. 12). This limits the extent of comparability of experimental and clinical findings as well as the value of experimental findings. The existing models are often vague about the physical characteristics of the shockwave and disclose information only about the static pressure that does not reveal real physical conditions causing the injury. We have built a system that is able to reproduce both simple and complex blast wave signatures, and provides highly

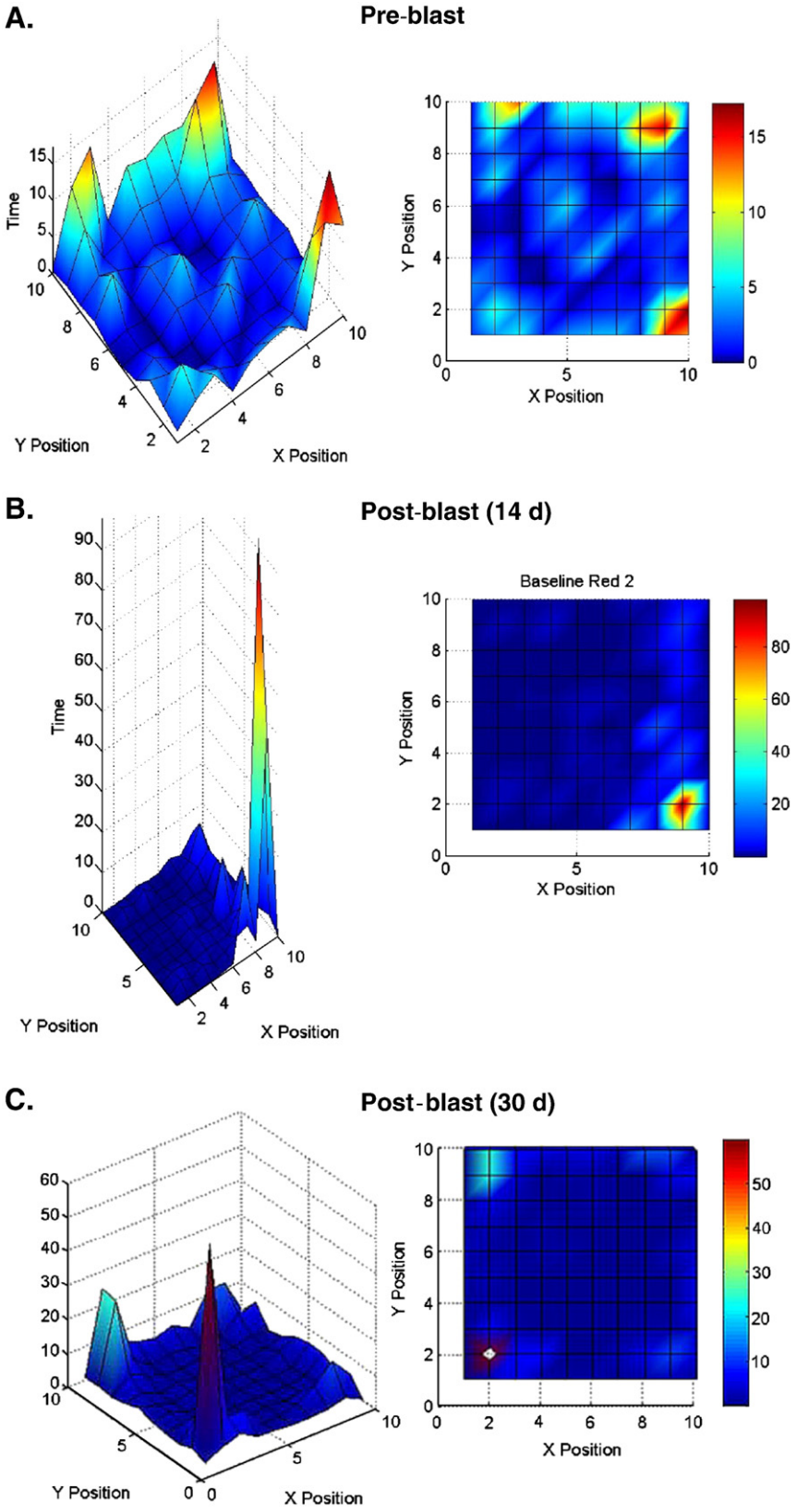

Fig. 8. 3-D and 2-D density maps showing the pattern of the exploratory activity of a representative animal with mild blast injury calculated based on time-distance signals (A) before blast, (B) 14 days after blast, and (C) 30 days after blast. Colors spanning from light blue to yellow, orange, and red indicate regions the animals visited more often and/or spent more time. The animal's hypoactivity and preference for a corner clearly demonstrates its "freezing" response and lack of interest toward environment, a response comparable to post-traumatic depression in humans.

controllable physical environment. As such, it can be used as a reliable and highly reproducible tool to investigate the effects of military-relevant blast wave signatures on injury outcomes in mice.

The Bowen criteria from 1968 (Bowen et al., 1968a; Damon et al., 1968) are still the standard for current primary blast injury criteria and related outcomes. The iso-damage pressure-duration curves have

Group	Osteopontin	MRP8	GFAP	CCL2/MCP1	ED1
	Hippocampus; Brainstem	Hippocampus; Brainstem	Hippocampus; Brainstem	Hippocampus; Brainstem	Hippocampus; Brainstem
Naïve	0.52±0.01; 1.00±0.00	0.54±0.02; 0.52±0.02	0.54±0.01; 0.59±0.02	0.20±0.00; 0.29±0.01	0.73±0.02; 0.65±0.02
Sham	0.53±0.01; 1.00±0.00	0.52±0.01; 0.55±0.02	0.60±0.02; 0.58±0.02	0.33±0.01; 0.30±0.01	0.64±0.01; 0.60±0.01

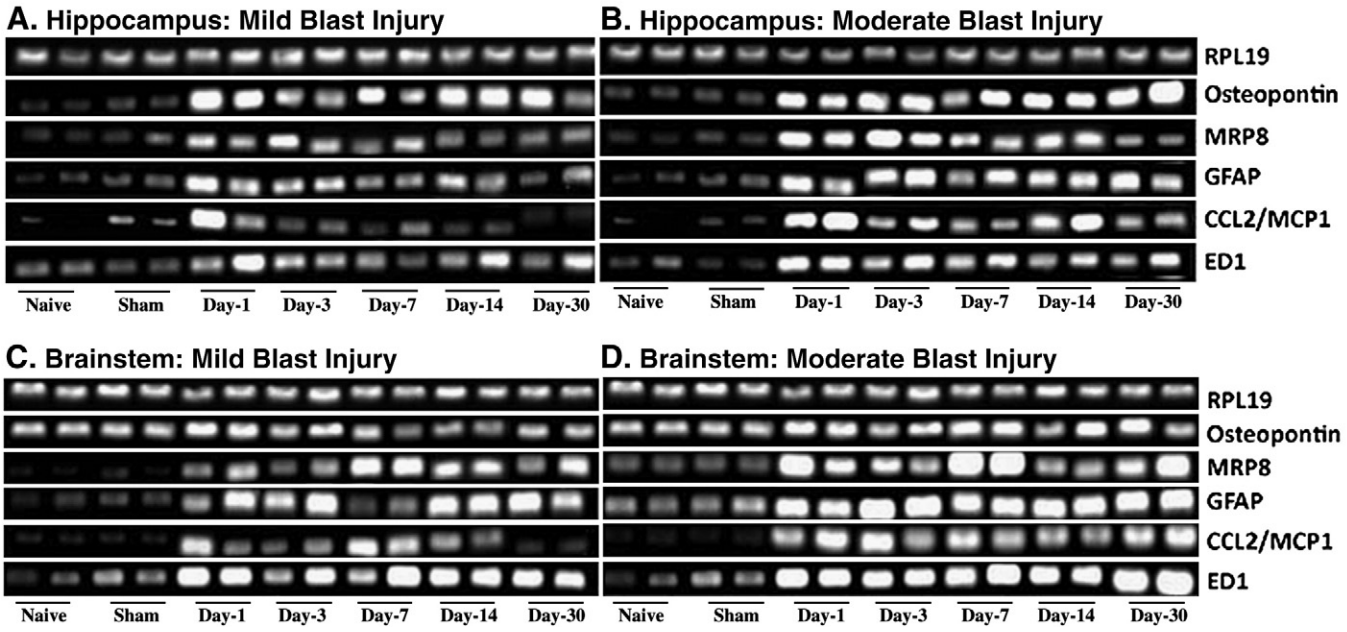

Fig. 9. The table shows expression levels of five genes involved in inflammation measured with RT-PCR in the hippocampus and brainstem of naïve and sham control mice. Data, expressed as intensity of the cDNA band, are the mean ± SEM of five independent samples. Representative gels showing cDNAs from RPL19 (used as an internal control to normalize gel loading), osteopontin, Myeloid related protein 8 (MRP8), glial fibrillary acidic protein (GFAP), chemokine CC ligand-2 (CCL2/MCP1), and ED1 in the (A) hippocampus of mice with mild blast injury; (B) hippocampus of mice with moderate blast injury; (C) brainstem of mice with mild blast injury; and (D) brainstem of mice with moderate blast injury. Semi-quantitative analysis of cDNAs was carried out by Quantity One 1-D Analysis as described in Materials and methods and shown in Figs. 10 and 11.

been constructed for 24-hour lethality levels without medical care. As an outcome measure, besides lethality, threshold lung damage is also given as one-fifth of the 50% lethality curve. These curves are given for an ambient pressure of one atmosphere, and for an average large mammal weighing 70 kg (approximating a human being). Additional curves were provided scaled for the appropriate ambient pressure, animal mass, and species (Richmond et al., 1967). Recently, there have been several concerns about the Bowen curves (Gruss, 2006). It has been posited that there is a significant systematic error in the Bowen curves criteria due to the use of low-quality pulse duration data in the original criteria. Additionally, questions have been raised about the consistency of the methodology used in animal experiments to validate the curves (blast/shock tube versus open field blast, anesthesia, or positioning, etc.). Regardless of the criticisms, the most important problems are that: 1) the Bowen criteria involved lung damages and lethality as outcome measures; thus, as such, they are less reliable and/or useful for predicting functional deficits such as memory deficit or balance impairment as outcome parameters; and 2) physiological and biological responses to external injurious stimuli are significantly different in different species; thus, physical scaling based on animals' size and using pressure-duration factors could give misleading information about the intensity and nature of functional deficits. In establishing our model, we started with the Bowen curve criteria for mice, and then modified the physical environment to reach graded neurological (memory, motor, and behavioral) deficits, thus achieve causal relationship between the intensity of the physical environment and functional outcome measures. By achieving this, we have developed a model that is capable of reproducing not only structural damage but also functional impairments that are dependent on the intensity of the injurious factor. Moreover, since the blast injury criteria used are defined for functional deficits and not for tissue destruction, this model is capable of reproducing mild non-impact blast-induced traumatic brain injury.

In our model, we established a causal relationship between the intensity of the mechanical force (i.e., overpressure of the blast) and long-term functional (i.e., motor performance, cognitive performance, and behavior) outcomes. We have shown a graded decline in functional performance and clear, intensity-dependent difference between mild and moderate injury groups. Moreover, our model successfully reproduced the main systemic and neural dysfunctions seen in patients (Brenner et al., 2010; Peskind et al., 2010; Terrio et al., 2009; Warden et al., 2009) including weight loss, unstable heart and respiratory rates, motor deficits, memory decline, depression and loss of interest toward environment, among others. In animals with moderate blast injuries the alterations in vital functions suggesting impaired autonomous nervous system control, memory decline, and behavioral impairments did not show any tendency toward normalization at the end of the 30-day observation period, implying that those changes will remain irreversible. Interestingly, while motor and memory performance of mice with mild blast injuries were

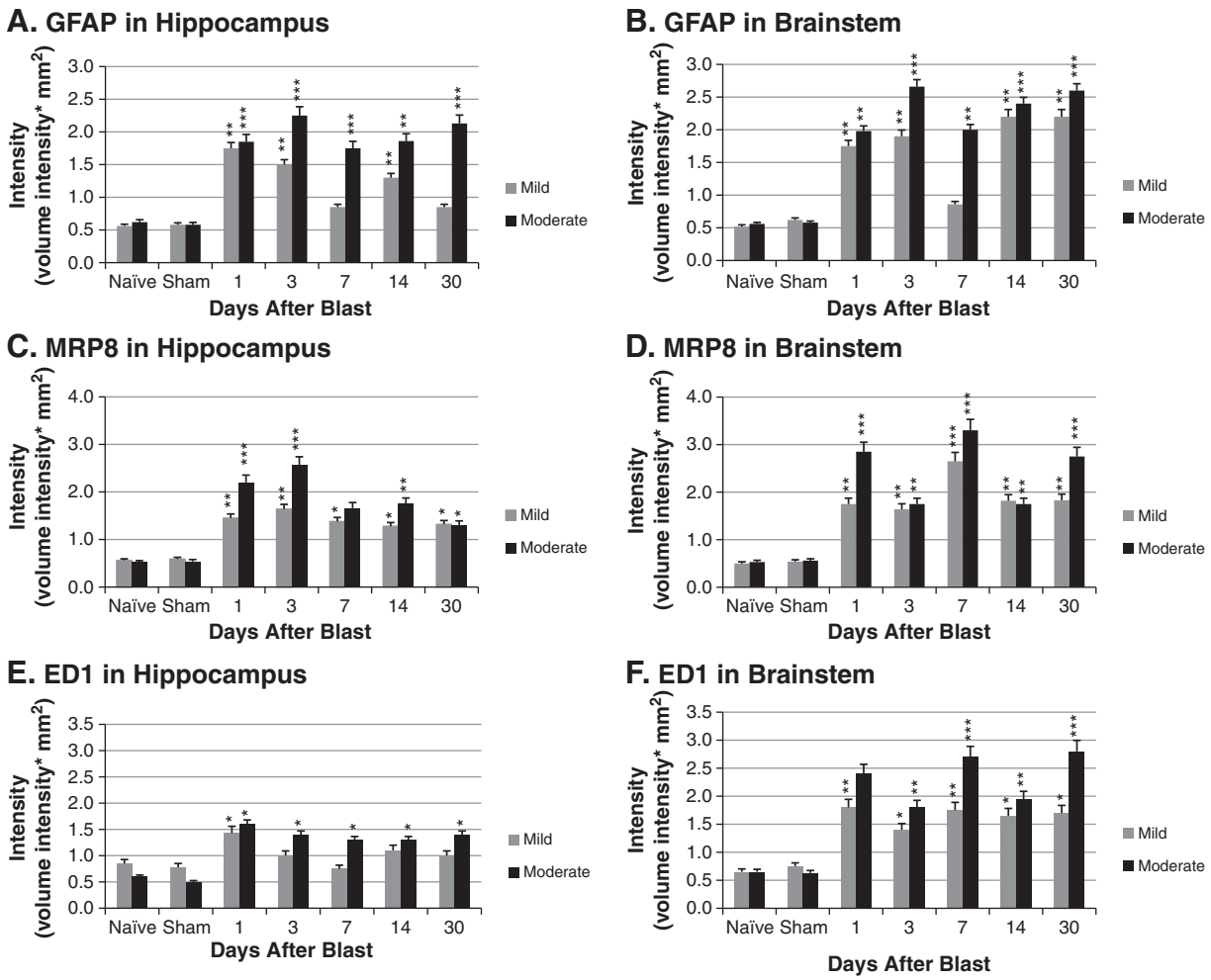

Fig. 10. Semi-quantitative analysis of cDNAs of the: Glial fibrillary acidic protein (GFAP) in the hippocampus (A) and brainstem (B); Myeloid related protein 8 (MRP8) in the hippocampus (C) and brainstem (D); and ED1 in the hippocampus (E) and brainstem (F) of mice exposed to either mild (gray bars) or moderate (black bars) intensity shockwave. Data, expressed as intensity of the cDNA band, are the mean ± SEM of five independent samples, and measured at 1, 3, 7, 14, and 30 days injury. *$p<0.05$, **$p<0.001$, and ***$p<0.001$ vs. pooled values of naïve and sham samples. Magnitude and pattern of gene expression of the genes shows significant induction.

normalized 1 month after the exposure, their behavior remained significantly changed with decreased exploratory activity and extended freezing response. Bearing in mind that mice between 1 and 6 months of age live 45 times faster than humans (Flurkey et al., 2007; The Jackson Laboratory, 2010), a 1-month observation of animals exposed to blast translates into a significant period in their lives, comparable to years in humans.

Similar to military clinical experience, mice with mild blast injury, thus mild TBI, showed no signs of structural damage at gross pathological examination. The limited mortality rate in animals was caused by imminent cardiorespiratory arrest most probable due to vago-vagal reflex activation as previously posited (Cernak et al., 1996; Irwin et al., 1999; Zuckerman, 1940). Importantly, the animals that died immediately after being exposed to mild intensity blast were in supine position. The supine position, i.e., a body position of facing the shockwave front, has been previously linked to increased mortality and morbidity both in animals and people (Bowen et al., 1968a; Chiffelle, 1966; Richmond et al., 1967, 1968, 2005) most probably due to interaction between the shockwave's kinetic energy and the elastic abdominal wall. Moreover, it has been shown that body position affects arterial oxygenation. Indeed, prone positioning has been shown to recruit collapsed lung tissue and improve gas exchange in trauma patients with blunt chest trauma and severe adult respiratory distress syndrome (Voggenreiter et al., 1999), whereas supine position had a depressive effect on respiratory frequency in anesthetized mice after brief hypoxia (Izumizaki et al., 2005).

In an attempt to link the functional deficits identified in mice exposed to blast to probable pathological mechanism underlying long-term neurological impairments, we analyzed five genes involved in the inflammation in the brain (Allan and Rothwell, 2003; Harting et al., 2008). Emerging evidence demonstrates the role of inflammation in the pathobiology of BINT (Bauman et al., 2009; Risling et al., 2010). It can occur within the neural tissue, where activated microglia and astrocytes release cytokines, chemokines, and reactive oxygen species (Harting et al., 2008). Reactive astrogliosis has been established as one of the key components of the cellular response to brain injury, and the transformation from quiescent to reactive astrocytes is associated with strong upregulation of GFAP (Stoll et al., 1998), predominantly expressed by mature astrocytes in the CNS. An increase in GFAP expression has been found to be a hallmark of many neurodegenerative conditions, such as Parkinson's disease (Banati et al., 1998), Alzheimer's disease (Wharton et al., 2009), and amyotrophic lateral sclerosis (ALS) (Liem and Messing, 2009). Moreover, GFAP has been widely utilized as one of the markers of cerebral ischemia-induced brain damage (Cordeau et al., 2008). Recent study, using a live-imaging method in GFAP-luciferase mice, demonstrated that the astrocyte activation after brain ischemia is initiated within the first few days and may persist up to 1 week or

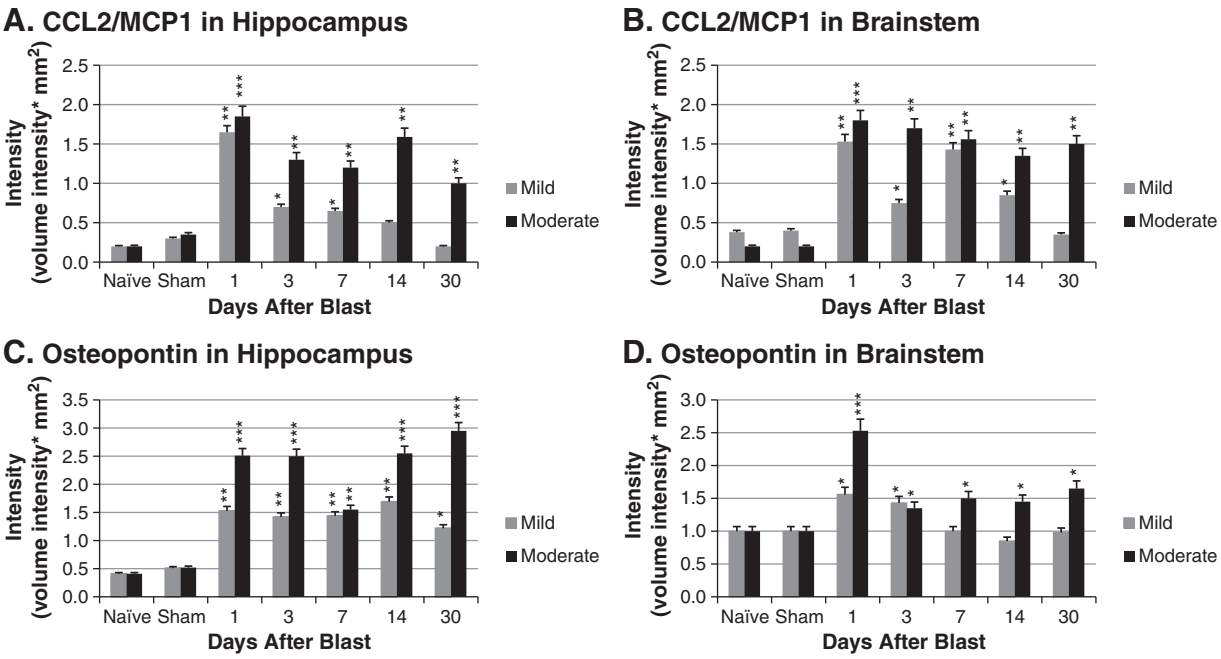

Fig. 11. Semi-quantitative analysis of cDNAs of the: Chemokine CC ligand-2 (CCL2/MCP1) in the hippocampus (A) and brainstem (B); and Osteopontin in the hippocampus (C) and brainstem (D) of mice exposed to either mild (gray bars) or moderate (black bars) intensity shockwave. Data, expressed as intensity of the cDNA band, are the mean ± SEM of five independent samples, and measured at 1, 3, 7, 14, and 30 days injury. $^{*}p<0.05$, $^{**}p<0.001$, and $^{***}p<0.001$ vs. pooled values of naïve and sham samples. Magnitude and pattern of gene expression of the genes shows significant induction.

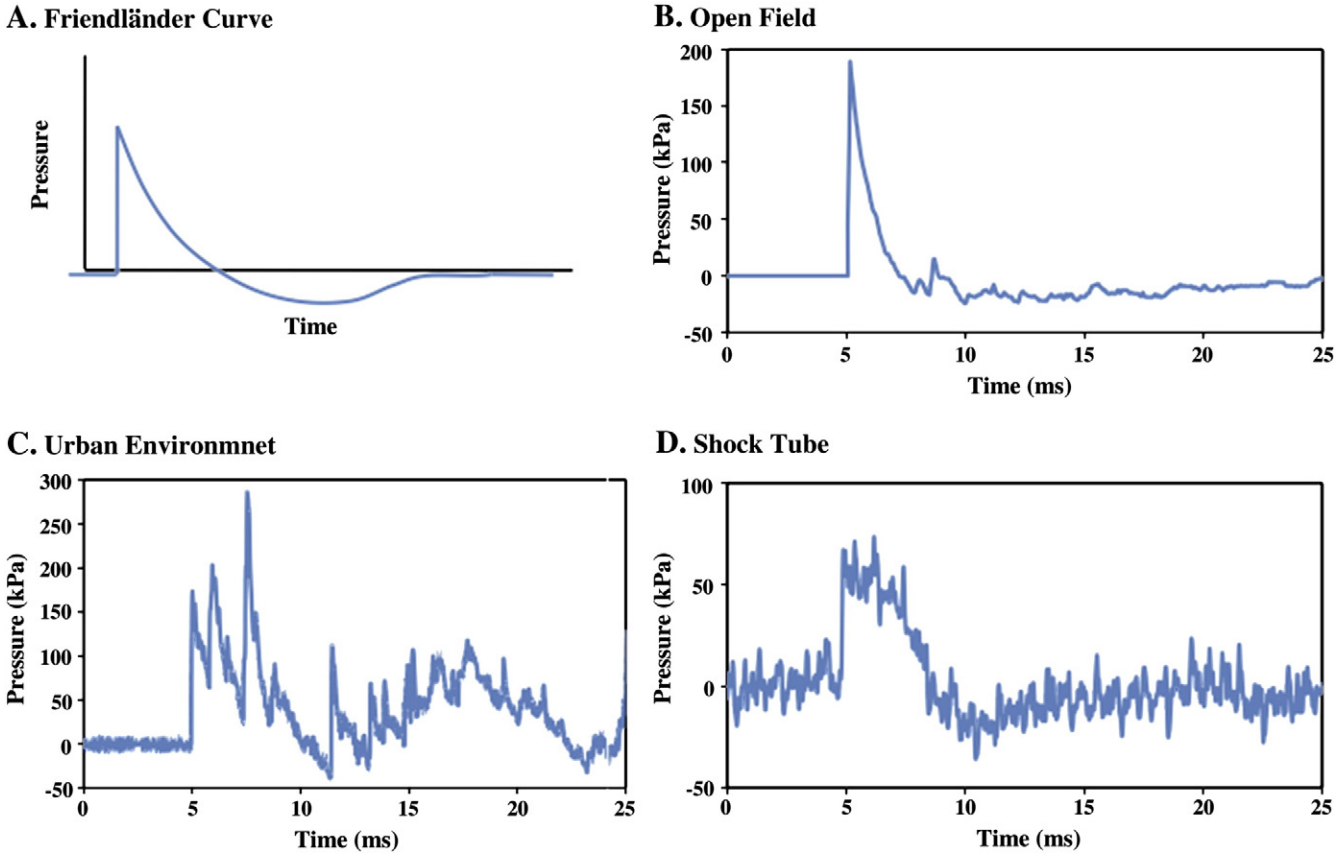

Fig. 12. Comparison of shockwave forms: (A) Friedländer waveform, a simplified qualitative depiction of an explosion-generated shockwave showing positive and negative phases of a pressure wave; (B) an open field shockwave generated by detonating 816.47 g (1.8 lbs) of a TNT-equivalent explosive charge in open field (even terrain, no surrounding objects) conditions. The static pressure was recorded 3.6 m from the source; (C) complex shockwave form generated by detonating 725.75 g (1.6 lbs) of a TNT-equivalent explosive charge in an urban-environment. The static pressure was recorded 2.3 m from the source; and (D) a moderate intensity shockwave form generated in our shock tube. The static pressure was recorded 4.5 m downstream from the shock tube diaphragm. Note a similarity between the shapes of the shock tube output and the open field shockwave; the intensity of the shock tube-generated ovepressure is modified based on the Bowen curve calculations.

longer (Cordeau et al., 2008). Interestingly, in our preliminary studies, we found that a single, mild blast exposure (11 psi, i.e., 76 kPa, on the surface of the body) is capable of inducing glial activation as measured either using the 3-D bioluminescence/fluorescence IVIS camera and imaging transgenic animals with luciferase reporter tagged to GFAP or performing GFAP immunocytochemistry (Cernak, unpublished data). ED1 antibody is often used to identify activated macrophages/microglia in brain injuries of different etiology (Souza-Rodrigues et al., 2008; Wasserman et al., 2008; Wilson and Molliver, 1994); since it predominantly labels lysosomes and is increased when macrophages/microglia become phagocytic, ED1 does not provide information about resident microglia and their contribution to brain pathology (Damoiseaux et al., 1994). Because our aim was to provide a gross analysis of the gene inflammatory response in the brain to blast exposure and not to analyze the relative contribution of activated vs. resident microglia, we included ED1 as one of the parameters into our assay platform. Myeloid related protein 8 (Mrp8), also called Calgranulin A or S-100 calcium binding protein A8 (S100A8), was characterized as endogenous Toll-like receptor-4 (Tlr-4) agonists expressed in activated macrophages and microglial cells (Engel et al., 2000; Vogl et al., 2007; Ziegler et al., 2009). It has been suggested that Mrp8 upregulation and signaling could play important role in ischemia- (Ziegler et al., 2009) and trauma-induced (Beschorner et al., 2000; Engel et al., 2000) neuroinflammation and damage progression. The chemokine CC ligand-2 (CCL2; formerly monocyte chemoattractant protein-1, MCP1) has been implicated in macrophage recruitment into damaged parenchyma after TBI, thus mediating post-traumatic secondary brain damage (Semple et al., 2010a,b). Osteopontin, a secreted glycoprotein, has been implicated in vascular injury by promoting cell adhesion, migration, and chemotaxis (Wang et al., 1998). Transient microglial and prolonged astroglial upregulation of OPN has been demonstrated after ischemic brain injury (Choi et al., 2007; Wang et al., 1998) and intracerebral hemorrhage (Suzuki et al., 2009; Yan et al., 2009). Our results showed significant upregulation of all tested genes in an injury severity-dependent fashion. The dynamics and multiphase response of gene changes resembled the pattern of functional outcome measures implying a potential causal relationship between inflammation and long-term neurological deficits due to blast. It is noteworthy the increase in inflammatory genes' expression other than OPN was more profound in the brainstem compared to the hippocampus suggesting the brainstem's sensitivity toward blast as mechanical factor of injury. The differing behavior of OPN compared to other inflammatory genes might be explained by its involvement in late tissue remodeling processes in brain structures selectively vulnerable to ischemia (Choi et al., 2007).

Conclusion

We have developed a new model for graded blast-induced neurotrauma, which induces physiological changes and functional deficits in a strictly controlled and defined experimental setting with a potential to generate a physical environment comparable to military scenarios. The alterations in vital functions, memory and cognitive performance, and behavioral impairments are comparable with the symptoms of mild and moderate TBI in Warfighters who are exposed to blast. Changes in genes involved in inflammation in the brain provide potential mechanistic explanation for long-term neurological deficits due to blast exposure.

Funding source

This work was supported by the JHU/APL internal research and development funds and the JHU/APL-JHU SOM Partnership Grant. The sponsor did not influence the study design; data collection, analysis and interpretation of data; or the writing of the report.

Disclosure statement

None of the authors had any actual or potential conflict of interest including any financial, personal, or other relationships with other people or organizations within 3 years of beginning the work submitted that could inappropriately influence (bias) their work.

This work has not been published previously; it is not under consideration elsewhere and its publication is approved by all authors. Moreover, the Johns Hopkins University Applied Physics Laboratory, i.e., the institution where the work was carried out, explicitly approves the publication of this article. The authors also declare that if accepted, this article will not be published elsewhere including electronically in the same form, in English or in any other language, without the written consent of the copyright-holder.

References

Allan, S.M., Rothwell, N.J., 2003. Inflammation in central nervous system injury. Philos. Trans. R. Soc. Lond. B Biol. Sci. 358, 1669–1677.
Anderson, J.D., 2003. Modern compressible flow: with historical perspective. McGraw-Hlll, Boston.
Axelsson, H., et al., 2000. Physiological changes in pigs exposed to a blast wave from a detonating high-explosive charge. Mil. Med. 165, 119–126.
Banati, R.B., et al., 1998. Glial pathology but absence of apoptotic nigral neurons in long-standing Parkinson's disease. Mov. Disord. 13, 221–227.
Bauman, R.A., et al., 2009. An introductory characterization of a combat-casualty-care relevant swine model of closed head injury resulting from exposure to explosive blast. J. Neurotrauma 26, 841–860.
Ben-Dor, C., et al., 2001. Handbook of shock waves. Academic Press, San Diego.
Beschorner, R., et al., 2000. Differential regulation of the monocytic calcium-binding peptides macrophage-inhibiting factor related protein-8 (MRP8/S100A8) and allograft inflammatory factor-1 (AIF-1) following human traumatic brain injury. Acta Neuropathol. 100, 627–634.
Boda, E., et al., 2009. Selection of reference genes for quantitative real-time RT-PCR studies in mouse brain. J. Mol. Neurosci. 37, 238–253.
Bowen, I.G., et al., 1968b. Estimate of man's tolerance to the direct effects of air blast. Defense Atomic Support Agency, Washington D.C., pp. 1–44.
Bowen, I.G., et al., 1968a. Biophysical mechanisms and scaling procedures applicable in assessing responses of the thorax energized by air-blast overpressures or by nonpenetrating missiles. Ann. NY Acad. Sci. 152, 122–146.
Brenner, L.A., et al., 2010. Traumatic brain injury, posttraumatic stress disorder, and postconcussive symptom reporting among troops returning from Iraq. J. Head Trauma Rehabil. 25, 307–312.
Cernak, I., Noble-Haeusslein, L.J., 2010. Traumatic brain injury: an overview of pathobiology with emphasis on military populations. J. Cereb. Blood Flow Metab. 30, 255–266.
Cernak, I., et al., 1999. Blast injury from explosive munitions. J. Trauma 47, 96–103 discussion 103-4.
Cernak, I., et al., 1996. Involvement of the central nervous system in the general response to pulmonary blast injury. J. Trauma 40, S100–S104.
Cernak, I., et al., 1990. The pathogenesis of pulmonary edema in sheep exposed to FAE charge. J. Trauma (China) 6 (Suppl), 267–271.
Cernak, I., et al., 2001. Ultrastructural and functional characteristics of blast injury-induced neurotrauma. J. Trauma 50, 695–706.
Chari, R., et al., 2010. A sequence-based approach to identify reference genes for gene expression analysis. BMC Med. Genomics 3, 32.
Chiffelle, T.L., 1966. Pathology of direct air-blast injury. Technical Progress Report DA-49-146-XY-055. Defense Atomic Support Agency, Department of Defense, Washington DC.
Choi, J.S., et al., 2007. Transient microglial and prolonged astroglial upregulation of osteopontin following transient forebrain ischemia in rats. Brain Res. 1151, 195–202.
Cordeau Jr., P., et al., 2008. Live imaging of neuroinflammation reveals sex and estrogen effects on astrocyte response to ischemic injury. Stroke 39, 935–942.
Damoiseaux, J.G., et al., 1994. Rat macrophage lysosomal membrane antigen recognized by monoclonal antibody ED1. Immunology 83, 140–147.
Damon, E.G., et al., 1968. Effects of ambient pressure on tolerance of mammals to air blast. Aerosp. Med. 39, 1039–1047.
Dennis, A.M., et al., 2009. Hemorrhagic shock after experimental traumatic brain injury in mice: effect on neuronal death. J. Neurotrauma 26, 889–899.
Dewitt, D.S., Prough, D.S., 2009. Blast-induced brain injury and posttraumatic hypotension and hypoxemia. J. Neurotrauma 26, 877–887.
Dodd, K.T., et al., 1990. Nonauditory injury threshold for repeated intense freefield impulse noise. J. Occup. Med. 32, 260–266.
Engel, S., et al., 2000. Dynamics of microglial activation after human traumatic brain injury are revealed by delayed expression of macrophage-related proteins MRP8 and MRP14. Acta Neuropathol. 100, 313–322.
Flurkey, K., et al., 2007. The mouse in aging research. In: Fox, J.G., et al. (Ed.), The Mouse in Biomedical Research. Elsevier, Burlington, M.A., pp. 637–672.
Gruss, E., 2006. A correction for primary blast injury criteria. J. Trauma 60, 1284–1289.
Hamm, R.J., et al., 1994. The rotarod test: an evaluation of its effectiveness in assessing motor deficits following traumatic brain injury. J. Neurotrauma 11, 187–196.

Harting, M.T., et al., 2008. Acute, regional inflammatory response after traumatic brain injury: implications for cellular therapy. Surgery 144, 803–813.
Irwin, R.J., et al., 1999. Shock after blast wave injury is caused by a vagally mediated reflex. J. Trauma 47, 105–110.
Izumizaki, M., et al., 2005. Effect of body position on ventilatory responses in anaesthetised mice. Comp. Biochem. Physiol. A Mol. Integr. Physiol. 141, 133–139.
Kaur, C., et al., 1997. Macrophages/microglia as 'sensors' of injury in the pineal gland of rats following a non-penetrative blast. Neurosci. Res. 27, 317–322.
Larsson, F., et al., 2002. Psychological stress and environmental adaptation in enriched vs. impoverished housed rats. Pharmacol. Biochem. Behav. 73, 193–207.
Liem, R.K., Messing, A., 2009. Dysfunctions of neuronal and glial intermediate filaments in disease. J. Clin. Invest. 119, 1814–1824.
Ling, G., et al., 2009. Explosive blast neurotrauma. J. Neurotrauma 26, 815–825.
Long, J.B., et al., 2009. Blast overpressure in rats: recreating a battlefield injury in the laboratory. J. Neurotrauma 26, 827–840.
Martin, E.M., et al., 2008. Traumatic brain injuries sustained in the Afghanistan and Iraq wars. Am. J. Nurs. 108, 40–47.
Martin, M., et al., 2002. Involvement of CB1 cannabinoid receptors in emotional behaviour. Psychopharmacology (Berl.) 159, 379–387.
Mellor, S.G., 1988. The pathogenesis of blast injury and its management. Br. J. Hosp. Med. 39, 536–539.
Moxon-Emre, I., Schlichter, L.C., 2010. Evolution of inflammation and white matter injury in a model of transient focal ischemia. J. Neuropathol. Exp. Neurol. 69, 1–15.
Nacken, W., et al., 2003. S100A9/S100A8: myeloid representatives of the S100 protein family as prominent players in innate immunity. Microsc. Res. Tech. 60, 569–580.
Nelson, L.A., et al., 2009. Relationship between processing speed and executive functioning performance among OEF/OIF veterans: implications for postdeployment rehabilitation. J. Head Trauma Rehabil. 24, 32–40.
Nishida, M., 2001. Shock tubes and tunnels: facilities, instrumentation, and techniques. Shock tubes. In: Ben-Dor, C., et al. (Ed.), Handbook of shock waves. Academic Press, San Diego, pp. 553–585.
Owen-Smith, M.S., 1981. Explosive blast injury. Med. Bull. US Army Eur. 38, 36–43.
Peskind, E.R., et al., 2010. Cerebrocerebellar hypometabolism associated with repetitive blast exposure mild traumatic brain injury in 12 Iraq war Veterans with persistent post-concussive symptoms. Neuroimage. doi:10.1016/j.neuroimage.2010.04.008.
Richmond, D.R., et al., 1967. Air-blast studies with eight species of mammals. Techn Progr Rep DASA 1854. Fission Prod. Inhal. Proj. 1–44.
Richmond, D.R., et al., 1968. The relationship between selected blast-wave parameters and the response of mammals exposed to air blast. Ann. NY Acad. Sci. 152, 103–121.
Richmond, D.R., et al., 2005. The relationship between selected blast-wave parameters and the response of mammals exposed to air blast.
Risling, M., et al., 2010. Mechanisms of blast induced brain injuries, experimental studies in rats. Neuroimage. doi:10.1016/j.neuroimage.2010.05.031.
Ritenour, A.E., et al., 2010. Incidence of primary blast injury in US military overseas contingency operations: a retrospective study. Ann Surg. 251, 1140–1144.
Robey, R., 2001. Shock tubes and tunnels: facilities, instrumentation, and techniques. Blast tubes. In: Ben-Dor, C., et al. (Ed.), Handbook of shock waves. Academic Press, San Diego, pp. 623–650.
Saljo, A., et al., 2001. Exposure to short-lasting impulse noise causes microglial and astroglial cell activation in the adult rat brain. Pathophysiology 8, 105–111.
Saljo, A., et al., 2009. Low levels of blast raises intracranial pressure and impairs cognitive function in rats. J. Neurotrauma 26, 1345–1352.
Salter, M.G., Fern, R., 2008. The mechanisms of acute ischemic injury in the cell processes of developing white matter astrocytes. J. Cereb. Blood Flow Metab. 28, 588–601.
Semple, B.D., et al., 2010a. Role of CCL2 (MCP-1) in traumatic brain injury (TBI): evidence from severe TBI patients and CCL2−/− mice. J. Cereb. Blood Flow Metab. 30, 769–782.
Semple, B.D., et al., 2010b. Role of chemokines in CNS health and pathology: a focus on the CCL2/CCR2 and CXCL8/CXCR2 networks. J. Cereb. Blood Flow Metab. 30, 459–473.
Souza-Rodrigues, R.D., et al., 2008. Inflammatory response and white matter damage after microinjections of endothelin-1 into the rat striatum. Brain Res. 1200, 78–88.
Stoll, G., et al., 1998. Inflammation and glial responses in ischemic brain lesions. Prog. Neurobiol. 56, 149–171.
Suzuki, H., et al., 2009. Protective effects of recombinant osteopontin on early brain injury after subarachnoid hemorrhage in rats*. Crit Care Med.
Terrio, H., et al., 2009. Traumatic brain injury screening: preliminary findings in a US Army Brigade Combat Team. J. Head Trauma Rehabil. 24, 14–23.
The Jackson Laboratory, 2010. Lifespan as a biomarker.
Trigo, J.M., et al., 2008. MDMA modifies active avoidance learning and recall in mice. Psychopharmacology (Berl.) 197, 391–400.
Urrea, C., et al., 2007. Widespread cellular proliferation and focal neurogenesis after traumatic brain injury in the rat. Restor. Neurol. Neurosci. 25, 65–76.
Vallee, M., et al., 1997. Prenatal stress induces high anxiety and postnatal handling induces low anxiety in adult offspring: correlation with stress-induced corticosterone secretion. J. Neurosci. 17, 2626–2636.
Voggenreiter, G., et al., 1999. Intermittent prone positioning in the treatment of severe and moderate posttraumatic lung injury. Crit. Care Med. 27, 2375–2382.
Vogl, T., et al., 2007. Mrp8 and Mrp14 are endogenous activators of Toll-like receptor 4, promoting lethal, endotoxin-induced shock. Nat. Med. 13, 1042–1049.
Wan, G., et al., 2010. Identification and validation of reference genes for expression studies in a rat model of neuropathic pain. Biochem. Biophys. Res. Commun. doi:10.1016/j.bbrc.2010.08.106.
Wang, X., et al., 1998. Delayed expression of osteopontin after focal stroke in the rat. J. Neurosci. 18, 2075–2083.
Warden, D.L., et al., 2009. Case report of a soldier with primary blast brain injury. Neuroimage 47 (Suppl 2), T152–T153.
Wasserman, J.K., et al., 2008. Glial responses, neuron death and lesion resolution after intracerebral hemorrhage in young vs. aged rats. Eur. J. Neurosci. 28, 1316–1328.
Wharton, S.B., et al., 2009. Population variation in glial fibrillary acidic protein levels in brain ageing: relationship to Alzheimer-type pathology and dementia. Dement. Geriatr. Cogn. Disord. 27, 465–473.
Wilson, M.A., Molliver, M.E., 1994. Microglial response to degeneration of serotonergic axon terminals. Glia 11, 18–34.
Yan, Y.P., et al., 2009. Persistent migration of neuroblasts from the subventricular zone to the injured striatum mediated by osteopontin following intracerebral hemorrhage. J. Neurochem. 109, 1624–1635.
Yelverton, J.T., 1996. Pathology scoring system for blast injuries. J. Trauma 40, S111–S115.
Zhou, L., et al., 2010. Normalization with genes encoding ribosomal proteins but not GAPDH provides an accurate quantification of gene expressions in neuronal differentiation of PC12 cells. BMC Genomics 11, 75.
Zhu, H., Dahlstrom, A., 2007. Glial fibrillary acidic protein-expressing cells in the neurogenic regions in normal and injured adult brains. J. Neurosci. Res. 85, 2783–2792.
Ziegler, G., et al., 2009. Mrp-8 and -14 mediate CNS injury in focal cerebral ischemia. Biochim. Biophys. Acta 1792, 1198–1204.
Zuckerman, S., 1940. Experimental study of blast injuries to the lungs. Lancet 236, 219–224.